

OPTIMIZATION OF BUILDING ENVELOPE DESIGN FOR DAYLIGHTING AND  
THERMAL PERFORMANCE

by

Benjamin Joseph Futrell

A dissertation submitted to the faculty of  
The University of North Carolina at Charlotte  
in partial fulfillment of the requirements  
for the degree of Doctor of Philosophy in  
Infrastructure and Environmental Systems

Charlotte

2015

Approved by:

---

Dr. Ertunga C. Ozelkan

---

Mr. Dale Brentrup

---

Dr. Robert Cox

---

Dr. David C. Weggel

---

Dr. Eric Delmelle

©2015  
Benjamin Joseph Futrell  
ALL RIGHTS RESERVED

## ABSTRACT

BENJAMIN JOSEPH FUTRELL. Optimization of building envelope design for daylighting and thermal performance. (Under the direction of DR. ERTUNGA C. OZELKAN and MR. DALE BRENTROP)

Buildings account for 40% of US energy usage. A building's energy usage is largely determined by decisions made during its design. Such decisions relate to the form and orientation of the building, the materials used, and location of windows. A bi-objective building design optimization method was developed to minimize heating and cooling energy usage and maximize natural lighting (daylighting). Four optimization algorithms were integrated and evaluated based on efficiency and consistency of results. Thermal performance was evaluated by enclosure elements' (windows, floors, walls, and roofs) impact on heating and cooling energy. Lighting performance was evaluated by the frequency and magnitude at which natural light levels deviated from a desired range. To ensure the accuracy of results, a method of thermal model calibration was developed based on room temperature responses to various weather conditions. The model used for simulation-based optimization was first calibrated to measured values, of the building it represented, such that predicted and measured hourly room temperatures ( $^{\circ}\text{F}$ ) deviated by an RMSE of 0.82 on hot and cold days. Optimization results show that thermal and lighting performance can be significantly improved from an initial design and the associated Pareto front aids evaluation of trade-offs between the two.

## DEDICATION

For Sarah, Henry, and Henry's little brother soon to arrive. Thanks for the support on the home front!

## ACKNOWLEDGMENTS

I would like to acknowledge the help and guidance I received from each of my committee members. I thank specifically Dale Brentrup for encouraging my analytical curiosity and allowing me the opportunity to “take apart the watch” and understand how it worked. He saw potential in me I did not see myself. I am glad our paths crossed! I thank Dr. Ozelkan (Oz) for guiding the curiosity of a former architecture student eager for analytical rigor. He gave me the knowledge and guidance necessary to develop and solve an interesting problem originating from a germ of an idea given by Dale in the School of Architecture’s Daylighting and Energy Performance Lab. Dr. Cox made sure my hammer of a solution hit the right nail of a problem, or at least closer to it. Thank you Dr. Cox for your critical examination of my work; I’m a much better researcher because of it. I would like to thank the faculty of the Infrastructure and Environmental Systems program and School of Architecture for the opportunity to solve a truly interdisciplinary problem. I would like also to acknowledge the National Science Foundation Industry & University Cooperative Research Program Center for Sustainably Integrated Buildings and Sites (SIBS) for its support and case study opportunities.

## TABLE OF CONTENTS

CHAPTER 1: INTRODUCTION	1
CHAPTER 2: REVIEW OF THE LITERATURE	6
2.1. Review of Related Building Design Optimization Work	6
2.2. Review of Related Energy Model Calibration Work	8
CHAPTER 3: BUILDING ENERGY MODEL CALIBRATION: A SIMULATED EXAMPLE	13
3.1. Demonstration of a Method of Energy Model Calibration	15
3.2. Results of Model Calibration Demonstration	17
CHAPTER 4: OPTIMIZATION OF DAYLIGHTING PERFORMANCE	19
4.1. Optimization Problem Formulation	25
4.2. Solution Method	30
4.2.1. Optimization Algorithms	31
4.2.2. Simplex Algorithm of Nelder and Mead with the Extension of O'Neill	33
4.2.3. Hooke Jeeves Algorithm	34
4.2.4. Particle Swarm Optimization Algorithm	35
4.2.5. Particle swarm Optimization and Hooke Jeeves Hybrid Algorithm	36
4.3. Results	36
4.3.1. Numerical Experiments and Results	36
4.3.2. Analysis of Thermal Performance	46
4.3.3. Description of Thermal Models	46
4.3.4. Summary of Thermal Analysis Results	52
4.3.5. Discussion and Conclusions	54
CHAPTER 5: BI-OBJECTIVE OPTIMIZATION OF DAYLIGHTING AND THERMAL PERFORMANCE	56

	vii
5.1. Methodology	59
5.1.1. Optimization Problem Formulation	59
5.1.2. Building Design Problem Definition	63
5.1.3. Optimization Algorithm	68
5.1.4. Lighting Simulations	69
5.1.5. Thermal Simulations	71
5.1.6. Determination of Pareto Fronts	72
5.1.7. Sensitivity Analysis of Lighting Simulation and PSO Algorithm Parameters	73
5.1.8. Optimization Process	80
5.2. Results and Discussion	81
5.3. Conclusions	86
CHAPTER 6: ENERGY MODEL CALIBRATION CASE STUDY	88
6.1. Energy Model Calibration	89
6.1.1. Description of Case Study Model Calibration	89
6.1.2. Energy Model Calibration Methodology through Thermal Response Analysis	94
6.1.3. Method of Thermal Response Analysis of Case Study Building	96
6.1.4. Results of Thermal Response Analysis and Model Calibration	101
6.2. Optimization of Retail Bank Building for Thermal and Daylighting Performance	109
CHAPTER 7: CONCLUSION	116
7.1. Summary	116
7.2. Limitations and Future Work	118
7.2.1. Building Element Performance	119
7.2.2. Analysis of Pareto Efficient Designs	119

	viii
7.2.3. Model Calibration Improvements	121
7.2.4. Integration into Building Design Practice	122
REFERENCES	123

## CHAPTER 1: INTRODUCTION

In buildings, thermal and lighting comfort conditions are sustained primarily by energy-intensive equipment. In 2012, operational energy in the commercial building sector accounted for 19% of total energy consumption in the United States [1]. Nationwide, lighting alone accounts for 20.5% of major fuel consumption in commercial buildings [2]. Major determining factors of heating, cooling, and lighting loads that must be met by HVAC and electrical light systems are climate, internal equipment, building use type, and occupancy profile and schedule, and the design of the building enclosure. Of these factors, building enclosure design is perhaps the most freely controlled by the design team. Building enclosure design includes building orientation, floor plan/footprint shape, window placement and size, material selection, etc. The building itself is a system of energy (in the form of sensible heat and radiation – including light) conducting, transmitting, and storing elements (walls, windows, and building mass, respectively) that interface between the exterior and interior environments. Because the design team has great control over these load-determining aspects of design, it is appropriate that they be investigated as a first tier energy efficiency strategy. For example, annual electric lighting consumption can be reduced by 20% to 77% by good daylighting practices, as others have shown across various building types and climates [3-9].

Robust and validated modeling tools exist for the performance evaluation of building designs; however, they are not commonly used to explore the performance of

many design alternatives [10]. In practice, their use is often limited to validating one or several designs. Building design optimization programs have been developed; however, most of these tools focus exclusively on the optimization of envelope thermal loads or use simple, lighting evaluation methods. Rigorous evaluation and optimization of holistic lighting performance can help identify building designs that consume less heating, cooling, and lighting energy.

This work, in part, analyzes the transmission of daylight by the building envelope to the building interior. Daylighting design has mainly to do with how windows and light-reflecting surfaces are located, sized, and assigned materials. Optimum daylighting design varies based on climate and geographic location, orientation, and surrounding exterior context. These considerations make optimizing for daylighting performance a unique problem for every building designed. During the building design process, the potential for daylighting to reduce electric lighting consumption is rarely analyzed or optimized. One aspect of the research presented here is to evaluate methods of optimizing building design for daylighting and, thereby, minimize the need for electric lighting.

Because the design of windows not only affects lighting performance but also heat gains and losses to and from a building, the thermal effects of window and envelope design decisions are integrated into this work. Larger windows admit more light but also allow for the potential of larger heat gains and losses. A successfully sustainable building design will balance the sometimes conflicting benefits of optimizing a building design for daylighting and thermal performance.

The work presented here is largely based on lighting and energy simulations, which are only trustworthy if the discrepancy between their predictions and reality is

acceptably small. The lighting simulation program used, RADIANCE, is well validated and trustworthy, as long as model input faithfully represents reality. Validation studies of RADIANCE include [11-15]. The major potential source of discrepancy between a RADIANCE lighting model and reality is how humans modify window condition (e.g., the use of blinds). This work focused on optimizing building design to provide the most comfortable levels of natural light, without the need for blinds. Therefore, an assumption of this work is that its lighting models do not account for modification by humans and are, therefore, reasonably trustworthy. Building energy/thermal models can also be trustworthy, if correct input is used. The building energy simulation program used in this work, EnergyPlus, has been validated by [16]. However, building energy models are based on input parameters that are difficult to determine, as [17] have shown. This work addresses the issue of underdetermined parameters by developing a method by which key parameters of an energy model are fine-tuned or calibrated such that the model predicts measured values, specifically zone temperatures, reasonably well for a given set of weather inputs.

In Chapter 2, a review of related literature is presented. Works focused on building design optimization are discussed, along with how this body of work relates to and expands upon them. Following this, works related to energy model calibration are discussed in detail.

Chapter 3 presents a brief simulation based demonstration of energy model calibration of a classroom design that is subsequently optimized in Chapters 4 and 5. In Chapter 4, a simulation based optimization method is developed to solve building daylighting design problems. An application of the proposed method is presented that

optimizes a prototype design of a grade school classroom. The prototype design optimizes the uniform delivery of daylight from windows to the classroom. The generic optimization program, GenOpt, was integrated into the method used to solve this design optimization problem [18]. Four of GenOpt's optimization algorithms were assessed for their speed of convergence to a solution and the distance of the found solution to the single best found solution of all algorithms. The four algorithms assessed were the Simplex Algorithm of Nelder and Mead with the Extension of O'Neill (SA), Hooke Jeeves (HJ), Particle Swarm Optimization using Inertia Weight (PSOIW), and a hybrid PSO Constriction/Hooke Jeeves (PSOC/HJ) algorithm.

Building upon the single objective optimization for daylighting performance, Chapter 5 presents a method of bi-objective optimization of daylighting and thermal performance. The daylighting optimization method was expanded to solve this bi-objective optimization problem. Thermal performance was evaluated by how heat transfer across enclosure elements impacts hourly heating and cooling loads. Lighting performance was evaluated based on the frequency and magnitude at which daylight levels, during occupied hours, deviate from a desired target illuminance range. A single-zone classroom design in Charlotte, NC was optimized for north, south, east, and west orientations. For each orientation, a Pareto front was approximated to help evaluate trade-offs between thermal and daylighting objectives. Results show that for the south orientation, thermal and daylighting objectives are not in strong conflict, however, for other orientations there is a more marked conflict between these objectives, particularly for the north orientation.

Chapter 6 presents a method of adapting the developed optimization method to calibrate an energy model to measured data, minimizing the difference between the two. This provides a means to ensure the energy model used for design optimization produces reasonably good results. The developed method of model calibration is relevant to building projects to be optimized where there is an existing building, such as a retrofit project or a standard design to be replicated, that can be measured and modeled. A case study example of such a project is presented. Hourly temperature and energy values were collected from an existing building to serve as the basis of design for other buildings. An energy model of this building was developed and calibrated to measured values. This was done by searching for the set of model parameter values that minimized the error between modeled and measured temperatures. The calibrated energy model was then used to optimize the prototype design for thermal and lighting performance. Since key parameters of the optimized energy model were calibrated, the results of the design optimization are more trustworthy than had a non-calibrated energy model been used.

## CHAPTER 2: REVIEW OF THE LITERATURE

This chapter first reviews related work about building design optimization and then reviews related work about building energy model calibration.

### 2.1. Review of Related Building Design Optimization Work

The application of optimization algorithms to the problem of energy efficient building design optimization has received much attention in recent years. For the problem of daylighting design, evolutionary-based optimization algorithms have been used more than other methods (see e.g. [19-23]), especially when the problem becomes intractable by a simple brute-force approach. This is due to the complex relationships between design parameters and performance. Gagne and Andersen apply a genetic algorithm (GA) to optimize façade design for daylighting performance and to facilitate “performance-based” design exploration with a specific focus on integration into the design process [20]. This work focused on a generative and goal-oriented design process that integrated a GA to search for high-performing/near optimum thermal and lighting design solutions as evaluated by DOE2.1E. Results showed that the GA could find near optimal designs for basic building massing and window dimensions for different orientations and climates. GAs for ceiling form optimization in response to daylight levels was discussed in [22]. This paper's focus was on the shape of the ceiling with regard to how well it reflects and diffuses sources of daylight for the satisfaction of interior illumination needs. Works focused on bi-objective thermal and daylighting optimization include [24, 25]).

Hu and Olbina developed a faster approach for predicting thermal and lighting performance of buildings. They performed a bi-objective optimization of basic fenestration parameters, window dimensions, glazing transmittances, and blind reflectance, for thermal and daylighting performance. Padovan optimized the design of an external shading device, accounting for its interaction with dynamic blinds, for thermal and daylighting performance.

In general, related work has shown that optimization algorithms are successful at finding high performing daylighting and thermal design solutions. The research presented in this paper builds upon the literature discussed above with some similarities but also several differences. Related work typically has investigate parameters that can be adjusted as single values in model input files. More complex parameters (e.g., ceiling height of complex room shapes and detailed fenestration elements such as lightshelves and external shading devices) have rarely been integrated in to optimization routines. Most works that do consider complex geometry evaluate either daylighting or thermal performance, but not both. When daylighting performance and thermal performance have been considered together, daylighting has been evaluated using simple methods. Additionally, the simultaneous optimization of solar and light transmittances of a window, with a dynamic constraint to ensure the physical feasibility of the window, has not been seen and is developed in this work. The stated dynamic constraint ensures that found solutions have realistic light to solar gain (LSG) values representative of commercially available products. In this work, a robust swarm based algorithm, GenOpt's hybrid PSO Constriction/Hooke Jeeves (PSOC/HJ), was used to optimize such parameters along with complex geometry. In addition, a method of evaluating daylighting

performance was developed that was found to aid optimization algorithms in “fine-tuning” complex daylighting designs. This method was based on state-of-the-art dynamic daylighting metrics. Additionally, the dynamic sizing and modeling of an economizer cycle for thermal performance has not been seen by the author in other works and, it too, has been developed in this work.

## 2.2. Review of Related Energy Model Calibration Work

Model calibration is important because optimization of a building model is only useful if the model closely predicts actual energy use for given weather and operational conditions. Because an energy model is a simplification of complex systems with many interactions, and the operation of buildings by humans is stochastic in nature, numerous studies have highlighted the discrepancies between modeled and measured quantities and are cataloged by [26]. Notable examples include [27] where model error was found to be 50% on average for the studied building. Many LEED certified buildings earn LEED certification points based on energy use predicted by an energy model based on ASHRAE’s Energy Cost Budget (ECB) method [28]. As such, LEED certified buildings have been the focus of several studies that compare predicted and actual energy use of buildings. In [29] modeled and measured energy use of LEED certified buildings was studied and it was found that energy use predictions for individual buildings were very inconsistent; measured energy use ranged from 50% to 275% of that predicted. [30] further highlights the discrepancy between predicted and actual energy use of LEED certified buildings, and [31] performed a detailed analysis of two LEED certified buildings and found that their models over predicted energy consumption by 14% and 25%.

As the works above have shown, building energy models have a reputation of being inaccurate. Because of this, much effort has been given to energy model calibration and several standards and example case studies have been developed [32-38]. However, these efforts and standards mostly focus on calibrating energy model results to monthly utility usage data, because these data are readily available. Studies have used hourly data as the basis of calibration [39, 40], and have correctly identified a major problem of calibrating to coarse data: many model solutions can closely match monthly utility data, making it difficult to identify which of the co-solutions is the most accurate representation of reality. In other words, there can exist many calibrated model instances because they each produce “acceptable” measures of calibration. The co-solutions problem stems from interactions and compensatory relationships between model parameters. For example, if internal heat from equipment is too low, the solar transmission of glazing could be increased to compensate. How is one to know whether the solar transmission of glazing is truly higher than originally thought, or if some other parameter, such as equipment heat gain, is the true source of greater heat gain?

Studies that have calibrated to hourly values focus on HVAC system energy use, which can suffer from a similar co-solution problem as coarse data. This issue arises from the interaction between the HVAC system and the building loads. The potential flaw in this approach is that compensatory relationships may exist between HVAC and load-affecting parameters (such as those related to the building envelope and internal heat gains). For example, if a cooling system is not functioning properly, and therefore using more energy than it normally would, envelope parameters in the energy model, with the cooling system modeled as properly functioning, can be adjusted to create artificially

high cooling loads. As a result, the modeled cooling system energy consumption will also be artificially high and may closely match that of the actual cooling system. Figure 2.1 illustrates such an example. Here, a close match between modeled and actual energy use was obtained by an artificially high infiltration rate. Upon closer examination of the “calibrated” model, the unrealistically high infiltration rate was discovered. Since the model assumed proper function of the cooling system, and air leakage is uncertain and difficult to measure, infiltration rates were adjusted until energy consumption matched measured values. After this discovery, it was determined that the cooling system was not operating properly, and thereby consuming excessive energy.

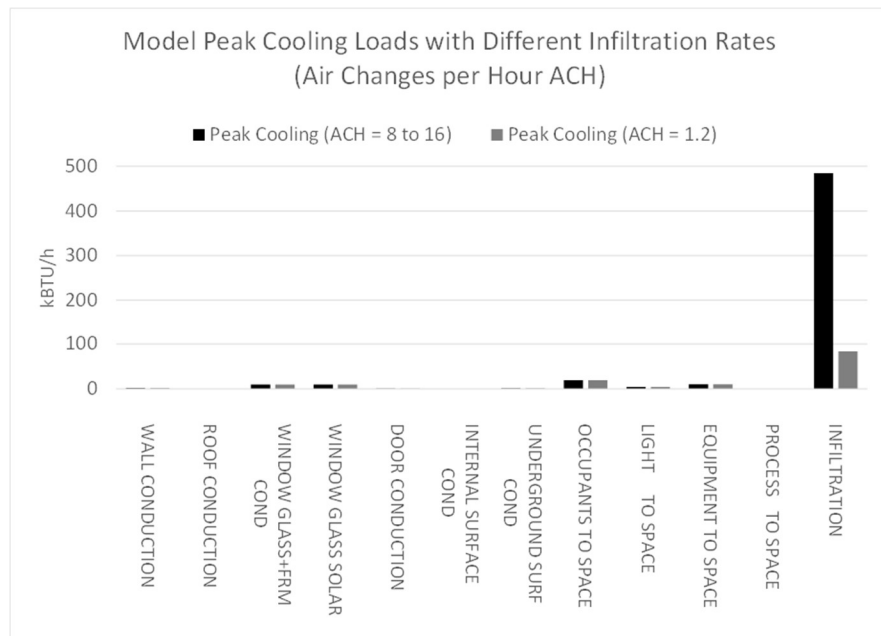


Figure 2.1: Component of peak cooling loads of “calibrated” energy models

With advancements in building automation systems (BAS) and building monitoring systems (BMS), and deeper market penetration of related products, often building energy and systems data (temperatures and flow rates) are available on a

granular time step and at an increasingly affordable cost. This increasing access to building performance data has opened new possibilities for higher fidelity building energy model calibration. Some have demonstrated the value to model calibration that such data can provide [41-44]. However, none have decoupled envelope loads and HVAC energy usage (i.e., the thermal loads from the systems responding to them) to address the potential compensatory relationship between the two.

The work presented here, specifically in Chapter 6, advances the related model calibration work by independently capturing the building heating and cooling loads, as determined by the building envelope and internal gains. Building internal gains from lights and equipment can be known at hourly, or in some cases sub-hourly, intervals because such data is monitored and reported by many BASs. BASs also have the ability to monitor room temperatures. Using these data, it is possible to measure building loads independent of effects from HVAC systems. This is done by temporarily disabling HVAC systems and recording the change in space temperature over time, the thermal response of the building. It is then possible to calibrate the modeled thermal response of a building to its measured thermal response. Internal heat gains from lights and equipment are determined by the BAS and input into the model. Actual weather conditions are also input into the model, leaving the envelope parameters as the only undetermined parameters that affect the thermal response. These envelope parameters can then be explored and optimized, with the goal of matching the actual thermal response of the building as close as possible. Subsequent to this, a properly functioning HVAC system can be modeled and used to audit the performance of the actual HVAC system.

For the purpose of building design optimization, accurately describing the building envelope, decoupled from the effects of the HVAC system, is an important first step. If a basic version of the envelope of the building to be optimized is characterized well, the optimized variant of the base design can be trusted with a reasonable degree of confidence. This approach is most appropriate in two cases. The first case is when there is an existing building similar to the one to be optimized. The base model can then be calibrated to data from the existing building. The second case is related to renovation projects. When an existing building is to be renovated, a base model can be calibrated to data from it before it is renovated. This model can then be used to optimize the renovation design.

## CHAPTER 3: BUILDING ENERGY MODEL CALIBRATION: A SIMULATED EXAMPLE

In this chapter, the design of a classroom building, subsequently optimized for lighting and thermal performance in Chapters 4 and 5, is used to demonstrate how an energy model can be calibrated to measured data. It is necessary to assess the accuracy of an energy model against actual performance data before using the model as a basis of design optimization. To this end, a method of energy model calibration, that is more fully described in Chapter 6, is used here to demonstrate how the quality and trustworthiness of an energy model can be increased before it is used for optimization purposes. The presented method is novel in that it is based on calibration to hourly end uses of energy and hourly zone temperatures, as opposed to daily or monthly aggregated energy usage, as is commonly done. The thermal characteristics of the building envelope are calibrated in isolation of the effects of the HVAC system. This allows for precise tuning of key envelope parameters and is significant because envelope parameters are the focus of subsequent optimization efforts.

To study the effects of the building envelope, namely how it responds to dynamic weather conditions, it is necessary to remove the effects of a building's HVAC systems. When this is done, heat is added to or removed from the air mass of spaces/zones in the building by "passive" means, causing changes in temperature over time. This is referred to as the thermal response of the building or, more precisely, the thermal response of the

thermal zones that compose the building. The thermal response, or profile of temperature changes over time, in a zone is determined by factors in three main categories.

- 1) Weather factors
  - a. Dry-bulb temperature
  - b. Relative humidity
  - c. Sun position
  - d. Direct solar radiation
  - e. Diffuse solar radiation
  - f. Ground temperature
  
- 2) Envelope factors
  - a. Thermal properties of envelope surfaces (floor, walls, roof, and fenestration)
  - b. U-values as determined by material thickness, conductivity, specific heat, and diffusivity
  - c. Solar transmittance of transparent surfaces (SHGC)
  - d. The amount of internal mass (e.g., furniture and interior walls) and its thermal properties
  - e. Infiltration and exfiltration of air
  
- 3) Internal heat gain factors
  - a. Heat gain from lights
  - b. Heat gain from equipment

Key parameters, not related to HVAC effects, that affect loads in buildings when they are occupied are heat gain from occupants, increased heat gain from lights and equipment used by occupants (although these may be measured and accounted for), and heat gains and losses from infiltration and exfiltration of air driven by occupant behavior such as the opening of doors when entering and exiting the building.

It is possible to largely determine all the factors impacting a zone's thermal response, except those in the envelope category. This is accomplished through measurement and data collection. For example, it is possible to measure the weather and internal heat gain factors impacting a zone's thermal response. The collection of hourly

local weather measurements is often available. Hourly energy usage data of key electrical circuits can be acquired from commercially available building automation systems (BASs) and Building Management Systems (BMSs). Thus, the effects of weather factors and heat gains from lights and equipment can be reasonably determined and accounted for in a building energy model. With these two categories of thermal response factors accounted for, a detailed study of envelope parameters, as the only undetermined values impacting the thermal response of a zone, can be conducted. It is here that energy model optimization methods can aid in the determining of envelope parameters. The below example describes the process of thermal response analysis, and subsequent model calibration, through a similar optimization framework as is presented in later Chapters 4 & 5 for the optimization of building design for lighting and thermal performance.

### 3.1. Demonstration of a Method of Energy Model Calibration

Figure 3.1 shows the basic classroom design that is later optimized. Here it is demonstrated, through simulation, how an energy model of the classroom may be calibrated. The method by which this is done follows. Using an initial model, based on the design optimization results from Chapter 5, hourly temperatures of the building interior are reported. On Saturdays and Sundays of the simulation, the modeled HVAC system was disabled so as to allow the space temperature to “float”. This was the thermal response of the building to the weather conditions on these test days. Saturdays and Sundays were used as test days because weekends are typically when a building is unoccupied and disabling the HVAC system will be least disruptive to people and operations. One thermal response “test” was conducted for each month of the simulation.

The simulation was run from January through the end of June, resulting in 6 thermal response test periods. TMY3 weather data for Charlotte, NC was used [45].

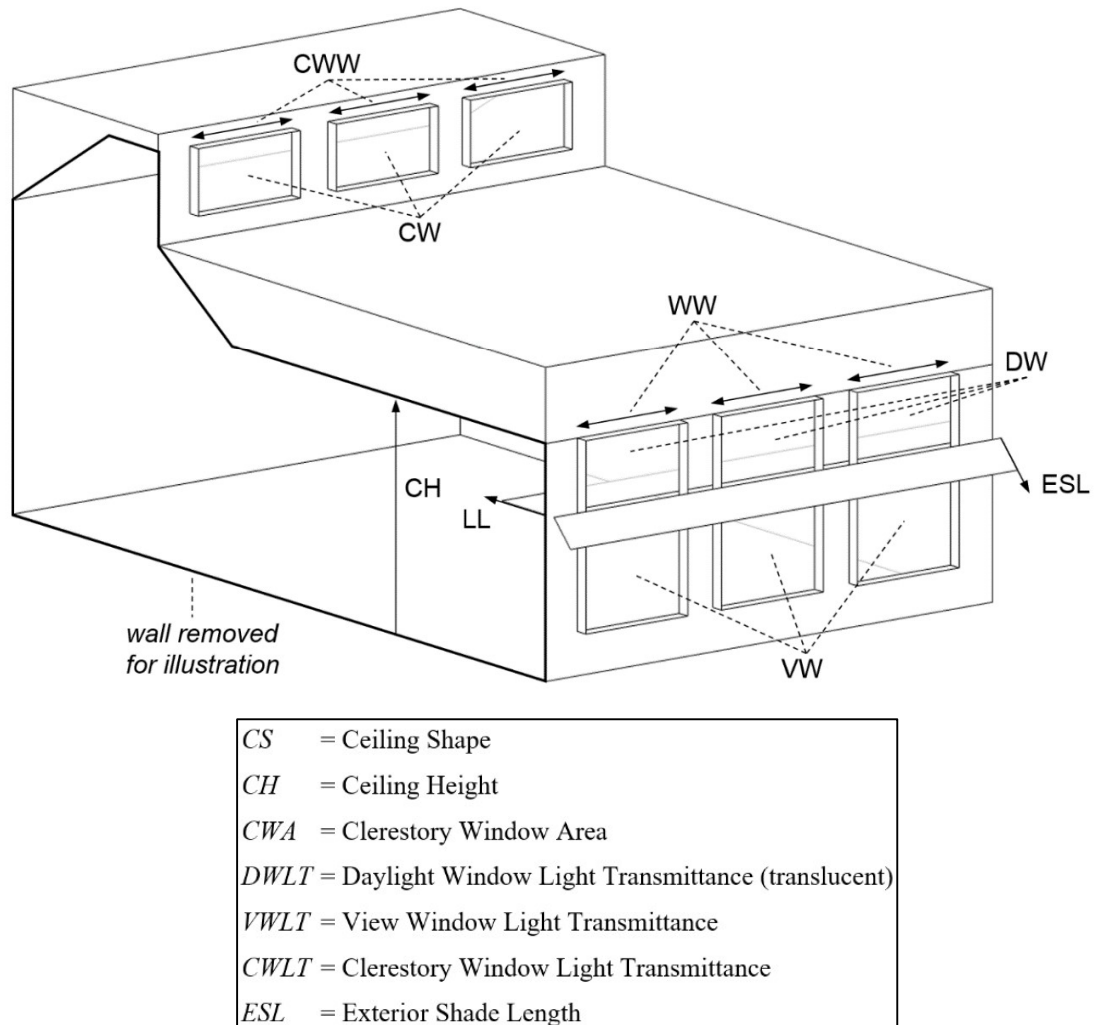


Figure 3.1: Illustration of building design used for energy model calibration

Certain envelope parameters of the model were intentionally changed and identified for optimization/calibration. These parameter values were searched and modified by an optimization algorithm with the objective of minimizing the Root Mean Square Error (RMSE) between the hourly thermal response temperatures of the base

model and the model being calibrated. It was assumed that the parameter set that minimized the RMSE between the models' outputs would be close to the "true" parameter set, as defined in the base model.

### 3.2. Results of Model Calibration Demonstration

Figure 3.2 shows the hourly temperatures of the base model's thermal response for the April thermal response test period. Also included on this graph are the hourly temperatures of the initial instance of the to-be-optimized version of the energy model. The initial model produced a thermal response that had an RMSE, with the base model's thermal response, of 2.1. It can be seen that there is a large discrepancy between the two thermal responses. Table 3.1 lists the intentionally modified parameters and the values they took on for the base model and initial to-be-optimized model.

An optimization procedure was then applied to the problem of calibrating the intentionally modified model. After about 150 simulations, the algorithm found a set of parameter values that resulted in a very good fit between the thermal responses (Figure 3.3). The calibrated model produced a thermal response that had an RMSE, with the base model's thermal response, of 0.013. The parameters values found by the optimization algorithm closely matched those of the base model, as seen in Table 3.1.

The results of this demonstration show that the theory of model calibration through thermal response analysis is potentially useful for determining key envelope parameters of an energy model to be subsequently optimized. In Chapter 6, this theory is more fully developed and applied to the calibration of an energy model of an actual building with measured data. This calibrated model is then used in a demonstration of

optimizing the envelope design of the existing building for lighting and thermal performance.

Table 3.1: Model parameters of base model and initial and calibrated models

Model Parameter	Base Model Value	Initial Model (to be calibrated)	Calibrated Model
Roof Conductivity	0.049	0.03	0.049
Window U-value	2.67	2.2	2.66
Window SHGC	0.69	0.15	0.69

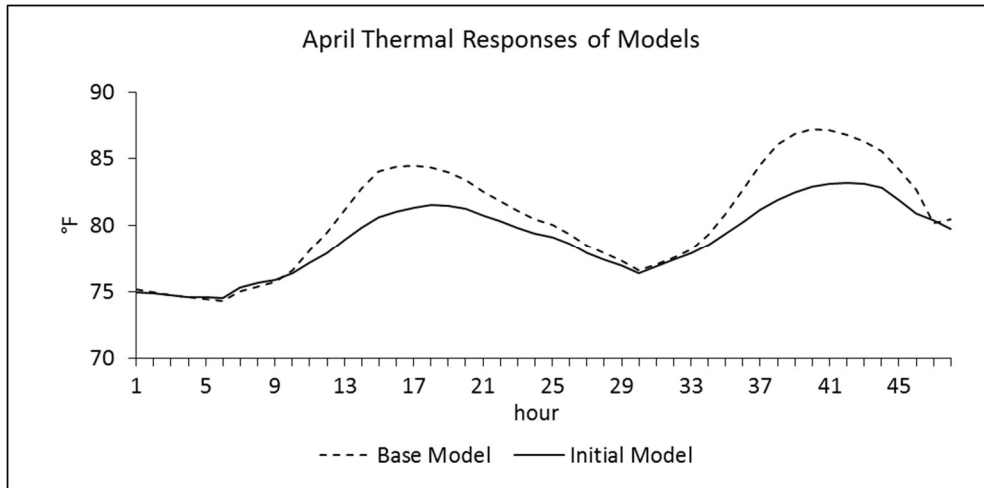


Figure 3.2: Thermal response of base mode and initial model to be calibrated

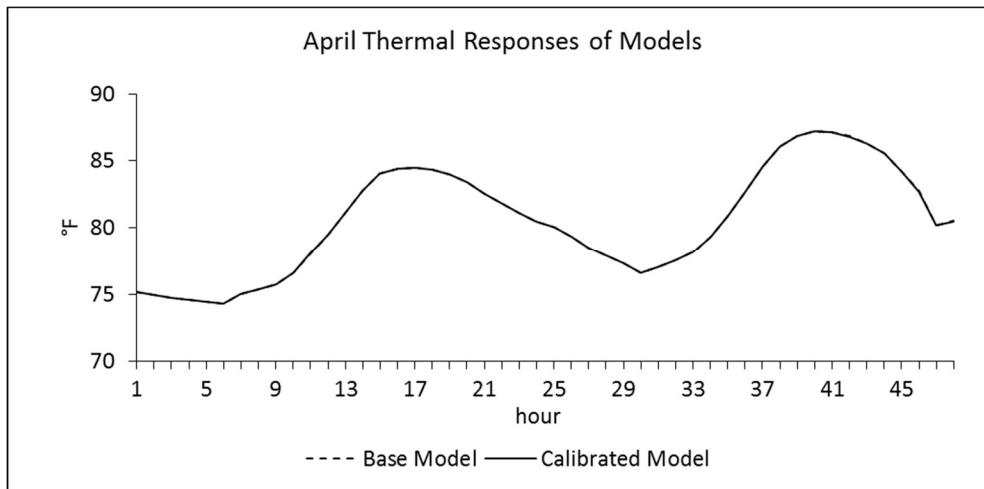


Figure 3.3: Thermal response of base model and calibrated model

## CHAPTER 4: OPTIMIZATION OF DAYLIGHTING PERFORMANCE

In this chapter, a method of optimizing building design is developed such that the illuminance needs of occupants is satisfied, to the greatest degree possible, through the admission and distribution of natural light. Key design parameters of the building were identified for optimization and feasible ranges for them were searched by optimization algorithms with the goal of achieving, as close as possible, ideal natural lighting conditions for each occupied hour of the year. The results of this chapter include the identification of optimum building designs for daylighting and the analysis of the performance of four optimization algorithms in their ability to efficiently and constantly find such designs.

Before defining the specific objective function in consideration, illuminance and related terms are defined. Illuminance (i.e., incident light) at a point ( $E$ ) is determined by integrating over the hemispherical field of luminance (i.e., surface brightness) seen by that point (Eq. 4.1) [46]). It is measured in lux, lumens per square meter, or foot-candles (fc), lumens per square foot. Besides the location of the point within the building/room, there are multiple external parameters ( $\Omega$ ) that influence the light field seen at any point in the building, including the building surface geometry, surface material properties (e.g., reflectance and/or transmittance), and a sky and sun model derived from historical climate/location data (month, day, hour, latitude, longitude, global horizontal irradiance and direct normal irradiance).

$$E(\Omega) = \int_0^{2\pi} \int_0^{\pi} L(\theta, \phi | \Omega) \cos \theta \sin \theta d\theta d\phi$$

$$\begin{aligned} \text{where } \theta &= \text{polar angle} \\ \phi &= \text{azimuthal angle} \\ \Omega &= \text{external factors} \end{aligned} \quad (4.1)$$

$L(\theta, \phi | \Omega)$  = luminance from direction  $(\theta, \phi)$  and for given external factors  $(\Omega)$

To approximate Eq. (4.1), a backwards ray-tracing method can be used based on a discrete number of sampling rays ( $2n^2$ , where  $n$  is an integer parameter) as shown in Eq. (4.2) [46]. The amount of luminance associated with each ray is calculated and, accordingly, the illuminance of the point is determined as a summation of the individual luminance values.

$$E(\Omega) \approx \frac{\pi}{2n^2} \sum_{j=1}^n \sum_{k=1}^{2n} L(\theta_j, \phi_k | \Omega)$$

$$\begin{aligned} \text{where } \theta_j &= \sin^{-1} \left( \sqrt{\frac{j - X_j}{n}} \right) \\ \phi_k &= \pi \frac{(k - Y_k)}{n} \end{aligned} \quad (4.2)$$

$X_j, Y_k$  = uniform random numbers between 0 and 1

$2n^2$  = total number of sampling rays

$L(\theta_j, \phi_k | \Omega)$  is the luminance in the direction  $\theta_j, \phi_k$  as seen by the calculation point

Next, the external parameters  $(\Omega)$  are explained in greater detail. Without loss of generality, external parameters can be divided into two groups: design parameters or decision variables  $(\Omega_1)$  and fixed parameters or inputs  $(\Omega_2)$ . Thus,  $\Omega = \Omega_1 \cup \Omega_2$ . Let  $\omega_1$

denote an individual design parameters such that  $\omega_1 \in \Omega_1$ . Typically, these decisions will need to be within allowed minimum and maximum specifications, which are denoted as  $\omega_{\min}$  and  $\omega_{\max}$ , respectively. Similarly,  $\omega_2$  denotes an individual fixed parameter or input such that  $\omega_2 \in \Omega_2$ . The  $L(\theta_j, \phi_k | \Omega)$  function is based on the luminance in the direction  $\theta_j$ ,  $\phi_k$  as seen by the calculation point.

For daylighting evaluation, illuminance is typically measured at calculation points at workplane height (0.75 m above the floor). An illuminance ( $E$ ) measurement is said to be within target if it is within  $E_{\min}$  and  $E_{\max}$  (typically, 100 lx and 2000 lx [47], however, here, a narrower range of 500 lx to 1000 lx is used in a modified manner described below to better distinguish between the performances of designs. Therefore, here, the objective is to identify a design that yields the maximum number of measurements within or in close proximity to the target range (denoted here using  $P$  which is formally defined below).

$$\max_{\omega_1 \in \Omega_1} P = \sum_{\omega_2 \in \Omega_2} \begin{cases} 1 & \text{if } E_{\min} \leq E(\omega_1 | \omega_2) \leq E_{\max} \\ E(\omega_1 | \omega_2) / E_{\min} & \text{if } E(\omega_1 | \omega_2) < E_{\min} \\ E_{\max} / E(\omega_1 | \omega_2) & \text{if } E(\omega_1 | \omega_2) > E_{\max} \end{cases} \quad (4.3)$$

subject to

Equation (3.2)

$$\omega_{\min} \leq \omega_1 \leq \omega_{\max}$$

Several daylighting metrics based on hourly measurements have been developed. These include Daylight Autonomy (DA), Continuous Daylight Autonomy (CDA), Useful Daylight Illuminance (UDI), Spatial Daylight Autonomy (sDA), and Annual Sun Exposure (ASE) [47-50]. DA is the percentage of illuminance values above a minimum

desired illuminance. Because DA has no upper threshold for illuminance, it does not capture whether a design is over-illuminated and, therefore, possibly visually uncomfortable. CDA gives partial credit to illuminance values below the minimum desired illuminance, but has the problem of not accounting for visual comfort. sDA is the percentage of area (based on the fraction of calculation points) that are above 300 lx for at least 50% of the annual hours evaluated. This metric also has the problem of not accounting for visual comfort; however, it is intended to be used in conjunction with ASE, which is a proxy measurement for visual comfort. ASE is the percentage of area (based on the fraction of calculation points) that is above a maximum threshold, typically 1000 lx, by direct sunlight alone for more than 250 annual hours evaluated. UDI is the percentage of illuminance values above a desired minimum, typically 100 lux, and below a desired maximum, typically 2000 lx. Unlike other metrics, UDI's "target range" of illuminance captures the daylight sufficiency and visual comfort of a design solution because values above the upper threshold are likely to cause visual discomfort/glare [49]. The measure of daylighting performance used here was based on UDI because a good daylighting solution meets both the illuminance and visual comfort requirements of occupants, and UDI is a good single indicator of both. However, based on experience, UDI and other metrics score too generally for optimization algorithms to converge efficiently. This is because these metrics give full credit to illuminance values above the minimum threshold or within the large target range and no credit to other values (except for CDA which gives partial credit to values below the minimum threshold), which leads to "crisp" binary based scores that do not always distinguish well enough between designs for algorithms to efficiently search the design space.

In addition to aiding the optimization process, a narrow target range of 500 lx to 1000 lx is more rigorous than the typical 100 lx to 2000 lx range, with regard to guarding against visual discomfort/glare, and is therefore used here. Even though the traditional 2000 lx upper limit is accepted as a good guard against visual discomfort, others have found a 500 to 1000 lx target range to be the best metric for measuring how well the illuminance and visual comfort needs of occupants are met [51, 52]. Calculated values within this range were given full credit (a value of 1) while outside values were given partial credit (a value between 0 and 1) proportional to the distance away from either the upper or lower boundary of the target range, as defined by Eq. (4.3) and seen in Figure 4.1. This scoring system ensured a unique score for every design solution and aided the optimization algorithm to converge quickly upon optimum solutions. As can be seen in Figure 4.1, the performance function is not symmetric about the target range because the benefit of values below the target range quickly diminishes while values above the target range can still be beneficial. The nature of the performance score curve helps to distinguish between designs. For example, if 0 value scores were given to all points above the upper threshold, then there would be no way to distinguish between the designs that grossly over-illuminate the classroom and those that moderately over-illuminate the classroom. The possibility of not optimizing to the best, least glare causing, solution is guarded against by the optimization algorithm finding the design solution that minimizes the magnitude of over-illuminated points. This effectively created a fuzzy membership function, which has been shown to work well in other types of optimization problems [53]. Using 88 calculation points, this method was found to give a unique score to each design solution and, therefore, a more precise representation of daylighting performance.

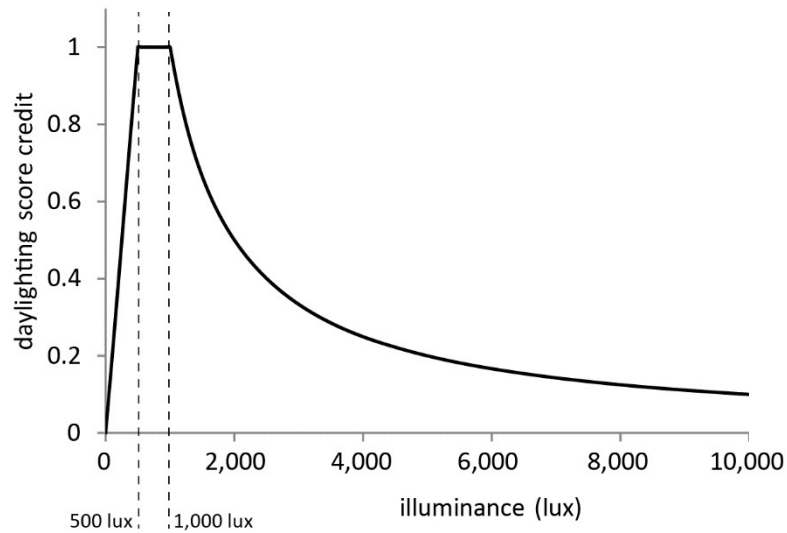


Figure 4.1: Graph of Eq. (4.3) used to score hourly illuminance values.

In this case, the following design parameters or decision variables ( $\Omega_1$ ) were selected:

- $CS$  = Ceiling Shape
- $CH$  = Ceiling Height
- $CWA$  = Clerestory Window Area
- $DWLT$  = Daylight Window Light Transmittance (translucent)
- $VWLT$  = View Window Light Transmittance
- $CWLT$  = Clerestory Window Light Transmittance
- $ESL$  = Exterior Shade Length

And the fixed parameters or inputs ( $\Omega_2$ ) included the following:

$x$  = x-coordinate of the illuminance calculation point

$y$  = y-coordinate of the illuminance calculation point

$m$  = month of year

$d$  = day of month (varies between 28 and 31 depending on month)

$h$  = hour of day (only occupied daylight hours used)

$\alpha$  = simulation parameters (including number of sampling rays)

$\beta$  = static model geometry and material properties

#### 4.1. Optimization Problem Formulation

Eight rows of calculation points on the  $x$ -axis and 11 rows of calculation points on the  $y$ -axis were used to sample illuminance. This resulted in 88 calculation points on a  $0.91 \text{ m} \times 0.91 \text{ m}$  grid centered in the classroom.  $E_{\min} = 500 \text{ lx}$  and  $E_{\max} = 1000 \text{ lx}$  were selected and the design parameters were normalized such that the minimum and maximum values corresponded to 0 and 1. Thus the following specific optimization problem was obtained:

$$\max P = \sum_{x=1}^8 \sum_{y=1}^{11} \sum_{m=1}^{12} \sum_{d=1}^{31} \sum_{h=0}^{23} \begin{cases} 1 & \text{if } E_{\min} \leq E(\text{CS}, \text{CH}, \text{CWA}, \text{DWLT}, \text{VWLT}, \text{CWLT}, \text{ESL} | x, y, m, d, h, \alpha, \beta) \leq E_{\max} \\ E(\text{CS}, \text{CH}, \text{CWA}, \text{DWLT}, \text{VWLT}, \text{CWLT}, \text{ESL} | x, y, m, d, h, \alpha, \beta) / E_{\min} & \text{if } E(\text{CS}, \text{CH}, \text{CWA}, \text{DWLT}, \text{VWLT}, \text{CWLT}, \text{ESL} | x, y, m, d, h, \alpha, \beta) < E_{\min} \\ E_{\max} / E(\text{CS}, \text{CH}, \text{CWA}, \text{DWLT}, \text{VWLT}, \text{CWLT}, \text{ESL} | x, y, m, d, h, \alpha, \beta) & \text{if } E(\text{CS}, \text{CH}, \text{CWA}, \text{DWLT}, \text{VWLT}, \text{CWLT}, \text{ESL} | x, y, m, d, h, \alpha, \beta) > E_{\max} \end{cases} \quad (4.4)$$

subject to

Equation (3.2)

$$0 \leq \text{CS}, \text{CH}, \text{CWA}, \text{DWLT}, \text{VWLT}, \text{CWLT}, \text{ESL} \leq 1$$

Eq. (4.4) can be modified to

$$P_i = \frac{P}{(\text{number of calculation points})(\text{number of occupied hours})} \quad (4.5)$$

which transforms  $P$  to  $P_i$ , a value between 0 and 1 where 1 represents perfect daylighting performance. Representing daylighting performance with  $P_i$  allows for simple comparison between the performances of solutions found within a specific problem, and also between different design problems.

The design of a classroom, shown in Figure 4.2, for daylighting performance was chosen as an optimization problem. As discussed before, seven design parameters were selected for optimization: ceiling shape (CS), ceiling height (CH) (note: daylight window height increased with CH), clerestory window area (CWA), daylight window (translucent) light transmittance (DWLT), view window light transmittance (VWLT), clerestory window light transmittance (CWLT), and exterior shade length (ESL). These design parameters are identified in Figure 4.2.

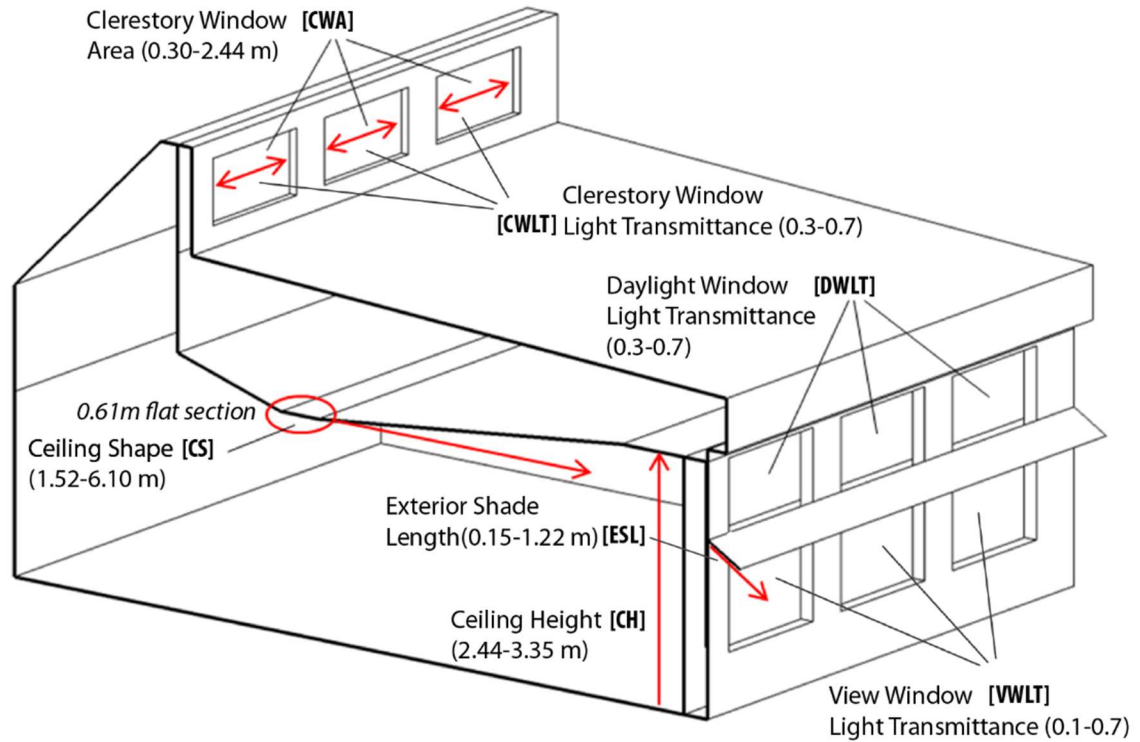


Figure 4.2: Building design parameters optimized.

CWA was increased or decreased by uniformly varying the width of the three clerestory windows from their centers. The clerestory windows' centers remained fixed. CS was varied by "sliding" a 0.61 m flat section of the ceiling perpendicular to the side windows. The ceiling sloped up to both ends of the room from this 0.61 m flat section, thus varying the position of the flat section changed the shape of the ceiling. CH was varied by increasing the height of the ceiling. The top of the daylight window (the upper glass of the side window) moved with the CH. The 0.61 m flat section of the window also moved with CH. ESL was varied by extending the distance away from the building the exterior shade reached. DWLT, VWLT, and CWLT were varied by uniformly changing the light transmittance of their associated windows.

Some of the main reasons for choosing these design parameters include:

- 1) CS influences how light admitted by windows is inter-reflected and delivered to calculation points.
- 2) Greater CH allows for a larger daylight window, thus admitting more daylight into the classroom.
- 3) Greater CWA increases the daylight delivered to calculation points located at the back of the classroom.
- 4) Greater DWLT increases the daylight delivered to calculation points throughout the classroom. The daylight window was modeled as a translucent material and delivers diffuse light to the classroom.
- 5) Greater VWLT increases the daylight delivered to calculation points close to the view window.
- 6) Greater CWLT increases the daylight delivered to calculation points located at the back of the classroom.
- 7) ESL can help reduce excessive daylight close to the window, while also reducing solar heat gain.

Table 4.1 shows the minimum and maximum settings of the investigated design parameters. Note that each design parameter was normalized such that 0 and 1 corresponded to the low and high settings, respectively.

Table 4.1: Minimum and maximum settings of the investigated design parameters

Design Parameter	Minimum -Maximum
CS (distance from window)	1.52 m- 6.10 m
CH (height of ceiling above floor)	2.44 m – 3.35 m
CWA (width of clerestory windows)	0.30 m – 2.44 m
DWLT	30% - 70%
VWLT	10% - 70%
CWLT	30% - 70%
ESL	0.15 m – 1.22 m

Daylighting performance was evaluated by measuring daylight illuminance delivered to 88 calculation points at workplane height (0.75 m above the floor), evenly spaced on a  $0.91 \text{ m} \times 0.91 \text{ m}$  grid (11 rows by 8 columns) centered in the classroom, for every hour of the year that the classroom is scheduled to be occupied. This was accomplished by using the daylight coefficient method [54] and its associated programs available in the ray-tracing software RADIANCE, along with hourly climate data for Charlotte [45]. The RADIANCE programs used were *gendaymtx*, *rcontrib*, and *dctimestep*. For daylight coefficient calculations using *rcontrib*, the sky was divided into 578 patches and the following key ray-tracing parameters were used: 12 ambient bounces (*ab*), 50,000 ambient divisions, and 0.00002 for the minimum contribution of each traced ray (*lw*). BASH shell scripts were written to calculate the *Pi* scores from the hourly illuminance values output by the RADIANCE programs. Each design solution took about 2 minutes to evaluate. As described in formulation (4.3), calculation point values within a desired illuminance range (i.e., between  $500 \text{ lx } E_{\min}$  and  $1000 \text{ lx } E_{\max}$ , neither too bright nor too dark) were fully rewarded while calculation point values outside of this range were partially rewarded based on their distance from either the upper or lower threshold. This narrow target illuminance range was found to help the optimization algorithm converge more quickly to near-optimal solutions. A wider target illuminance range, e.g., between  $300 \text{ lx}$  and  $2000 \text{ lx}$ , is representative of appropriate illuminance levels for office and school work, but was found to produce longer convergence times. The narrower illuminance range helps distinguish better between designs when approaching near-optimal solutions.

## 4.2. Solution Method

The optimization problem in Eq. (4.4) is relatively complex due to the physical relationship described in Eq. (4.2). “If-then” statements make the problem discontinuous as well. The “if-then” statements in the objective function can be replaced by binary decisions (thus yielding a mixed integer non-linear optimization problem) but this does not simplify the problem either due to the complexity of the illuminance function. As discussed in the literature, there are simulation programs for computing the illuminance function [55-57]. As previously described, one of these packages, RADIANCE [57], is utilized here in conjunction with GenOpt. GenOpt was created to allow for the integration of optimization algorithms and any simulation program that reads and writes text files as input and output. GenOpt essentially acts as a dispatcher, or controller, between optimization algorithms and simulations programs. GenOpt includes methods of manipulating simulation input files and reading variables from simulation output files. Because of its generic functionality, it is fairly easy to “plug and play” different direct search and meta-heuristic optimization algorithms in the solution of a particular simulation-based problem. Direct search and meta-heuristic algorithms do not require computation of directional derivatives and are, therefore, appropriate for simulation-based design problems that contain coding features that introduce discontinuity in the objective function.

#### 4.2.1. Optimization Algorithms

The performance of four optimization algorithms that are implemented in GenOpt is compared. In this section, the key concepts of how each algorithm operates are discussed; however, a comprehensive description of each is not provided. A detailed description of each algorithm may be found in [58], which contains technical information for each, as well as references related to the original development of each. The performance of an algorithm (the number of simulations required to converge to a solution, if not stopped by a limit on the number of simulations, and the performance value of the found solution), is dependent on its parameter settings. The evaluation of the effect of parameters settings on algorithm performance is not addressed by the work presented here. Instead, the parameters of each algorithm are set to values demonstrated to perform well for energy related building design problems [51]. The parameters chosen for each algorithm are listed in Table 4.2. Future work may include a detailed study of the influence of key parameters of each algorithm on performance and the identification of optimal parameters for daylighting design problems. The algorithms described below belong to the “direct search” and “meta-heuristic” classes of optimization algorithms; they make search decisions by the direct evaluation of the performance of solutions and do not require the derivative of the performance function to operate. As discussed above, these algorithms are appropriate for the daylighting design problem solved here which contains discontinuities in its performance function.

Table 4.2: Parameters of algorithms.

Common Stopping Criteria for all Algorithms	
Maximum Iterations	2000
Maximum Equal Results	100
SA	
Accuracy	0.01
Step Size Factor	0.1
Block Restart Check	10
Modify Stopping Criterion	TRUE
HJ	
Mesh Size Divider	2
Initial Mesh Size Exponent	0
Mesh Size Exponent Increment	1
Number of Step Reductions	4
PSOIW	
Neighborhood Topology	Von Neumann
Neighborhood Size	5
Number of Particles	20
Number of Generations	20
Seed	1
Cognitive Acceleration	2.8
Social Acceleration	1.3
Maximum Velocity Gain Continuous	0.5
Initial Inertia Weight	1.2
Final Inertia Weight	0
PSOIW/HJ	
<i>PSOIW Component</i>	
Neighborhood Topology	Von Neumann
Number of Particles	10
Number of Generations	10
Cognitive Acceleration	2.8
Social Acceleration	1.3
Maximum Velocity Gain	0.5
Constriction Gain	0.5
Mesh Size Divider	2
Initial Mesh Size Exponent	0
<i>HJ Component</i>	
Mesh Size Divider	2
Initial Mesh Size Exponent	0
Mesh Size Exponent Increment	1
Number of Step Reductions	3

#### 4.2.2. Simplex Algorithm of Nelder and Mead with the Extension of O'Neill

This direct search algorithm begins by constructing a simplex in the solution space of the design problem composed of vertices that represent unique design solutions [59]. The size of the simplex is always one more than the number of design parameters being optimized. At each vertex, the performance of the associated design solution is simulated and recorded. For each iteration, the vertex with the worst performance is replaced by another, causing the simplex to “crawl” around the design space in search of an optimum solution. The vertex to be replaced is reflected outside of the simplex along a line defined by its position and the centroid of the opposing side of the simplex. If the performance value of the new vertex is better than those of all other vertices, it is moved further along the reflection line and used to define the simplex of the next generation. This is known as expansion and causes the algorithm to be aggressive or “greedy” in its search for an optimum. If the performance value of the new vertex is equal to or worse than that of the best stationary vertex, and better than that of at least one other stationary vertex, it is accepted and used to define the simplex for the next generation. If the performance value of the new vertex is worse than those of all stationary vertices, it is moved along the reflection line toward its original position. This is known as contraction. If the performance value of the vertex generated by contraction shows no improvement over the original performance of the vertex before reflection, the entire simplex is shrunk such that the vertex with the best performance value remains fixed while all other vertices move toward it. Key parameters of this algorithm are the step size factor, which controls the distance between simplex vertices, and the minimum variance of the performance values of the vertices that must be met to achieve convergence. Advantages of this

algorithm include few simulations needed for each iteration and rapid improvement during initial runs. However, the algorithm has been demonstrated to sometimes fail at reaching convergence and often only finds a local optimum. Starting the algorithm at multiple random locations can often overcome the latter issue.

#### 4.2.3. Hooke Jeeves Algorithm

This direct search algorithm starts with a single point in the design space, referred to here as the “head”, from which it searches in a predefined distance (step size) in both directions of all coordinates for a better performing solution [60-63]. After simulating the performance values of all design solutions emanating in the coordinate directions from the head, the solution with the best performance is identified. The head is moved along the line between it and the best performing solution a distance scaled by a parameter call the acceleration factor. The process of evaluating solutions is repeated at this new head location. When a solution better than the head cannot be found, the step size is reduced, allowing for the search to continue within the region of the design space defined by the extents of the previous set of non-head design solutions. This process is continued for a predefined number of step size reductions. After the maximum number of step size reductions have been made and a design better than the head cannot be found, the algorithm terminates. In GenOpt, the parameters mesh size divider, initial mesh size exponent, and mesh size exponent increment controlled the incremental reductions in step size. The reader is referred to the literature for specific information about these parameters.

#### 4.2.4. Particle Swarm Optimization Algorithm

This meta-heuristic algorithm is a population based algorithm that developed out of evolutionary computational theory and social behavior theory [64-66]. It was originally developed to model the social behaviors of birds in a flock, or swarm. A basic concept of this algorithm is that a swarm of particles with dynamic velocities influenced by the location of found high-performing solutions “flies” through the design space in search of an optimum solution. During each iteration of the algorithm, the performance values associated with the particles’ positions are simulated and used to control where the particles move next. This algorithm begins by choosing random points in the design space for the initial positions of the particles composing the swarm. Each particle remembers the position of the best performing solution it has visited (personal best) and that of the best solution found by its neighbors (neighborhood best). Neighboring particles are determined by the neighborhood topology parameter. The velocity of every particle is controlled by its current position relative to the positions of its personal best and neighborhood best solutions such that it accelerates toward both potentially optimal positions. During each iteration, a particle's magnitude of acceleration in the direction of its current neighborhood best solution is made proportional to its distance from the neighborhood best solution, a constant parameter value, and a random scalar between 0 and 1 that is dynamically generated. The same is true of a particle's magnitude of acceleration in the direction of its personal best solution. In addition to these coefficients of acceleration, a dynamic inertia weight coefficient can be added. This coefficient starts large and gets smaller, with each iteration. When the inertia weight is large, it aids global search of the design space by allowing high acceleration of particles. When it is small, it

aids local searching and convergence by slowing down the movement of particles. An alternative approach to the inertia weight coefficient is called the constriction coefficient. During each iteration, this method scales the acceleration of a particle in each direction by a randomly generated scalar that can be greater than 1. A scalar less than one is then applied to the overall velocity of the particle. These operations constrain the overall velocity of a particle. This is important because unconstrained velocity of particles has been demonstrated to be problematic; particles tend to accelerate back and forth about optimal solutions and convergence is not reached.

#### 4.2.5. Particle swarm Optimization and Hooke Jeeves Hybrid Algorithm

In addition to the three algorithms described above, the PSO/Hooke Jeeves hybrid algorithm implemented in GenOpt is evaluated. This algorithm begins by running the PSO algorithm using the constriction coefficient method. Once complete, the optimum solution found is used as the starting point for the Hooke Jeeves algorithm. The intent of this hybrid algorithm is that the PSO run will locate the optimal region of the design space and the Hooke Jeeves run will perform a refined search of that area.

### 4.3. Results

#### 4.3.1. Numerical Experiments and Results

For each of the four algorithms evaluated, 12 optimization runs were conducted, starting at random locations in the design space. Figure 4.3 illustrates the optimization/convergence process of each algorithm in which the best found solution is plotted against the number of simulations conducted to find it. It should be remarked that the number of runs was determined based on the required computation time for the experiments and the number of computers available. All simulations were run on

computers running Linux OS with 3.4 GHz quad-core processors. Each simulation took approximately 2 minutes to converge. Thus, an optimization run requiring 250 simulations took between 8 and 9 hours to complete. Since the PSO algorithms are population based, their simulations could be run in parallel on the quad-core processors. Convergence times for the algorithms varied from 2 to 9 hours.

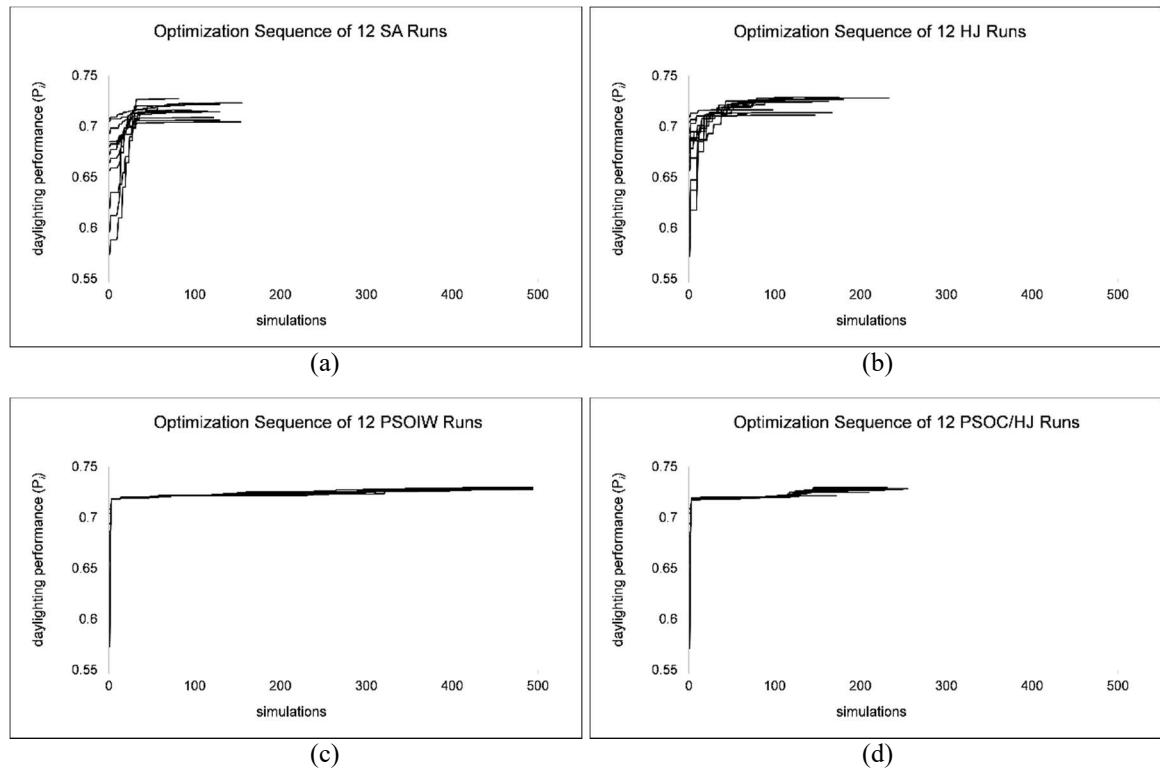
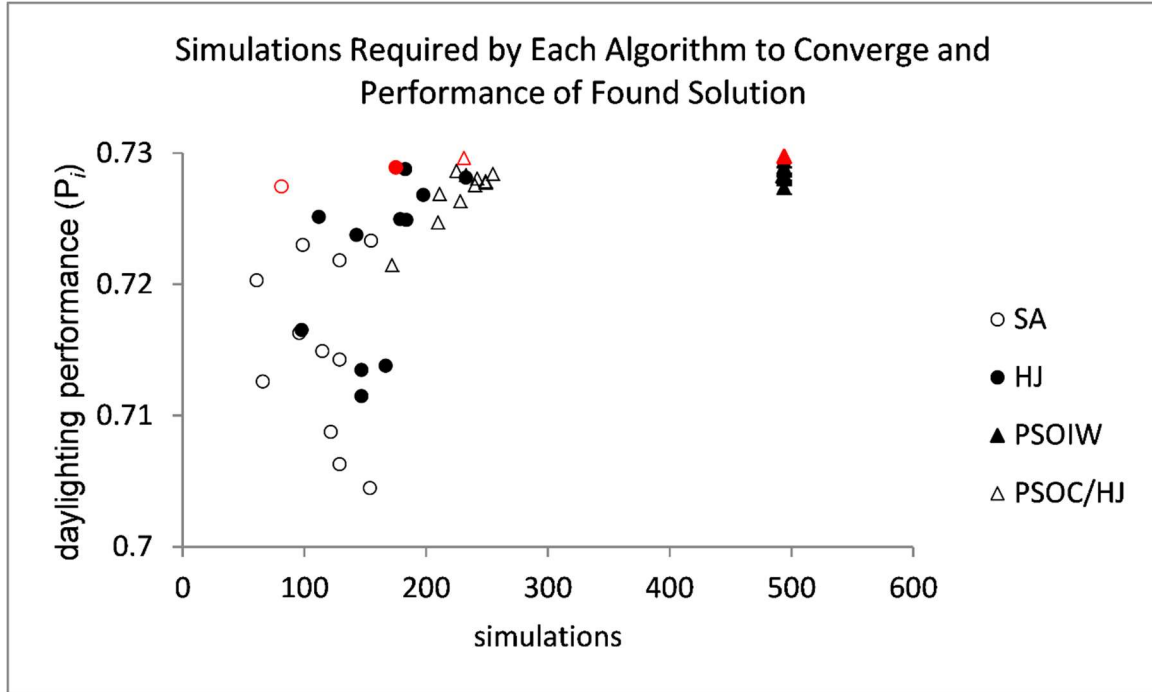


Figure 4.3: Optimization sequences of 12 optimization runs for (a) Simplex Algorithm of Nelder and Mead with the Extension of O'Neill; (b) Hooke Jeeves; (c) Particle Swarmusing Inertia Weight; and (d) hybrid PSO Constriction/Hooke Jeeves.

Figure 4.3(a) shows that the SA quickly reached convergence (ranging from 61 to 155 simulations); however, found solutions were not consistently close to the best overall found solution (found by PSOIW with a  $P_i$  value of 73.0%). SA produced solutions with

$P_i$  values ranging from 70.4% to 72.7%. Figure 4.3 (b) shows that the HJ algorithm runs reached convergence in 97 to 233 simulations. Like the SA, the HJ algorithm produced inconsistent results;  $P_i$  values of found solutions ranged from 71.1% to 72.9%. Figure 4.3(c) shows that the PSOIW algorithm found the highest performing solution (73.0%) and consistently found solutions extremely close to it, ranging from 72.7% to 73.0%. In all 12 PSOIW runs, convergence was not reached before the 500 simulation limit that was set. Figure 4.3(d) shows that the PSOC/HJ algorithm also produced more consistent results than SA and HJ; however, its results were slightly less consistent than those of PSOIW, with  $P_i$  values ranging from 72.4% to 73.0%. In Figure 4.3(d) the benefit of the HJ run after PSOC is evident. After the PSOC sequence of found solutions “flattens” between 50 and 100 simulations, the HJ algorithm finds designs with improved  $P_i$  values. The PSOC/HJ algorithm runs took between 172 and 255 simulations to reach convergence.

Similar conclusions can be drawn from Figure 4.4, which plots the solutions found by each run of each algorithm and the number of simulations required to reach either convergence or the maximum number of simulations allowed. It can be seen that the SA typically reached convergence in the fewest number of simulations, but did not produce constant performance values of found solutions. HJ typically took about 50 more simulations to converge than SA and its performance values of found solutions were slightly less varied than those of SA. PSOC/HJ took about 25 to 75 more simulations to converge than HJ and found very high performing and more consistent solutions than SA and HJ. PSOIW found solutions are tightly clustered near the best overall solution of 73.0%, but took the greatest number of simulations, 500, to find.



The nature of found solutions varied somewhat. A description of the architectural characteristics of the best overall solution found by PSOIW follows. As seen in Figure 4.5, the best overall solution had the following characteristics: a ceiling height of 3.35 m, a ceiling sloping down from the window wall such that the flat section of ceiling is 6.10 m from the window wall, 1.52 m wide clerestory windows with 0.7 light transmittance, a 1.22 m exterior shade, a daylight window light transmittance of 0.3, and a view window light transmittance of 0.35.

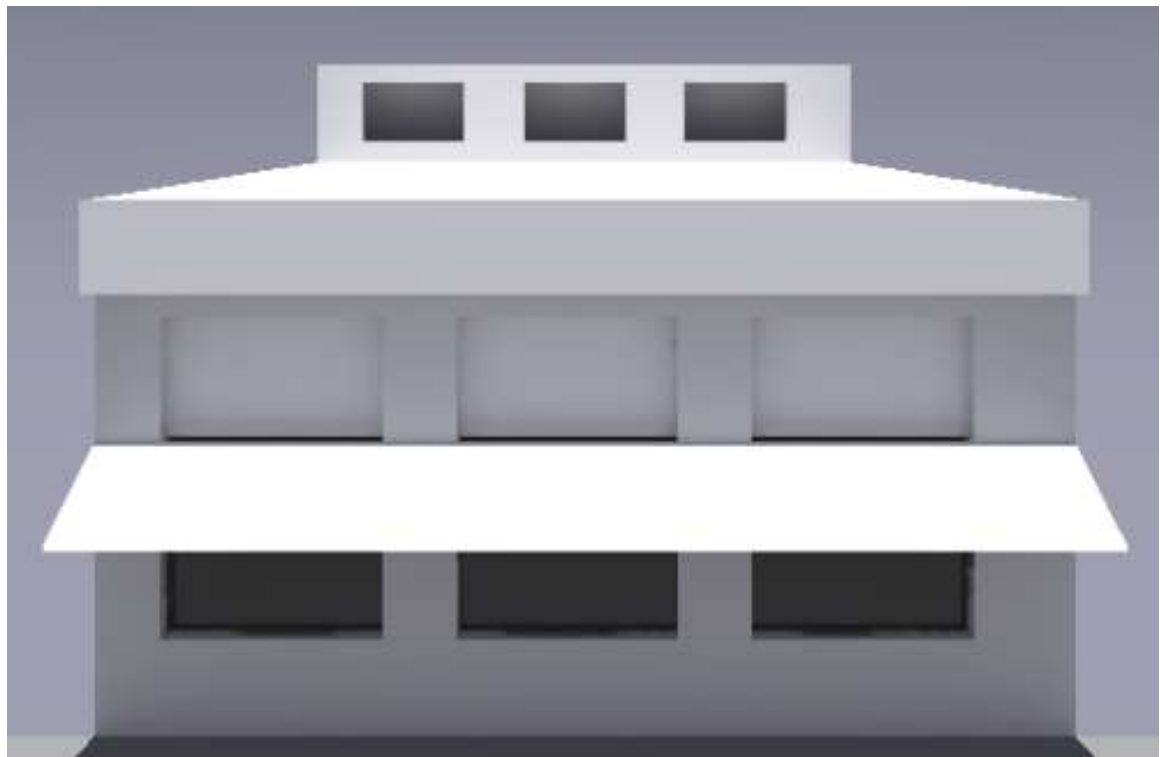
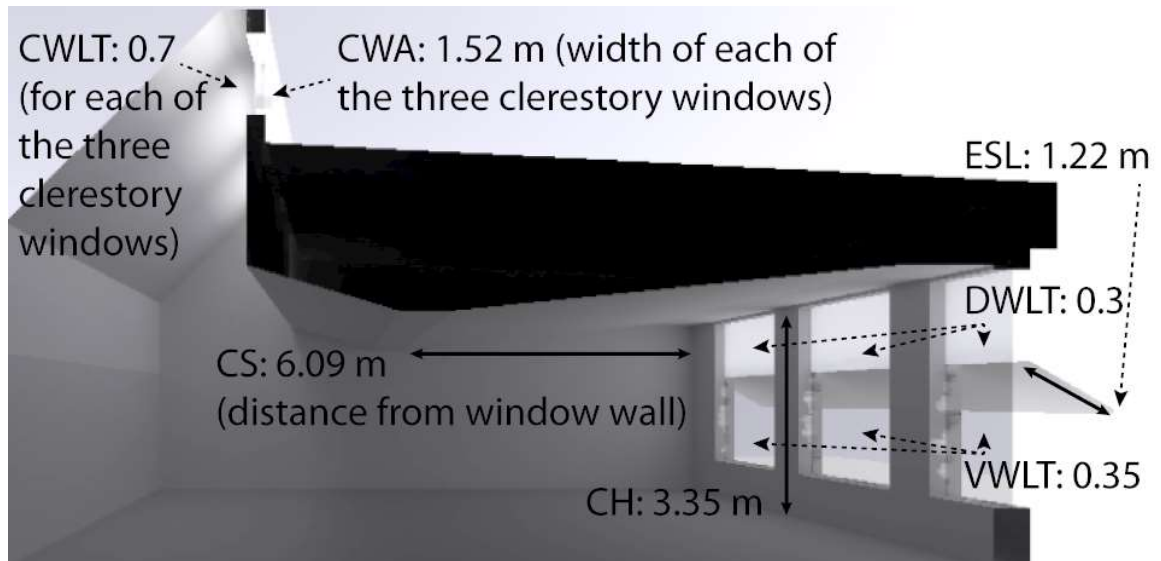


Figure 4.5: Best overall solution found by PSOIW; section perspective (a), exterior elevation (b).

Several insights can be made by analyzing the results of the optimization runs. Figure 4.6 shows the parameter values of the best found design solution of each algorithm. Although each algorithm found at least one solution within 2% of the overall best found solution (Figure 4.5), and similar in design parameter values, variation existed in the design parameter values of each algorithm's set of found solutions. Figure 4.7 shows the dispersion of the parameter values of found solutions by each algorithm. It can be seen that SA and HJ did not find consistent design solutions, while PSOIW and PSOC/HJ found much more consistent design solutions. By examining the design parameter values of solutions found by PSOIW in Figure 4.7(a), it is evident that the highest performing solutions have large CH, CS, and ESL values; a VWLT value in the middle of its range; a small DWLT value; and CWA and CWLT values in the upper half of their ranges. All design parameter values of solutions found by PSOIW have little variance, except for CWA and CWLT. This is likely due to the interaction between CWA and CWLT; both regulate the amount of light delivered through the clerestory windows. When one decreases the other may increase and result in a similar amount of total admitted light.

### Parameter Values of Best Found Solution of Each Algorithm

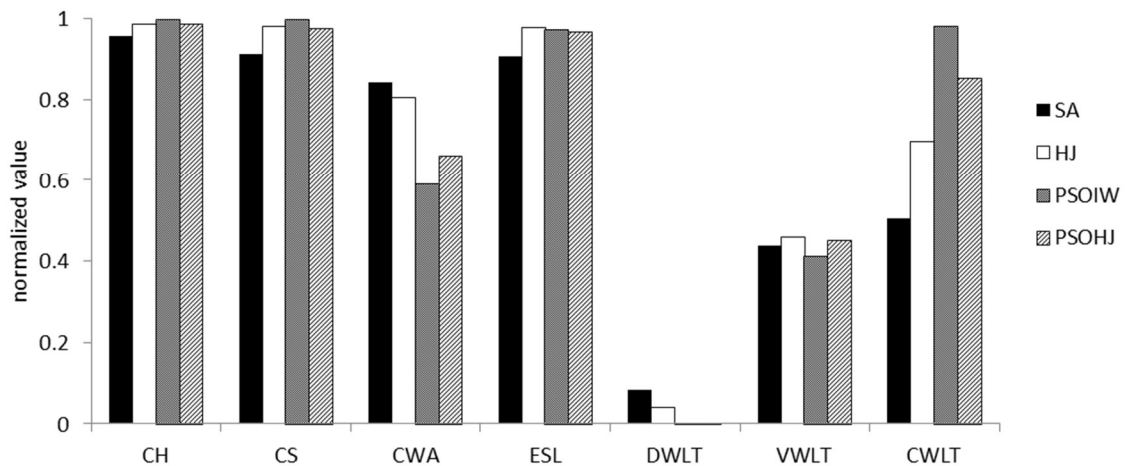


Figure 4.6: Parameter values of best design solution found by each algorithm.

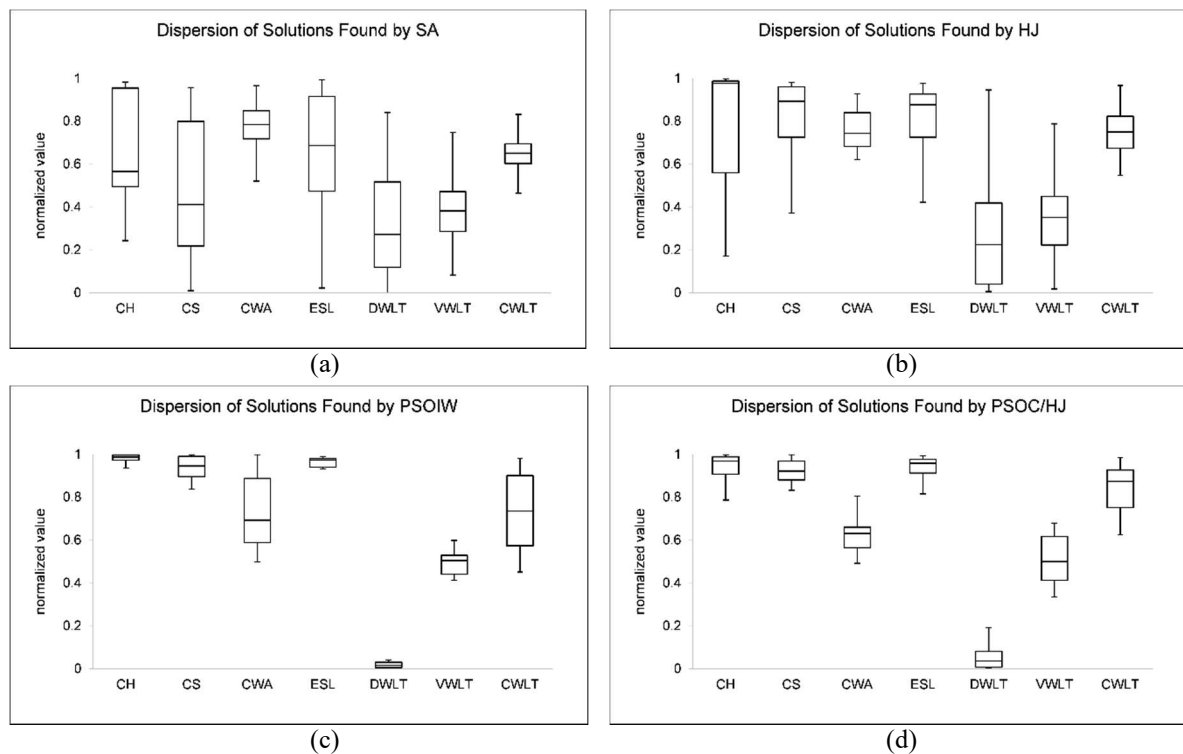
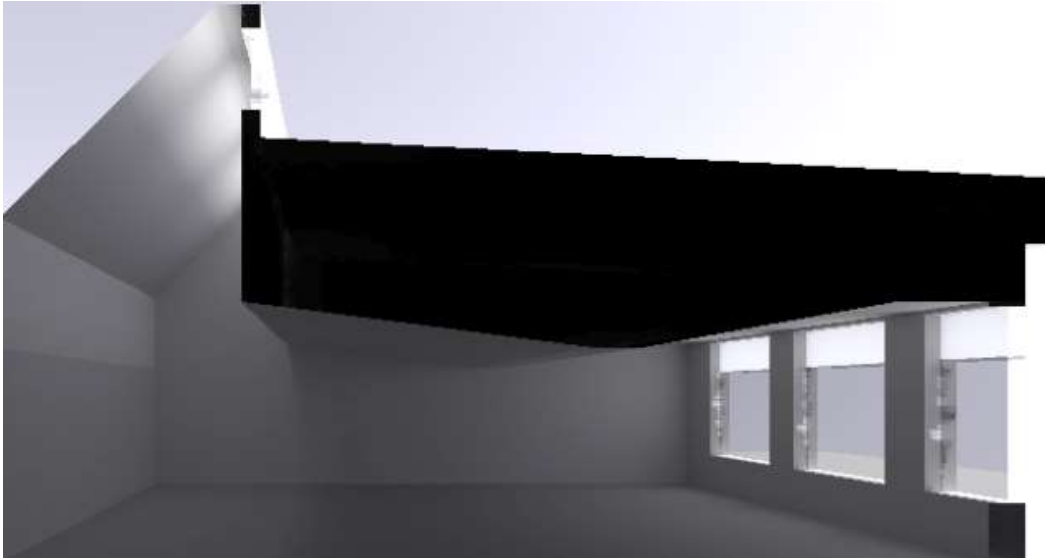


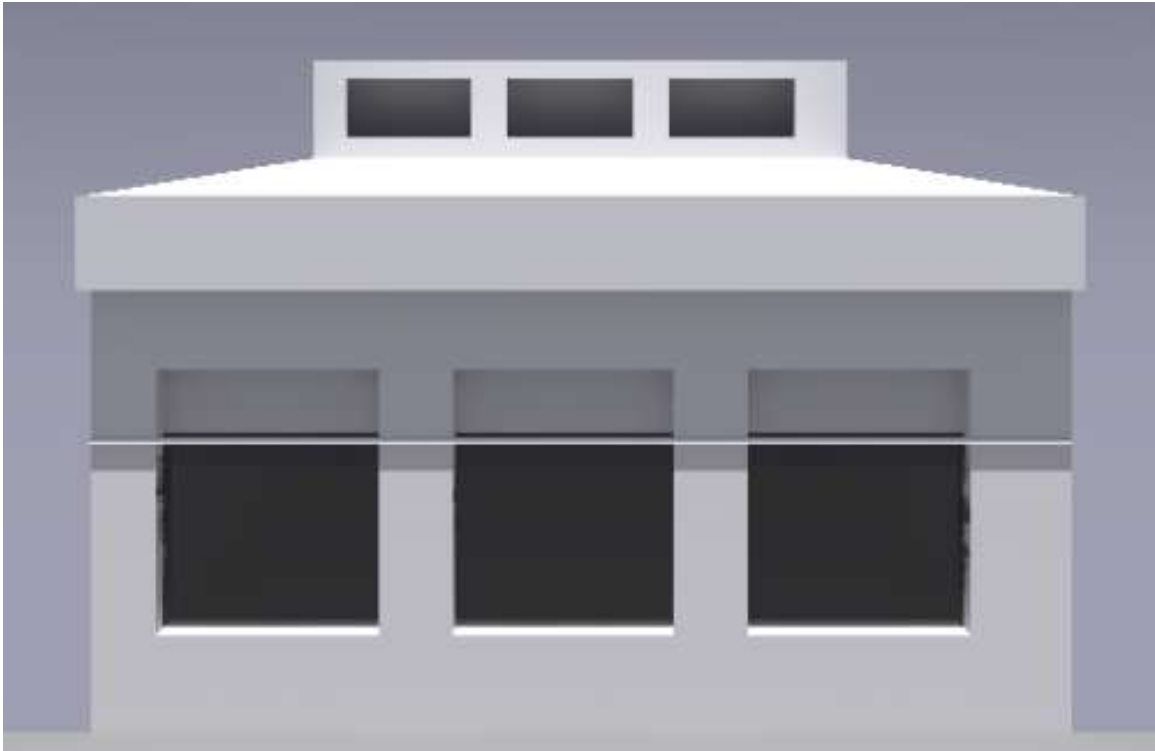
Figure 4.7: Dispersion of design parameters values of optimal solutions found by each algorithm. (a) Simplex Algorithm of Nelder and Mead with the Extension of O'Neill; (b) Hooke Jeeves; (c) Particle Swarm using Inertia Weight; and (d) hybrid PSO Constriction/Hooke Jeeves.

It is evident that the best solutions have a large translucent daylight window with a light transmittance value of 0.3. This low of a value of light transmittance for an upper daylighting window is usually not considered good practice; however, in this design it creates a large, but not too bright, light source. Because the daylight window faces south, large amounts of direct sunlight are mitigated and delivered in a diffuse manner to calculation points throughout the space, which all have a large view of this high window.

While other designs appear to be maximizing the daylighting delivered through the daylight window to the entire room, Figure 4.8 shows a very different design solution found by one of the runs of SA with a  $P_i$  of 70.4%. This design appears to focus on providing the appropriate amount of light to the back of the room, by increased CWA and CWLT, while sacrificing appropriate daylighting at the front of the room. A short exterior shading device will result in uncontrolled direct sunlight in winter months near the view window. However, with only a 2.6% lower  $P_i$  than the best overall found solution, the reduced ceiling height of this design solution may have a relatively low construction cost, and therefore be a more desirable solution to the design team.



(a)



(b)

Figure 4.8: Solution found by SA with a lesser  $P_i$  value (70.4%), lower ceiling height, and different ceiling shape, as compared to best performing solutions. Section perspective (a), exterior elevation (b).

In conclusion, the nature that each algorithm demonstrated at solving this complex daylighting problem reveals that PSOIW and PSOC/HJ can be relied on to consistently find solutions likely close to the absolute best solution. SA and HJ can find lower, albeit slightly, performing solutions more economically, but with less consistency of found solutions. Nonetheless, the variety of solutions found by SA and HJ may be of interest to a design team, who may be willing to sacrifice some amount of performance for other design criteria, such as construction cost or aesthetics. Likewise, design solutions found by PSOIW and PSOC/HJ on their way to converging can be explored for such tradeoffs. Analyzing found solutions' design parameter values can lead to insights such as the interaction between clerestory window area and clerestory window light transmittance.

#### 4.3.2. Analysis of Thermal Performance

Thus far, this work has focused on optimizing building design for daylighting performance without regard for how thermal loads, sensitive to envelope design, are affected. Because of this, the overall energy performance of found solutions is unknown. And it is not known if the benefits of daylighting optimization are negated by large heating and cooling loads stemming from solar gains and conducted losses through windows. While the method presented in this paper is intended to be part of an overall integrated method that includes evaluation of thermal loads, an examination of the thermal performance of the daylighting optimal designs found here is warranted.

#### 4.3.3. Description of Thermal Models

The analysis of thermal performance consisted of three parts. In the first part, the annual thermal and lighting performance of a reference classroom building energy model

is analyzed for the purpose of establishing a benchmark performance value and standard settings of key energy model parameters. Heating and cooling loads were defined as the annual sum of hourly thermal energy needed to be added or removed from the room air mass to maintain a thermostat set point for temperature and humidity. For all analyzed models, heating loads, cooling loads, and lighting energy were normalized to kW h/m<sup>2</sup>. In the second part, these key parameters are used in an optimization process of an energy model of the daylit classroom design presented above. The classroom design was optimized for thermal performance without regard for daylighting, serving as a reference for understanding how a design might be traditionally optimized. In the third part, the best daylighting design of the classroom found by the PSOIW algorithm is optimized for thermal performance. Its optimized parameters include the solar heat gain coefficients of the daylight, view, and clerestory windows for thermal performance. Solar heat gain coefficients were constrained to values realistic for the daylighting optimized light transmittance of each window group. In this energy model, the benefit of daylight to reduce electric lighting energy was taken into account. All energy models were simulated on an annual hourly basis using TMY3 weather data of Charlotte, NC [45].

EnergyPlus 8.1.0 was used to model energy performance. Of principal interest was knowing how the building envelope design affected annual heating and cooling loads placed on HVAC systems and annual lighting energy use. Analyzing thermal loads simplified the energy simulations and allowed for focused analysis on the building envelope. The goal was to identify the building envelope design that minimized the annual energy use of any HVAC system design for the building. EnergyPlus's "Ideal Loads Air System" HVAC object accommodates such an analysis as it "...can be thought

of as an ideal unit that mixes air at the zone exhaust condition with the specified amount of outdoor air and then adds or removes heat and moisture at 100% efficiency in order to produce a supply air stream at the specified conditions” [67]. In addition, the sensible and latent heating and cooling loads can be reported easily.

The first model analyzed was the Primary School in ASHRAE climate zone 3A from the U.S. Department of Energy Commercial Reference Building Models of the National Building Stock [68]. This set of reference buildings was developed to “assess new technologies; optimize designs; analyze advanced controls; develop energy codes and standards; and to conduct lighting, daylighting, ventilation, and indoor air quality studies.” The models are based on “reasonably realistic building characteristics and construction practices.” Since this model was a realistic reference of actual building use and energy performance, its key parameters (envelope constructions, lighting power density, equipment power density, occupant density, thermostat set points, and associated schedules) were also used in the two thermal optimization models of the classroom design, described below. Key parameters common to all three energy models analyzed are listed in Table 4.3. Parameters specific to the reference model are listed in Table 4.4. For the purpose of this study, which focused on the design of a single classroom, the south facing classroom zone of the reference model, most similar to the classroom design being optimized, was isolated and given an Ideal Loads Air System. Interior walls of the classroom that interfaced other thermal zones in the complete model were made adiabatic surfaces.

Table 4.3: Energy model parameters common to all energy models.

Parameter Description	Value
Lighting Power Density (LPD)	15.06 W/m <sup>2</sup>
Equipment Power Density (EPD)	15.00 W/m <sup>2</sup>
Exterior Wall U-Value	0.79 W/m <sup>2</sup> -K
Floor U-Value	3.40 W/m <sup>2</sup> -K
Ceiling U-Value	0.38 W/m <sup>2</sup> -K
Window U-Value	3.24 W/m <sup>2</sup> -K
Occupancy Density	4 m <sup>2</sup> /person
Sep – Jun Occupancy Rates	8:00 AM – 5:00 PM: 75%; 5:00 PM – 9:00 PM: 15%
Jul – Aug Occupancy Rates	8:00 AM – 9:00 PM: 15%
Infiltration Rate	0.39 ACH

Table 4.4: Energy model parameters of reference classroom model.

Parameter Description	Value
South Window SHGC	0.25
Window to Wall Area Ratio	0.35

The second model analyzed for optimal thermal performance was the classroom design presented in Section 4.1 and 4.2, but instead of investigating light transmittance of daylight, view, and clerestory windows, solar heat gain coefficients (SHGC) of the window groups was investigated. All other optimized envelope variables were optimized within their ranges outlined above. SHGCs were allowed to range from 0.15 to 0.6. Twelve optimization runs using the PSOIW algorithm were conducted. PSOIW was chosen because it was found to most consistently find near-optimal solutions for the daylighting optimization runs. The annual sum of heating loads, cooling loads, and lighting energy in kW h/m<sup>2</sup> was minimized. The east, west, and north walls of the classroom were made adiabatic, as they would interface other thermal zones with similar

thermostat set points in a complete school building. Parameters specific to the reference model are listed in Table 4.5.

Table 4.5: Energy model parameters of design optimized for thermal performance without regard for daylighting performance.

Parameter Description	Value
CH (height of ceiling above floor)*	3.35 m
CWA (width of clerestory windows)*	1.52 m
ESL*	1.22 m
Daylight Window SHGC*	0.16
View Window SHGC*	0.16
Clerestory Window SHGC*	0.16
Window to Wall Area Ratio	0.38

\* Optimized parameter

The third model analyzed was the best overall daylighting solution found by PSOIW, described in Section 4.3.1 and show in Figure 4.5. All parameters optimized for daylighting were left unchanged. The SHGCs of the daylight, view, and clerestory windows were optimized for thermal performance. Commercially available 1” insulated glazing units (IGU) were surveyed to identify realistic minimum SHGCs to associate with the LT of each glass group. The minimum SHGC values identified were, for the daylighting windows (LT 0.3), 0.2; for the view windows (LT 0.35), 0.2; and for the clerestory windows (LT 0.7), 0.35. SHGCs were allowed to be no greater than the LT of their window group. The reduction of hourly lighting energy made possible by daylight illuminance was accounted for in the following way. Hourly average workplane daylight illuminance values in three zones were calculated and used to create a fractional (0 to 1) hourly lighting schedule. The lighting schedule was used in the energy model to scale hourly lighting power (LP) values to levels appropriate to supplement daylight

illuminance, effectively modeling a continuously dimming daylighting control system. The classroom was divided into three lighting zone rows of equal size running parallel to the lower daylighting wall. In each zone and for each hour, if the average daylight illuminance was greater than 450 lx (90% of the 500 lx target illuminance), its fractional LP value was set to 0.1 (assuming a continuous dimming system with a minimum output of 10%). For values below 450 lx, the fractional LP value was set to the quotient of the average daylight illuminance and 500 lx. For each hour of the year, the fractional LP values of each zone were averaged to arrive at a grand average of fractional LP for the entire classroom. These hourly values were modified by the building occupancy schedule (lights were assumed to be fully off when unoccupied) and used as a continuous dimming lighting schedule for the EnergyPlus model. As with the second model, twelve optimization runs using the PSOIW algorithm were conducted to minimize the annual sum of heating loads, cooling loads, and lighting energy, and the east, west, and north walls of the classroom were made adiabatic. Parameters specific to the reference model are listed in Table 4.6.

Table 4.6: Energy model parameters of design optimized for thermal performance that was based on the daylighting optimal design.

Parameter Description	Value
CH (height of ceiling above floor)	3.23 m
CWA (width of clerestory windows)	2.17 m
ESL	1.21 m
Daylight Window SHGC*	0.20
View Window SHGC*	0.21
Clerestory Window SHGC*	0.35
Window to Wall Area Ratio	0.35

\* Optimized parameter

#### 4.3.4. Summary of Thermal Analysis Results

Table 4.5 and Table 4.6 list the optimized envelope design parameters of the second and third models. Table 4.7 lists the annual energy performance of each model. Figure 4.9 illustrates the monthly heating loads, cooling loads, and lighting energy of the three analyzed models. For all models, the largest load was cooling, followed by lighting and heating. For all models, heating loads were significantly less than cooling loads and lighting energy. The noticeably small heating loads are due to internal gains from relatively high lighting and equipment power densities and winter solar gains from south-facing glass. The thermal optimal solution minimized cooling loads by minimizing SHGC values and maximizing the length of the exterior shade. Even though its ceiling height, exterior shade, and window areas were optimized for daylighting without regard for thermal impacts, the third model of the daylighting optimal solution had annual loads 40%, and 33% lower than the reference and thermal optimal models, respectively. In this case, the benefit of daylight to reduce electric lighting use, and associated internal heat gain, significantly reduced the two largest energy loads of cooling and lighting, without causing excessive solar gains during the summer or thermal losses during the winter. The presented method of daylighting optimization has a steep penalty for over-illumination by daylight (Figure 4.1), which likely guards against excessive solar gains and is evident in the best design's low LT values of the view and daylight windows (allowing for lower SHGC values) and its relatively long exterior shading device. It is important to note that, without the benefit of reduced lighting energy from daylighting, the daylighting optimal design had a poor annual performance of 145.8 kW h/m<sup>2</sup>. This underscores the importance of properly working lighting control to achieve the energy reduction potential

of a daylighting optimal design. It should be stated that the thermal performance of a design optimized for daylighting performance will likely vary by building orientation, and, as done here, a design optimized for daylighting performance should always be critically evaluated for overall energy performance.

Table 4.7: Annual energy performance of energy models.

Model	Sum of annual heating, cooling, and lighting loads (kW h/m <sup>2</sup> )
Reference classroom	154.7
Thermally optimized classroom	137.3
Daylighting optimized classroom	92.4

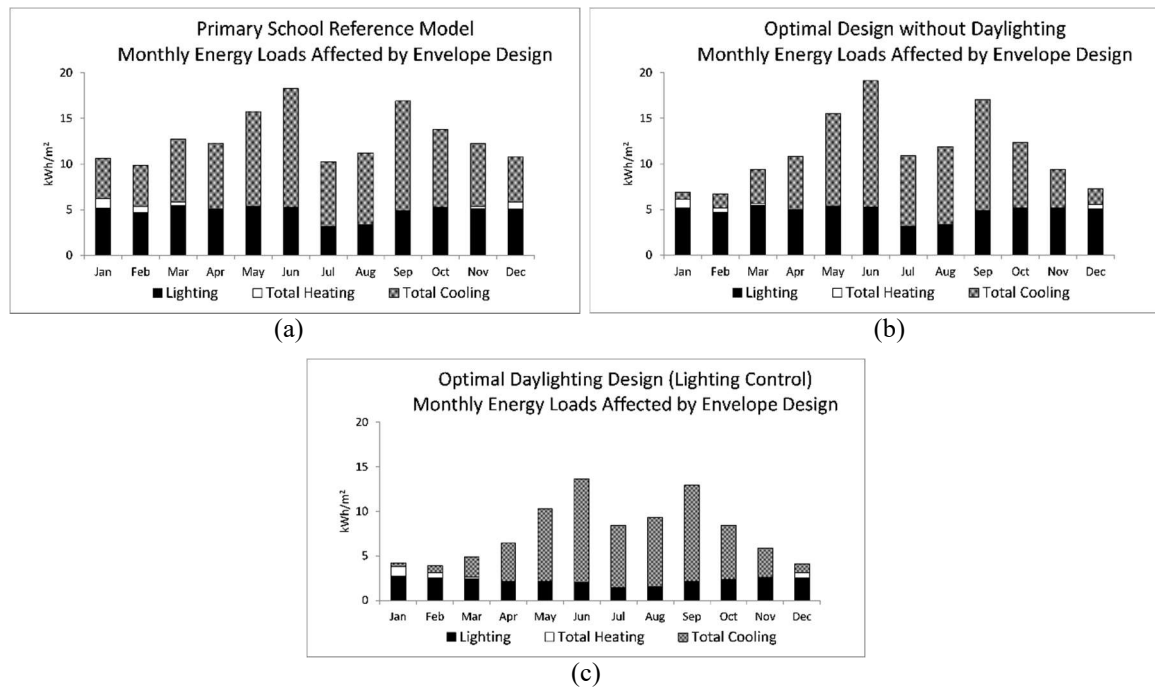


Figure 4.9: Monthly energy performance; reference classroom (a), classroom optimized for thermal performance without regard for daylighting (b), and thermal optimization of best daylighting design (c).

#### 4.3.5. Discussion and Conclusions

A new methodology to optimize building design for daylighting performance that uses state-of-the-art dynamic climate-based lighting simulations was presented. Four optimization algorithms were evaluated for their performance at finding an optimally performing solution. The four algorithms were Simplex Algorithm of Nelder and Mead with the Extension of O'Neill (SA), Hooke Jeeves (HJ), Particle Swarm Optimization using Inertia Weight (PSOIW), and a hybrid PSO Constriction/Hooke Jeeves (PSOC/HJ) algorithm. Each algorithm was run twelve times and in each case was able to improve daylighting performance above a randomly chosen base design. The SA algorithm produced inconsistent results and reached convergence in the fewest number of simulations (from 61 to 155), typically. The HJ algorithm reached convergence in fewer simulations (from 97 to 233) than PSOIW and PSOC/HJ, typically, but also produced inconsistent results. Compared to SA and HJ, The PSOC/HJ hybrid algorithm produced more consistent solutions closer to the overall best solution found, but with more simulations (from 172 to 255) required. The PSOIW found the best overall design solution and produced the most consistent design solutions. PSOIW required the greatest number of simulations and did not reach convergence before reaching the maximum number of simulations specified (500). In addition, the SHGCs of the best daylighting design's window groups were optimized for thermal performance. This design had an annual energy performance (the sum of hourly heating loads, cooling loads, and lighting energy) 40% lower than the DOE reference classroom model and 33% lower than the classroom design that was optimized for thermal performance without regard for daylighting. The steep penalty for over-illumination by daylight applied in this method

likely guards against excessive solar gains. It is suggested that, when time allows, the PSOIW algorithm is the preferred algorithm for this and similar optimization problems; any increase in search time is worth the certainty of the quality of the design solutions found. When analysis time is constrained, PSOC/HJ will likely find a solution close to the absolute best in a reasonable amount of time. When only a good solution, or a variety of good solutions, is/are desired, multiple runs of SA may be appropriate.

The use of optimization algorithms in complex daylighting design problems allows building design decision makers to identify high-performing designs that would have otherwise been unidentified. In addition, the results of an optimization run can be analyzed to identify a collection of near-optimal solutions, which likely have different design attributes that the design team may consider.

The optimization method presented was used to solve a design problem with only vertical daylighting apertures; however, it is expected to be relevant to optimizing all types of building apertures, including horizontal ones, because it operates on the design factors that impact transmitted light from the sky vault, the sun disk, and that which is reflected off of exterior surfaces. Therefore, the presented method and conclusions about the performance of algorithms are expected to also apply to designs with horizontal skylights.

## CHAPTER 5: BI-OBJECTIVE OPTIMIZATION OF DAYLIGHTING AND THERMAL PERFORMANCE

In this chapter, a challenging problem is addressed: optimizing early building design for daylighting and thermal performance with the objectives of passively satisfying occupant thermal and luminous needs, to the greatest degree possible, therefore minimizing energy demand for heating, cooling, and lighting. A bi-objective optimization method using GenOpt and its implementation of a Hooke Jeeves and Particle Swarm Optimization algorithm is demonstrated that investigates how building enclosure design influences the above objectives. Thermal performance was evaluated by how heat transfer across enclosure elements impacts hourly heating and cooling loads. Lighting performance was evaluated based on the frequency and magnitude at which daylight levels, during occupied hours, deviate from a desired target illuminance range. A single-zone classroom design in Charlotte, NC was optimized for north, south, east, and west orientations. For each orientation, a Pareto front was approximated to help evaluate trade-offs between thermal and daylighting objectives. Results show that for the south, east, and west orientations, thermal and daylighting objectives are not in strong conflict, however, for the north orientation there is a more marked conflict between these objectives.

In Charlotte's South Atlantic region, where this investigation was conducted, heating, cooling, and lighting represent the three largest end uses of energy in commercial and institutional buildings, 23.4%, 12.4%, and 24.2%, respectively [2].

Optimizing the building enclosure to minimize one of these quantities will likely have a negative influence on at least one of the others. This conflict between thermal and lighting objectives is largely because the windows that provide daylight to a space are also the weakest thermal barrier between the inside and outside environments and have a significant impact on heating and cooling loads. Optimum thermal and daylighting design varies based on climate and geographic location, orientation, and surrounding exterior context. These considerations make optimizing for thermal and daylighting performance a unique problem for every building designed. The purpose of this study is to demonstrate a method of optimizing building enclosure design such that annual thermal and lighting energy is minimized while providing a high-quality lighting environment for occupants.

Presented is a simulation-based optimization method to solve this problem, integrated with GenOpt and its implementation of a hybrid Generalized Pattern Search implementing Hooke Jeeves and Particle Swarm Optimization algorithms [58]. An application of the proposed methodology is demonstrated that optimizes a grade school classroom prototype design (Figure 5.1). Key prototype design parameters are optimized to minimize the frequency and magnitude of hourly daylight levels, during occupied times, outside a desired illuminance range. Design parameters are also optimized to minimize the annual sum of hourly heating, cooling, and lighting energy. Heating and cooling loads are defined as the thermal energy necessary to add to or extract from the room air to maintain the thermostat set point temperature.

Daylighting performance was accounted for by simulating daylight illuminance at calculation points evenly distributed throughout the room on a 0.91 m by 0.91 m grid. This was done for every occupied hour of the year. The daylighting performance score of a particular design solution was based on that solution's population of occupied hourly illuminance values. Each illuminance value was given a score between 0 and 1 that diminished proportionally with its distance from a narrow target range. Thus, an ideally daylit room would have all occupied hourly illuminance values given a score of 1. To calculate the overall daylighting performance score of a particular design, its illuminance value scores were summed and then divided by the sum of illuminance values scores if it had achieved ideal performance (all hourly illuminance values scores equal to 1). This resulted in a value between 0 and 1 that represented how close the design was to ideal performance. The calculation of daylighting performance is described in detail in Chapter 4.

Thermal performance was accounted for by performing annual energy simulations of design solutions. Thermal performance was defined as the sum of annual hourly energy consumption affected by envelope design, namely heating system energy, cooling system energy, and lighting energy. Annual hourly energy for each of these was summed and used as a measure of the thermal performance of a design. To account for the benefit of using outdoor air to cool a zone, when in cooling mode and the outdoor air temperature is below that of the zone's return air, an economizer cycle was modeled.

## 5.1. Methodology

### 5.1.1. Optimization Problem Formulation

The objective of this optimization problem is to maximize daylighting and thermal performance of a building across various scenarios. Before defining the specific objective function in consideration, thermal performance and daylight illuminance, along with related terms, are defined.

The evaluation of daylighting performance in this chapter is based on the formulation of daylighting performance described in Chapter 4. In this chapter, the  $n$  parameter of Eq. (4.2) is considered in detail. The  $n$  parameter controls the number of sampling rays used in the daylighting simulation and is a critical parameter for calculating daylight illuminance at a point. Therefore, it was studied, along with other key parameters, below in a sensitivity analysis that determined parameter values that balanced simulation time and accuracy of results.

For thermal performance, a heating or cooling load is defined as the amount of heat needed to be added to or removed from the room air mass to maintain the room air mass temperature at the thermostat set point temperature. Heat is transferred from the room air mass by heat exchange across the building envelope. These exchanges include conduction through all envelope elements, shortwave (solar) and longwave (infrared) radiation between the external environment and building interior through windows, and infiltration and exfiltration of air through cracks and gaps in the building envelope. Ultimately, heat is transferred to and from room air by convection with interior surfaces, which are warmed or cooled by conducted and/or radiated heat. Because of their transient nature caused by dynamic weather conditions and thermal capacitance of materials, a full

description of how these heat transfer processes are modeled, is not possible here.

However, the thermal load of a room can be generalized and expressed as:

$$q_{sys} = q_{ce} + q_{iv} + q_{conv}$$

where

$$q_{sys} = \text{heat transfer to air needed to maintain thermostat setpoint temperature}$$

$$q_{ce} = \text{convective part of people, lights, and equipment}$$

$$q_{iv} = \text{load due to infiltration and ventilation air}$$

$$q_{conv} = \text{convected heat transfer from room surfaces}$$
(5.1)

In Eq. (5.1), the terms  $q_{ce}$ ,  $q_{iv}$ , and  $q_{conv}$  are determined each through non-linear differential equations which are omitted here to keep the presentation concise and focus on the optimization aspects. For more details the reader may refer to [69]. For thermal evaluation, the sum of annual hourly heating loads and annual hourly cooling loads, modified by a heating efficiency of 0.85 and cooling system coefficient of performance (COP) of 3, was used. These system efficiencies were chosen to keep the found optimal solutions general with respect to HVAC system type. For ease of comparison with other buildings, this sum was converted to kWh/m<sup>2</sup> of building floor area (denoted here as  $Q$ ).

Next, as in Chapter 4, the external factors ( $\Omega$ ) are elaborated. Without loss of generality, external factors were divided into two groups: design parameters or decision variables ( $\Omega_1$ ) and fixed parameters or inputs ( $\Omega_2$ ). Thus,  $\Omega = \Omega_1 \cup \Omega_2$ . Let  $\omega_1$  denote an individual decision variable such that  $\omega_1 \in \Omega_1$ . Typically, these decisions will need to be within allowed minimum and maximum specifications, which are denoted as  $\omega_{\min}$  and  $\omega_{\max}$ , respectively. Similarly, let  $\omega_2$  denote an individual fixed parameter or input such that  $\omega_2 \in \Omega_2$ .

For daylighting evaluation, illuminance was simulated at calculation points at workplane height ( $\sim 0.75$  m above the floor). Calculation points were uniformly distributed at workplane height on a  $0.91$  m x  $0.91$  m grid. This resulted in a 9 by 13 grid of calculation points in the optimized classroom described below (thus there are 9 values for  $x$  coordinates and 13 for  $y$  coordinates). Illuminance values were measured for every occupied hour of the year. An illuminance ( $E$ ) value was said to be within target if it was within a desired  $E_{\min}$  and  $E_{\max}$  representative of a comfortable luminous environment favorable for usual classroom activities, typically  $300\text{lx}$  and  $2500\text{lx}$  [49]. However, here, a narrower primary target range was used such that  $E_{\min} = 500\text{lx}$  and  $E_{\max} = 1000\text{lx}$ , which is different than daylighting metrics recently developed, or being developed, based on hourly climate specific measurements as described in detail in Chapter 4. Using 117 calculation points, this method was found to give a unique score to each design solution and, therefore, a more precise representation of daylighting performance.

The objective of the daylighting performance optimization was to find the design that maximized the sum of annual hourly daylighting scores of the calculation points. The objective of the thermal performance optimization was to minimize annual  $Q$ . These objectives, denoted  $P$  and  $Q$ , respectively, are captured in the formulation of the bi-objective optimization problem in Eq. (5.2).

$$\max_{\omega_1 \in \Omega_1} P = \sum_{o_{first}}^{o_{last}} \sum_{c_{first}}^{c_{last}} \begin{cases} 1 & \text{if } E_{\min} \leq E(\omega_1 | \omega_2) \leq E_{\max} \\ E(\omega_1 | \omega_2) / E_{\min} & \text{if } E(\omega_1 | \omega_2) < E_{\min} \\ E_{\max} / E(\omega_1 | \omega_2) & \text{if } E(\omega_1 | \omega_2) > E_{\max} \end{cases}$$

$$\min_{\omega_1 \in \Omega_1} Q = \sum_{h_{first}}^{h_{last}} \{ q_{sys} \} / m^2$$

where

$o$  = occupied hour

$c$  = illuminance calculation point

$h$  = hour of the year

subject to

$$\omega_{\min} \leq \omega_1 \leq \omega_{\max}$$

(5.2)

In this case, the following design parameters or decision variables ( $\Omega_1$ ) were selected:

$CH$	= Ceiling Height
$CW\_LT$	= Clerestory Window Light Transmittance
$CW\_ST$	= Clerestory Window Solar Transmittance
$CWW$	= Clerestory Window Width
$DW\_LT$	= Daylight Window Light Transmittance
$DW\_ST$	= Daylight Window Solar Transmittance
$ESL$	= Exterior Shade Length
$LL$	= Lightshelf Length
$VW\_LT$	= View Window Light Transmittance
$VW\_ST$	= View Window Solar Transmittance
$WW$	= Window Width

And the fixed parameters or inputs ( $\Omega_2$ ) included the following:

$x$  = x-coordinate of the illuminance calculation point

$y$  = y-coordinate of the illuminance calculation point

$m$  = month of year

$d$  = day of month (varies between 28 and 31 depending on month)

$h$  = hour of day (only occupied daylit hours used)

$\alpha$  = simulation parameters (including number of sampling rays)

$\beta$  = static model geometry and material properties

In subsequent descriptions of found solutions,  $P$  has been converted to  $P_i$  based on Eq. (4.5), which normalized daylighting performance on a scale of 0 to 1 with 1 being the best possible daylighting score.

#### 5.1.2. Building Design Problem Definition

The design of a classroom in Charlotte, NC, shown in Figure 5.1, was chosen as an optimization problem. Charlotte (35.2° N, 80.8° W) is located in ASHRAE Climate Zone 3A and is warm and humid with mild winters. Charlotte has 1327 heating degree days (15.5 °C base) and 1585 cooling degree days (15.5 °C base). The dimensions of the classroom were 8.1 m by 11.1 m. Windows were placed on one of the shorter side of the classroom. The orientation of the classroom, referenced in simulations runs described below, was such that the windows faced the stated orientation. The static parameters of the building enclosure design were based on constructions appropriate for a steel frame building in ASHRAE Climate Zone 3A, where Charlotte, NC is located. Table 5.1 gives the details of the thermally important materials used for the exterior walls, roof, and floor.

Table 5.1: Building enclosure materials.

Material (from outside to inside)	Thickness (m)
Floor	
Concrete	0.101
Carpet	0.005
Exterior Wall	
Sheathing	0.002
Insulation (0.045 W/m-K)	0.078
Gypsum Board	0.013
Roof	
Roof Membrane	0.009
Insulation (0.049 W/m-K)	0.211
Metal Decking	0.002

As discussed before, eleven design factors were selected for optimization: ceiling height (CH), clerestory window light transmittance (CW\_LT), clerestory window solar transmittance (CW\_ST), clerestory window width (CWW), daylight window light transmittance (DW\_LT), daylight window solar transmittance (DW\_ST), exterior shade length (ESL), lightshelf length (LL), view window light transmittance (VW\_LT), view window solar transmittance (VW\_ST), window width (WW).

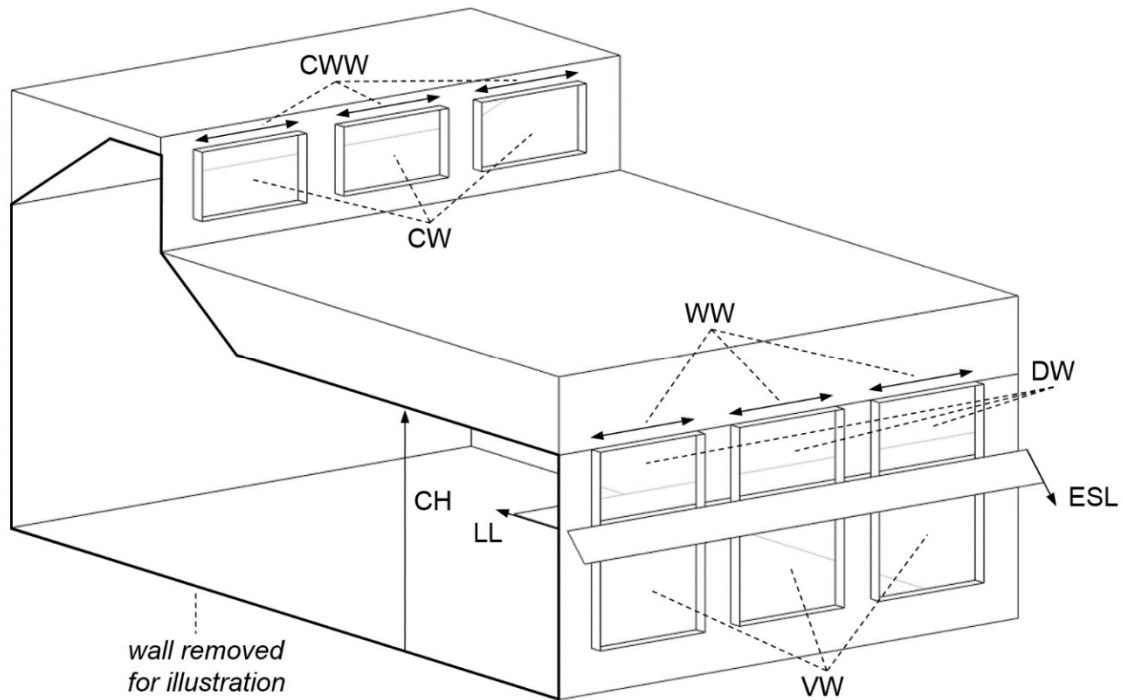


Figure 5.1: Building design factors optimized

CH was varied by increasing the height of the ceiling. The top of the daylight window (the upper glass of the side window) moved with the CH. The bottom of the daylight window and the top of the view window always met at two-thirds the distance from the bottom of the view window to the top of the daylighting window (this is good daylighting design practice). Likewise, the lightshelf and top edge of the exterior shade remained at the meeting of the daylight window and view window. CWW was increased or decreased by uniformly varying the width of the three clerestory windows from their centers. The clerestory windows' centers remained fixed. The exterior shade length increased and decreased along its 45 degree angle from the exterior wall. Lightshelf length increased and decreased perpendicularly from the exterior wall. WW was increased or decreased by uniformly varying the width of the three daylight and view

window pairs from their centers. The pairs' centers remained fixed. Table 5.2 shows the minimum and maximum settings of the investigated design factors.

Table 5.2: Minimum and maximum settings of the investigated design factors.

Design Factor	Minimum -Maximum
CH (height of ceiling above floor)	2.4 m – 3.7 m
CW_LT	0.3 – 0.8
CW_ST	0.1 – 0.7
CWW	0.9 m – 2.4 m
DW_LT	0.3 – 0.8
DW_ST	0.1 – 0.7
ESL	0 m – 1.2 m
LL	0' – 1.1m
VW_LT	0.3 – 0.8
VW_ST	0.1 – 0.7
WW	0.9 m – 2.4 m

Some of the reasons for choosing these design parameters include:

- 1) Window sizes have a large impact on solar gains and conducted gains and losses.
- 2) ST values have a great impact on solar gains.
- 3) ESL can aid in control of solar gains while allowing for greater LTs of glass and thus more daylight admission.
- 4) CH allows for a larger daylight window, thus admitting more daylight into the room. Also, the light admitted from the daylight window is delivered deeper into the room where it is usually more needed.
- 5) VW\_LT controls the daylight delivered to calculation points close to the view window.
- 6) CW\_LT controls the daylight delivered to the back of the room.
- 7) DW\_LT controls daylight delivered deeper into the room from the main daylighting wall.
- 8) CWW and WW control the mount of light admitted through their respective windows and thus the locations to which those windows deliver light.

In short, these parameters independently affect the distribution of daylight throughout the space while having a large impact on solar gains and conducted gains and losses. Changing a parameter in one direction to improve either daylighting or thermal performance will usually result in a trade-off with the other objective, making the search for parameter value combinations that optimize both lighting and thermal performance an interesting optimization problem.

Table 5.3 lists key static parameters of the classroom design used in the energy model. These values are based on ASHRAE 90.1 2010 standards [28] and the Department of Energy's commercial reference buildings [70].

Table 5.3: Key parameters used in energy model of classroom.

Energy Model Parameter	Value
Wall U-value (W/m <sup>2</sup> -K)	0.43 W/m <sup>2</sup> -K
Floor U-value	2.193 W/m <sup>2</sup> -K
Roof U-value	0.223 W/m <sup>2</sup> -K
Window (all) U-value	2.672 W/m <sup>2</sup> -K
Cooling Thermostat Set Point	25 °C
Heating Thermostat Set Point	21 °C
Lighting Power Density	10.76 W/m <sup>2</sup>
Equipment Power Density	5.38 W/m <sup>2</sup>
Ventilation Rate	0.08 m <sup>3</sup> /s - person
Infiltration Rate	0.19 air changes/h
Occupancy Density	0.25 people/m <sup>2</sup> m
Occupancy Schedule Week Days Sep-May	0.25 people/m <sup>2</sup> m
Occupancy Schedule Weekends Sep-May	Unoccupied
Occupancy Schedule Jun-Jul	Unoccupied

For the daylighting model, basic daylighting principles were followed for the assignment of light reflectance values to surfaces with 80%, 60%, and 30% assigned to the ceiling, walls, and floor, respectively.

### 5.1.3. Optimization Algorithm

The optimization problem in Eq. (5.2) is relatively complex due to the physical relationship described in Eq. (4.2 & 5.1). If-then statements make the problem discontinuous, as well. The if-then statements in the objective function can be replaced by binary decisions (thus yielding a mixed integer non-linear optimization problem) but this does not simplify the problem either, due to the complexity of the illuminance function.

GenOpt can interface with any simulation program that reads and writes text files for input and output. GenOpt includes several direct/pattern search and meta-heuristic optimization algorithms that do not require computation of directional derivatives. Because of the characteristics of Eq. (5.2), GenOpt was chosen as the optimization “controller” to execute daylighting and thermal simulations, read daylighting and thermal performance scores, and search the design space for optimal solutions. Here, GenOpt’s hybrid meta-heuristic (Particle Swarm Optimization using a constriction coefficient) and pattern search (Hooke Jeeves) algorithm, referred to as PSOC/HJ, is used. In Chapter 4, this algorithm was found to give good results with relatively few simulations.

The PSO algorithm is a population based algorithm that was developed out of evolutionary computational theory and social behavior theory [64-66]. It is more fully described in Chapter 4. Here, several parameters (NP, NS, SA, CA, and CG) are highlighted again because they were investigated in the sensitivity analysis below. The number of particles composing the swarm is controlled by the NP parameter. Each particle remembers the position of the best performing solution it has visited (personal best) and that of the best solution found by its neighbors (neighborhood best).

Neighboring particles are determined by the neighborhood topology parameter and the NS parameter, which determines the number of particles in a neighborhood. The velocity of every particle is controlled by its current position relative to the positions of its personal best and neighborhood best solutions such that it accelerates toward both potentially optimal positions. During each iteration, a particle's magnitude of acceleration in the direction of its current neighborhood best solution is made proportional to its distance from the neighborhood best solution, a constant parameter value known as SA, and a random scalar between 0 and 1 that is dynamically generated. The same is true of a particle's magnitude of acceleration in the direction of its personal best solution, CA. In addition to these coefficients of acceleration, a constriction coefficient is used to limit the velocity of particles so that they more efficiently converge to an optimum point. When the constriction coefficient is large, it aids global search of the design space by allowing high acceleration of particles. When it is small, it aids local searching and convergence by slowing down the movement of particles. During each iteration, this constriction method scales the acceleration of a particle in each direction by a scalar controlled by the CG parameter. A scalar less than one is then applied to the overall velocity of the particle. These operations constrain the overall velocity of a particle. This is important because unconstrained velocity of particles has been demonstrated to be problematic; particles tend to accelerate back and forth about optimal solutions and convergence is not reached.

#### 5.1.4. Lighting Simulations

There are several simulation packages (i.e., ray-tracing programs) available for computing the illuminance function [55-57]. One of these packages, RADIANCE [57], is

utilized here in conjunction with EnergyPlus [71], to calculate thermal performance, and GenOpt, to control the optimization procedure.

Hourly illuminance values were simulated using the daylight coefficient method [54] and its associated programs available in the ray-tracing software RADIANCE, along with hourly climate data for Charlotte [45]. The RADIANCE programs used were *epw2wea* (which converted the EPW weather file to the WEA format), *gendaymtx* (which took the WEA formatted weather file and output hourly sky luminance models), *rcontrib* (which took the classroom model and calculation points as input and output daylight coefficients for each calculation point), and *dctimestep* (which took daylight coefficient values of calculation points and hourly sky models as input and output hourly illuminance values of calculation points). For daylight coefficient calculations using *rcontrib*, the sky was divided into 578 patches. Key ray-tracing parameters are discussed below in the Section 5.1.4. BASH and GNU Octave scripts were written to calculate the *Pi* scores from the hourly illuminance values output by the RADIANCE programs. In addition, these scripts calculated hourly lighting schedules for the EnergyPlus simulations that accounted for the offsetting of electric lighting power made possible by daylight illuminance. Lighting schedules were produced for three lighting zones running parallel to the main daylighting wall and which divided the room equally into thirds. For each hour and for each zone, a scalar between 0.1 and 1 was produced that scaled the lighting power density to a level that complemented the amount of daylight present in the zone. By doing this, the energy models accounted for the reduction in electricity consumption from daylighting, and also the associated reduction in internal heat gain from lighting.

Hourly lighting schedule scalar values were calculated according to Eq. (5.3), which is based on a target illuminance of 500 lx.

$$L = \begin{cases} 0.1 & \text{if } \bar{E} \geq 450 \\ 1 - (\bar{E}/500) & \text{if } \bar{E} < 450 \end{cases} \quad (5.3)$$

where

$L$  = lighting power scalar value for current hour

$\bar{E}$  = average zone illuminance for current hour

### 5.1.5. Thermal Simulations

EnergyPlus was used to perform the annual thermal simulations. Basic parameters of the energy model are given in Section 5.1.5. The energy model was simulated using the same EPW weather file of Charlotte, NC used to generate the hourly sky luminance models for the calculation of daylight illuminance. EnergyPlus's Ideal Loads Air System object was used to calculate heating and cooling loads, which were scaled according to a generic heating system efficiency of 0.85 and a cooling system COP of 3. To account for the benefit of using outdoor air to cool a zone, when in cooling mode and the outdoor air temperature is below that of the zone's return air, an economizer cycle was modeled. This required a sizing run to be performed, before the annual energy simulation, to size the maximum air flow rate of the system when cooling. For each building design solution, the process of performing this sizing run and subsequent annual simulation was automated through BASH scripts.

To keep glass properties within realistic ranges, ST values were not allowed to be less than ½ of LT values. This constraint was implemented in GenOpt as a dynamic penalty function, which is described in detail in the GenOpt manual [58]. Design

solutions were penalized based on the magnitude by which they violated this constraint. The penalty increases with the number of simulations performed. This allowed for exploration of regions of the design space that violated the constraint but ensures that non-violating solutions are eventually converged upon.

#### 5.1.6. Determination of Pareto Fronts

A Pareto front allows one to understand the trade-offs between conflicting objectives of design solutions that are said to be “Pareto efficient” [72]. In the context of a bi-objective problem, Pareto efficient means that neither objective can be improved without worsening the other. Such solutions are called non-dominated. Because of this property, a population of Pareto efficient solutions will tend to form a Pareto front on a scatter plot whose axes represent the objectives. The front represents the farthest extent possible that design solutions can go in the directions of improving objective values. A Pareto front for the presented bi-objective problem allows decision makers to evaluate the trade-offs between daylighting performance and thermal performance and decide on a solution that best balances these conflicting objectives. Here, the Epsilon Constraint Method is used to determine the Pareto front of design solutions for the north, south, east, and west orientations of the classroom design [73]. The Epsilon Constraint Method finds points on the Pareto front by placing a constraint on one objective (determined a priori) and optimizing for the other objective. This creates a single objective problem and results in an optimized solution constrained in one objective dimension but fully optimized in the other. This process is repeated for multiple values of the constraint placed on the one objective until the Pareto front is approximated at a sufficiently good resolution. Thermal performance was chosen as the objective to be constrained in the Epsilon Constraint

Method. Different values for the constraint were automatically explored, through automated scripts, until a well-defined Pareto front was established.

#### 5.1.7. Sensitivity Analysis of Lighting Simulation and PSO Algorithm Parameters

Before optimization runs were performed, a sensitivity analysis was performed, by means of a Design of Experiment (DOE), on the lighting simulations and PSOC/HJ algorithm with the goal of determining appropriate parameter settings for each. A DOE is a method of performing experiments to understand the response of a system to multiple parameter conditions [74]. DOE is a tool by which one can understand why these changes happen, that is the relationship between change in a parameter(s) and change in the response(s). This is of interest because one can gain an understanding of how sensitive the response of a system is to specific parameter changes. Parameters with a strong influence on system response should be set to values that ensure good results, regardless of impact on simulation time. Parameters with little influence can be set to values that are economical with respect to simulation time. Here, full  $2^k$  factorial designs ( $k$  factors/parameters at 2 levels, low and high) were used to study how sensitive the lighting simulations and PSO algorithm runs were to key parameters, with the goal of determining appropriate parameter settings that balance accuracy and time. Key outputs of a DOE run are plots showing the main effects (how changing the value of one factor/parameter changes the response) and interaction effects (how changing the value of one factor/parameter changes the response with different settings of the other factors).

To better understand the effect of ray-tracing parameters on the calculation of illuminance values and daylighting performance  $P_i$  scores, key parameters of RADIANCE's *rcontrib* program were investigated, including ambient bounces (*ab*),

ambient divisions ( $ad$ ), and limit weight ( $lw$ ). Because *rcontrib*'s method of calculating illuminance values, based on daylight coefficients and described above, does not use ambient caching, these parameters are the key determinants of *rcontrib*'s behavior. A short description of *rcontrib*'s parameters follows. For a detailed description of *rcontrib* and its parameters, readers are referred to its manual [75].  $ab$  is the maximum number of diffuse bounces of light. It must be set to a number sufficiently large to account for the contribution of inter-reflected light to a point.  $ad$  is the number of ambient divisions and corresponds to the number of sampling rays,  $n$ , in Eq. (4.2). A large  $ad$  value will increase the probability of accurately sampling light entering a window as seen by a point.  $lw$  is known as the limit weight parameter. It requires the weight, or contribution, of each sampling ray to a point's illuminance to be at least its value. Sampling rays that are estimated to contribute less than  $lw$ 's value are dropped from the ray-tracing calculation. It is important to set  $ad$  and  $lw$  to aggressive values since ambient caching is not used and, therefore, interpolation of values between sample ray locations does not occur.

To verify the parameters initially used in this study, a  $2^3$  factorial design was created that used the initial parameter settings as the low factor levels and very aggressive parameter settings as high factor levels. These factor levels are given in Table 5.4. Daylighting simulations were performed on a south-facing classroom design with each design factor set to its center-point value. The  $P_i$  score was calculated and used as the response of the experiment. 10 replicates of this design were performed. The response values of replicates were averaged. As seen in Figure 5.2, the main effects of  $ab$  and  $ad$

are very small. While the main effect of  $lw$  is larger than those of  $ab$  and  $ad$ , it is still quite small (0.002  $Pi$ ).

Table 5.4: Factor levels for rcontrib sensitivity analysis.

Parameter/Factor	Low Setting	High Setting
$ab$	12	18
$ad$	$5 \times 10^4$	$1 \times 10^5$
$lw$	$2 \times 10^{-5}$	$1 \times 10^{-5}$

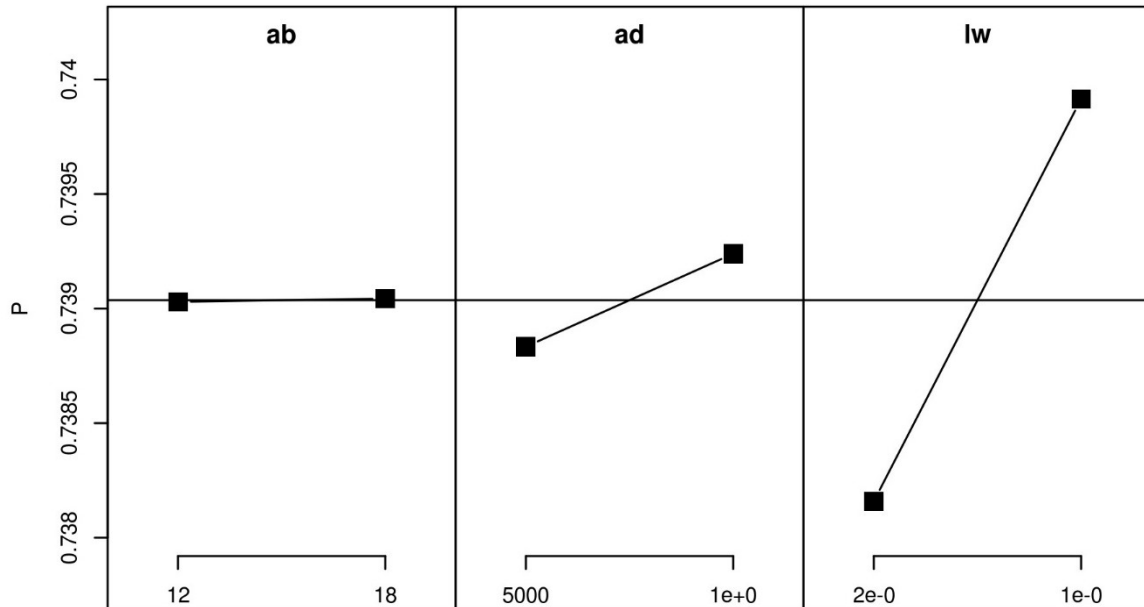


Figure 5.2: Main effects of rcontrib parameters

The interaction plot of this experiment (Figure 5.3) shows very little interaction between the parameters (factors have a similar effect regardless of the settings of the other factors). These results show that the initial parameter values for *rcontrib* produce very close  $Pi$  values to those of very aggressive parameters. The initial parameter values

were also associated with smaller simulation times. Therefore, the initial parameters were used in subsequent simulations.

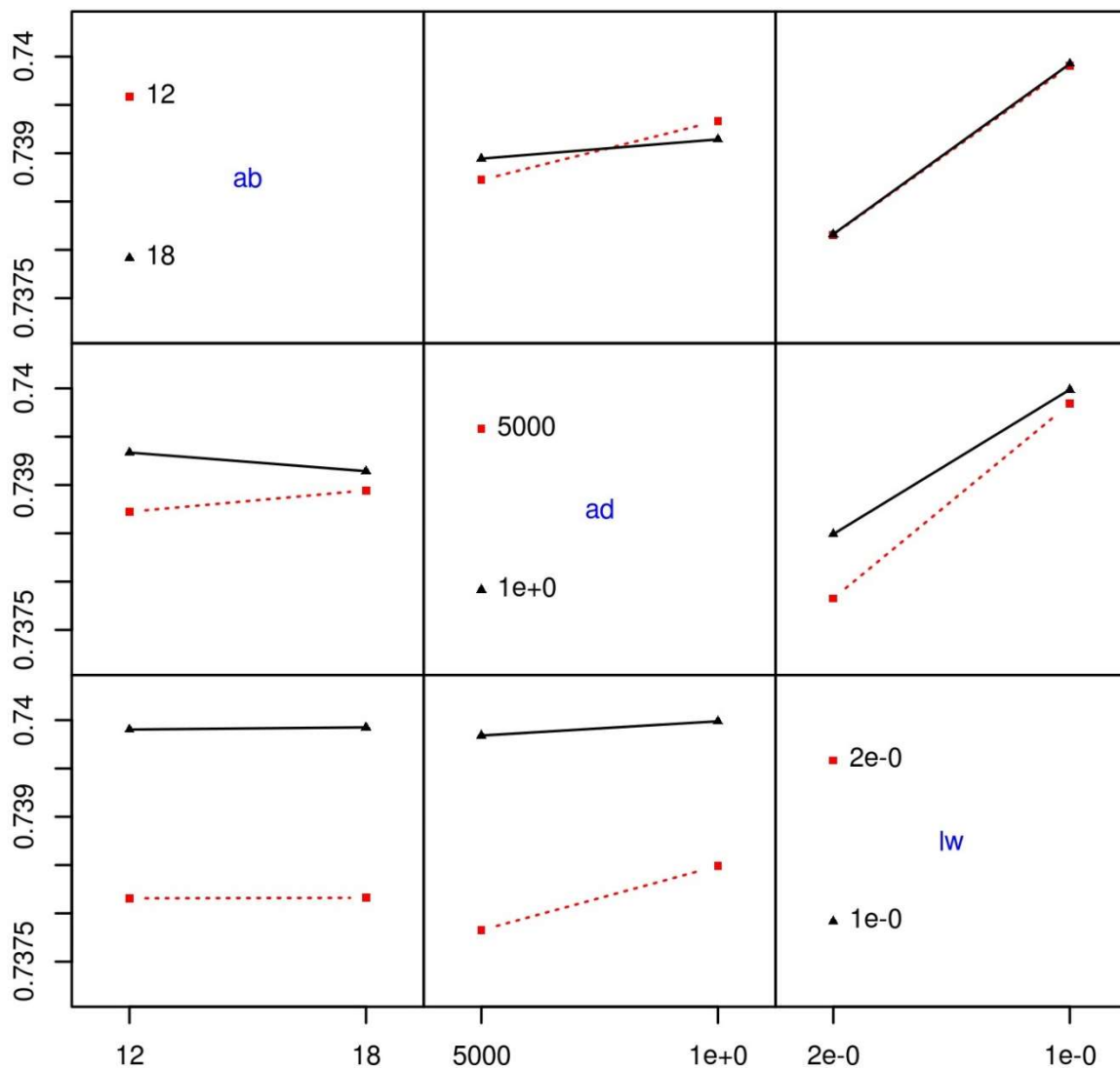


Figure 5.3: Interactions of rcontrib parameters

A sensitivity analysis of the PSOC algorithm parameters was performed since it is the main algorithm of GenOpt's PSOC/HJ hybrid algorithm. The goal of this sensitivity analysis was to identify PSOC parameters that reliably found near optimal solutions quickly so that the subsequent Hooke Jeeves algorithm run, which begins at the best solution found by PSOC, can search the region local to this solution for refinements. The PSOC algorithm parameter values were deemed to be more critical than those of the

Hooke Jeeves algorithm because when positioned at a near-optimal solution, the Hooke Jeeves algorithm will not have to search long to find a better solution, if it exists.

The chosen sensitivity analysis for PSOC algorithm parameters was a  $2^5$  factorial design, which was performed twice: once with the  $Pi$  score of the found solution as the response and once with the simulation time as the response factor. The parameters/factors chosen for investigation were NP, NS, SA, CA, and CG. These parameters are described in Section 5.1.3. Table 5.5 gives the factor levels for this sensitivity run.

Table 5.5: Factor levels for PSO sensitivity analysis

Parameter/Factor	Low Setting	High Setting
NP	10	20
NS	1/5 NP	1/2 NP
CA	1.3	2.8
SA	1.3	2.8
CG	0.5	1

Figures 5.4 and 5.5 shows that NP had a very strong effect on simulation time; NS, CA, SA, CG had much less of an effect time, and all parameters had relatively minor effects on the  $Pi$  value of the found solution. This experiment confirmed that the default setting for PSO in GenOpt balance well the quality of found results with simulation time. Therefore, the default settings, shown in Table 5.6 and Table 5.7, were used.

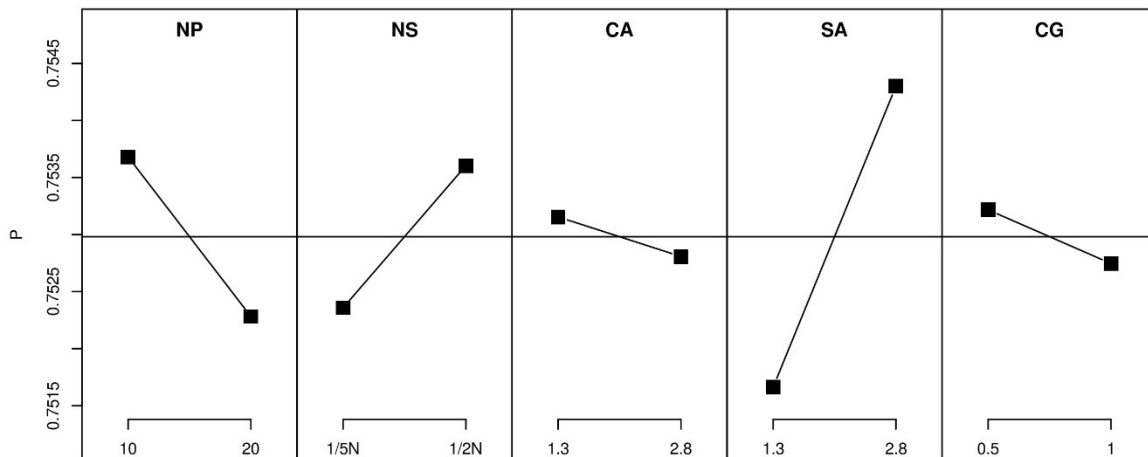


Figure 5.4: Main effects of PSO parameters on Pi scores

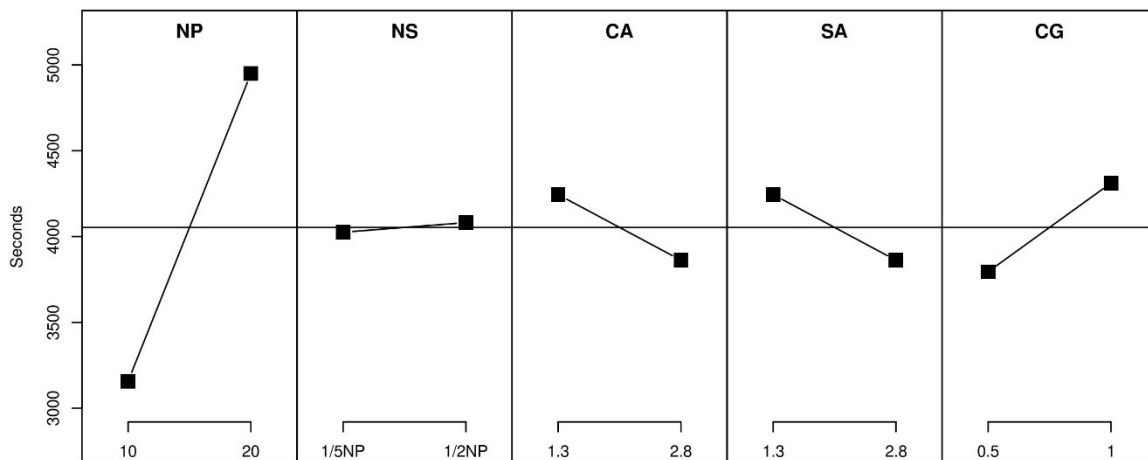


Figure 5.5: Main effects of PSO parameters on simulation time

Table 5.6: Parameters of the GPS Hooke Jeeves Algorithm

Parameter	Value
Mesh Size Divider	2
Initial Mesh Size Exponent	0
Mesh Size Exponent Increment	1
Number of Step Reductions	3

Table 5.7: Parameters of the Particle Swarm Optimization Algorithm

Parameter	Value
Neighborhood Topology	Von Neumann
Number of Particles	10
Number of Generations	10
Cognitive Acceleration	2.8
Social Acceleration	1.3
Maximum Velocity Gain	0.5
Constriction Gain	0.5
Mesh Size Divider	2
Initial Mesh Size Exponent	0

#### 5.1.8. Optimization Process

Figure 5.6 shows the sequence of operations and flow of data used to solve the optimization of the classroom model. GenOpt was used to control the optimization process. The optimization process was initiated by executing GenOpt, which accepted as input the parameters to be optimized ( $\omega_2$ ), along with their ranges and initial values. Secondly, GenOpt generated RADIANCE and EnergyPlus input files by replacing variables in template input files with the values of parameters for the initial run. Thirdly, GenOpt executed a BASH shell script that coordinated the execution of RADIANCE and EnergyPlus. RADIANCE was executed first and output hourly illuminance values that were used to calculate a  $P_i$  score and lighting schedules. EnergyPlus was then executed to perform a sizing run to determine the maximum air flow rate for the economizer. After this, an annual simulation of EnergyPlus was executed that output thermal and lighting load data which was converted into kWh/m<sup>2</sup> values for the design. With the simulations complete, GenOpt then accepted the thermal and daylighting performance scores as input

and used them to determine the region of the design space to search next. This process was continued until GenOpt reached its stopping or convergence criterion.

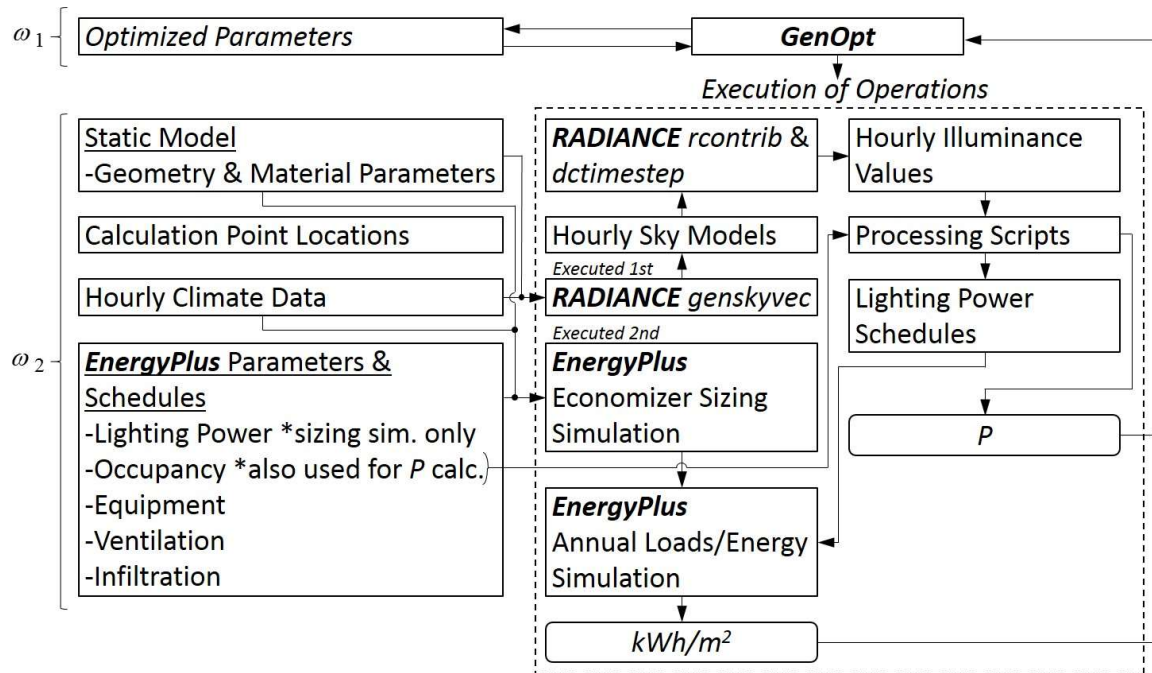


Figure 5.6: Sequence of operations used to solve classroom optimization process

## 5.2. Results and Discussion

Several observations of the nature of daylighting and thermal performance of this design for the cardinal orientations can be made from the Pareto fronts of each orientation (Figure 5.7) and their parameter values shown in Figure 5.8 and listed in Table 5.8. On each Pareto front, three designs, designated *a*, *b*, and *c*, are called out. For the north facing-orientation, much better daylighting performance was possible than in other orientations (87 *Pi*, which is approximately 10% better than the next best overall *Pi* score of all orientations), but this came at the cost of the overall poorest thermal performance score of all Pareto efficient solutions of all orientations (greater than 73 kWh/m<sup>2</sup>). In this

case, large windows admitted even, diffuse north daylight to the classroom but also caused large thermal losses in winter months, without direct solar gains during the day to help compensate for these losses. For the south facing-orientation, daylighting and thermal performances were constrained to a relatively narrow Pareto front, which contained the best overall thermal performance scores (less than  $55 \text{ kWh/m}^2$ , approximately 11% better than the next best thermal performance score of all orientations). The south-facing design's best daylighting scores were similar to those of the east, and west-facing designs' (approximately  $0.77 \text{ Pi}$ ). The very good thermal performance and relatively good daylighting performance of the south-facing orientation is a result of window sizes, LT values, and ST values that simultaneously provide appropriate amounts of daylight to the classroom when occupied, while minimizing negative solar gains during the cooling season and maximizing beneficial solar gains during the heating season. The south-facing orientation's windows were kept in the lower range of their possible dimensional values while the exterior shade and interior lightshelf were kept in the higher range of their possible values (Figure 5.8b). In short, the optimization of the south-facing orientation shows the benefits of traditional passive solar design. This is the only orientation that significantly benefits from winter gains, which have a large beneficial effect on overall thermal performance because of the disparity between heating and cooling system efficiencies. The east orientation showed more conflict between the objectives than the south orientation. Its range of thermal performance ( $61\text{--}63 \text{ kWh/m}^2$ ) was worse than that of the south orientation ( $54\text{--}58 \text{ kWh/m}^2$ ). While its minimum daylighting performance ( $0.73 \text{ Pi}$ ) was similar to that of the south orientation, its best daylighting score ( $0.78 \text{ Pi}$ ) was slightly better than that of

the south ( $0.77 Pi$ ). This may seem counter-intuitive, but it appears to result from the daily and seasonal occupancy patterns of the classroom and the physical characteristics of the east orientation optimized fully for daylighting. When fully optimized for thermal performance (the *a* solutions), the east-facing orientation's clerestory windows are smaller than those of the south-facing orientation. When fully optimized for daylighting performance (the *c* solutions), the east facing orientation's clerestory windows are larger than those of the south-facing orientation (Figure 5.8*b* and Figure 5.8*c*). This indicates that the east-facing orientation minimizes window area for thermal performance, since it has little potential for solar gain during the winter months and winter thermal losses by conduction dominate its overall thermal performance. The east-facing classroom, unoccupied in the summer, has fewer hours of low-altitude sun than the south-facing orientation. Therefore, when fully optimizing for daylighting, it guards less against it. It is also possible that early morning hours are relatively cloudy, making possible the east-facing orientation's higher daylighting performance.

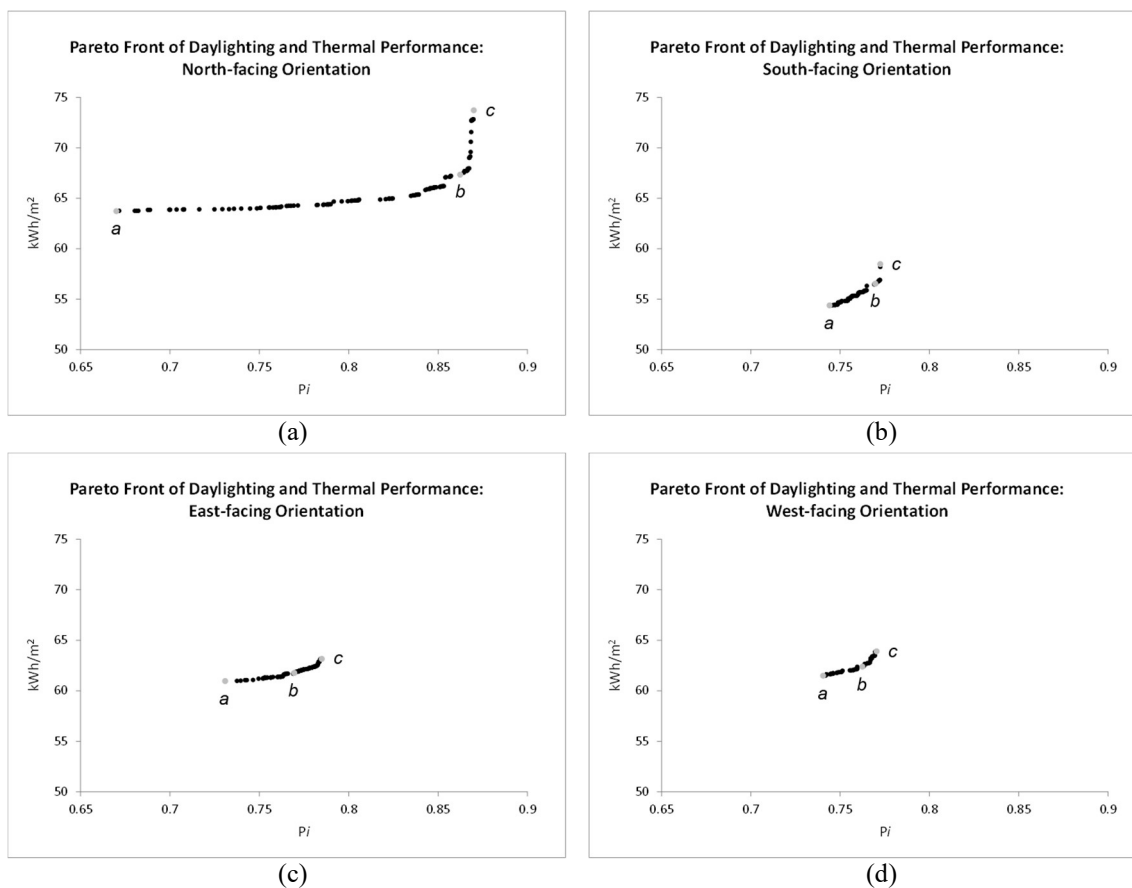


Figure 5.7: Pareto fronts of daylighting and thermal performance by orientation of classroom: (a) North-facing, (b) South-facing, (c) East-facing, and (d) West-facing

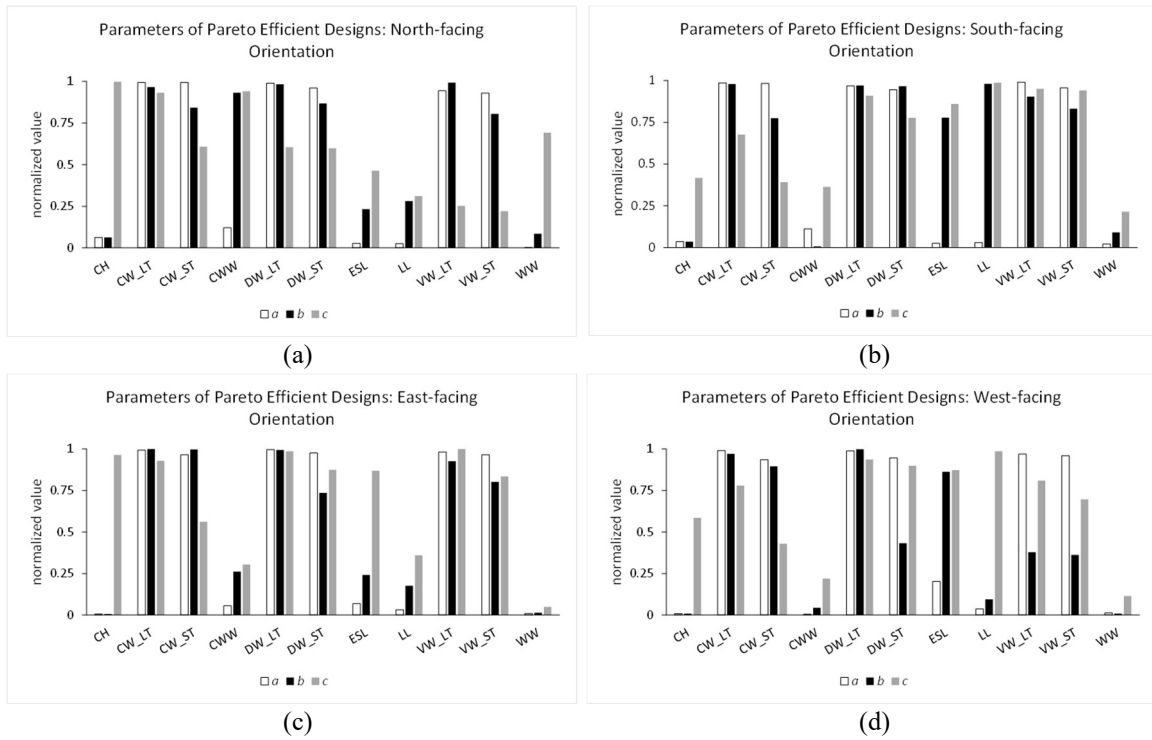


Figure 5.8: Samples of Pareto solutions by classroom orientation: (a) North-facing, (b) South-facing, (c) East-facing, and (d) West-facing

Table 5.8: Parameters of sample Pareto solutions

	CH(m)	CW_LT	CW_ST	CWW(m)	DW_LT	DW_ST	ESL(m)	LL(m)	VW_LT	VW_ST	WW(m)
North											
<i>a</i>	2.51	0.70	0.70	1.10	0.69	0.68	0.03	0.03	0.67	0.66	2.51
<i>b</i>	3.66	0.68	0.61	2.34	0.69	0.62	0.28	0.30	0.70	0.58	3.66
<i>c</i>	3.66	0.66	0.46	2.35	0.46	0.46	0.57	0.33	0.25	0.23	3.66
South											
<i>a</i>	2.48	0.69	0.69	1.08	0.68	0.67	0.03	0.03	0.69	0.67	2.48
<i>b</i>	3.20	0.69	0.56	0.92	0.68	0.68	0.95	1.05	0.64	0.60	3.20
<i>c</i>	2.95	0.51	0.33	1.47	0.65	0.57	1.05	1.05	0.67	0.66	2.95
East											
<i>a</i>	2.44	0.70	0.68	1.00	0.70	0.69	0.08	0.03	0.69	0.68	2.44
<i>b</i>	2.97	0.70	0.70	1.31	0.70	0.54	0.29	0.19	0.66	0.58	2.97
<i>c</i>	3.61	0.66	0.44	1.38	0.69	0.62	1.06	0.38	0.70	0.60	3.61
West											
<i>a</i>	2.45	0.69	0.66	0.92	0.69	0.67	0.25	0.04	0.68	0.68	2.45
<i>b</i>	2.92	0.68	0.64	0.98	0.70	0.36	1.05	0.10	0.33	0.32	2.92
<i>c</i>	3.15	0.57	0.36	1.25	0.66	0.64	1.06	1.05	0.59	0.52	3.15

The west-facing orientation generally had similar performance characteristics as the east, except that its daylighting performance was slightly worse. This is most likely a result of clearer skies in afternoon hours resulting in low-altitude sun over-illuminating the classroom.

Overall, the north-facing orientation exhibited the strongest conflict between daylighting and thermal performance, with daylighting performance scores ranging from 67 to 87  $P_i$  and thermal performance scores ranging from 64 to 74 kWh/m<sup>2</sup>. To gain a sense of the relative conflict between objectives of the different orientations, one can perform several operations on the Pareto front datasets. First, the daylighting and thermal performance scores are normalized over all orientations, with 0 representing the worst overall performance and 1 representing the best. Next, for each orientation, the distance between the best and worst thermal performance is determined. The same is done for daylighting performance. Finally, the product of the worst to best distances of thermal and daylighting performance is taken and represents the degree to which the objectives are in conflict for a particular orientation. These relative measures of conflict for the north, south, east, and west orientations were 0.52, 0.03, 0.03, and 0.02, respectively. Thus, the north orientation exhibited the greatest conflict while the south, east, and west orientations exhibited little conflict.

### 5.3. Conclusions

A hybrid GPS Hooke Jeeves/PSO algorithm was used in combination with the Epsilon Constraint Method to find Pareto efficient solutions to the daylighting and thermal optimization problem of a classroom design. Since windows admit light and provide weak resistance to heat conduction and radiation heat exchange, it was thought

that daylighting and thermal performance would be strongly conflicting objectives. However, the results show that, for the design problem with a south, east, or west orientation in the Charlotte climate, these two objectives are not strongly conflicting. This is evident in the Pareto front which ranges over relatively small differences in daylighting and thermal performances. Along the Pareto front, both objectives are close to their best possible value. For the north orientation, there is a much more pronounced conflict between the objectives, with much greater daylighting performance possible, with the consequence of poorer thermal performance. The east orientation showed better daylighting and thermal performance than the west orientation, most likely due to weather conditions. This information is valuable for design decision makers who are interested in understanding better the trade-offs between daylighting and thermal performance, beyond notional understanding and conventional wisdom. Future research on this problem may include the modeling of complex fenestration systems and dynamic shading systems along with advanced methods of accounting for glare and visual comfort.

## CHAPTER 6: ENERGY MODEL CALIBRATION CASE STUDY

In this chapter, the design of a prototypical retail bank building is optimized for thermal and lighting performance and is presented as a case study application of the optimization method presented earlier. Conveniently, an existing instance of the prototype design was available for empirical study. Thus, it was appropriate to assess the accuracy of the energy model to be optimized against actual performance data before using the model as a basis of design optimization. To this end, a method of energy model calibration was developed to serve as a valuable pre-optimization step that increases the accuracy of optimized building design results. The developed method is novel in that it is based on calibration to hourly end uses of energy and hourly zone temperatures, as opposed to daily or monthly aggregated energy usage, as is commonly done. In addition, the thermal characteristics of the building envelope were calibrated without the effects of the HVAC system. This allowed for precise tuning of key envelope parameters and is significant because envelope parameters are the focus of subsequent optimization efforts. This chapter is structured into two main parts. First, the method of model calibration is explained and demonstrated. Second, the optimization of the calibrated energy model for thermal and lighting performance is demonstrated.

## 6.1. Energy Model Calibration

### 6.1.1. Description of Case Study Model Calibration

As an example of model calibration, a retail bank building in the Miami, FL region was studied and modeled in detail. This bank serves as a prototype design that will be replicated; therefore, the results of model calibration can be used in the optimization of this design in other locations and belongs to the first case of model calibration presented in Chapter 3. Figure 6.1 is a floor plan of the bank and shows the major space types in the bank which include a customer teller line, open office space, teller area, and drive thru teller area. Other support spaces included a breakroom, electrical room, bathrooms, a workroom and a storage room. Figures 6.2 and 6.3 show exterior views of the bank with shading surfaces above windows colored purple. The walls of the building are made of insulated concrete forms (ICF). This made the building very airtight and also created a thermal mass effect in the building. The glazing of the building was electrochromic glass, which darkens or tints when direct sunlight is sensed on the glazing. The electrochromic glass varied from 0.4 SHGC (no incident direct sunlight) to 0.09 SHGC (incident direct sunlight). The bank also had a highly insulated roof; however, it was breached by aluminum support members for a photovoltaic system on the roof that caused a thermal bridging effect and increased the U-value of the roof. Table 6.1 outlines the major energy-impactful characteristics of the bank.

Table 6.1: Building attributes as specified in construction documents

Building Attribute	Value
Gross Floor Area	297 m <sup>2</sup>
Wall U-value	0.25 W/m <sup>2</sup> -K
Floor U-value	0.98 W/m <sup>2</sup> -K
Roof U-value	0.30 W/m <sup>2</sup> -K
Window U-value	2.00 W/m <sup>2</sup> -K
Electrochromic Glass SHGC	0.4,0.09 tinted
Electrochromic Glass LT	0.59,0.01 tinted
Cooling Thermostat Set Point	22.2 °C with 25.6 °C setback
Heating Thermostat Set Point	20 °C with 18.3 °C setback
Lighting Power Density	8.07 W/m <sup>2</sup>
Equipment Power Density	5.38 W/m <sup>2</sup>
Ventilation Rate	0.016 m <sup>3</sup> /s - person
Infiltration Rate	1.2 ACH occupied, 0.01 ACH unoccupied
Occupancy Density	0.07 people/m <sup>2</sup>
Operation Schedule	7:00 AM to 6:00 PM Mon. through Fri. 7:00 AM to 5:00 PM Sat. Unoccupied Sun.
HVAC System	Variable Refrigerant Flow (VRF) heat pump 35 kW cooling capacity 32kW heating capacity supplying single fan and coil unit in four thermal zones Dedicated Outdoor Air Supply (DOAS) 10 kW cooling capacity 8kW heating capacity

Figure 6.4 shows the three main thermal zones of the bank. A smaller fourth thermal zone, not labeled in Figure 6.4, was composed of the electrical room. Each thermal zone is served by a single indoor fan and coil unit (or air handling unit, AHU) with refrigerant supplied by the VRF outdoor heat pump unit. Each AHU's supply air is distributed to its zone by duct work. Air is returned to each AHU through a plenum return. The bank is also served by a dedicated outdoor air system (DOAS) which supplies ventilation air during occupied hours. The DOAS supply air was ducted directly into the plenum near the intakes of each of the three main AHUs.

The bank building was outfitted with an extensive BMS that reported hourly energy usage of each electrical circuit. The BMS also reported zone temperatures on an

“on change” basis in each zone as measured by their thermostats. This hourly data was valuable because it allowed for the precise description of equipment and lighting heat gains in the calibrated energy model and for modeled space temperatures to be calibrated to measured space temperatures.

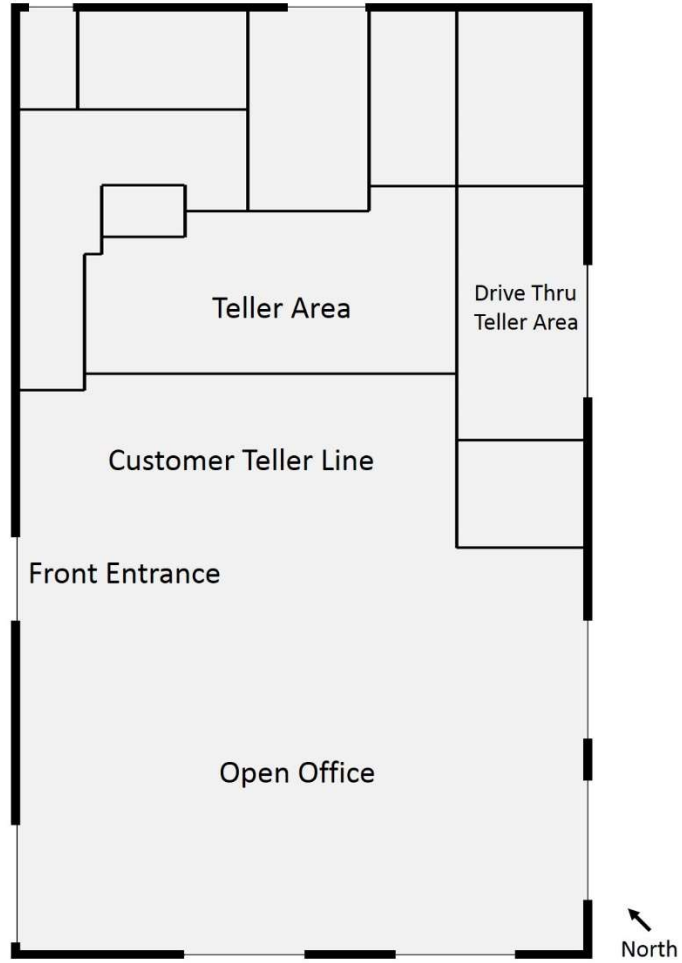


Figure 6.1: Floor plan of bank

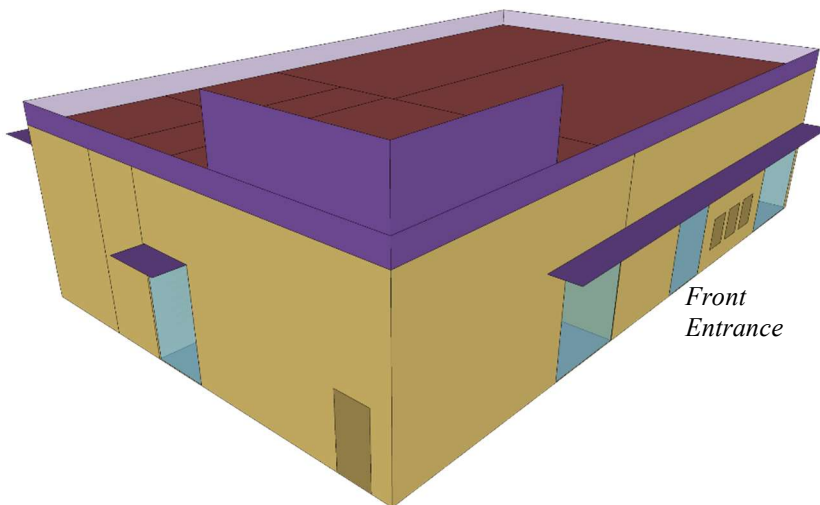


Figure 6.2: View of bank's north corner

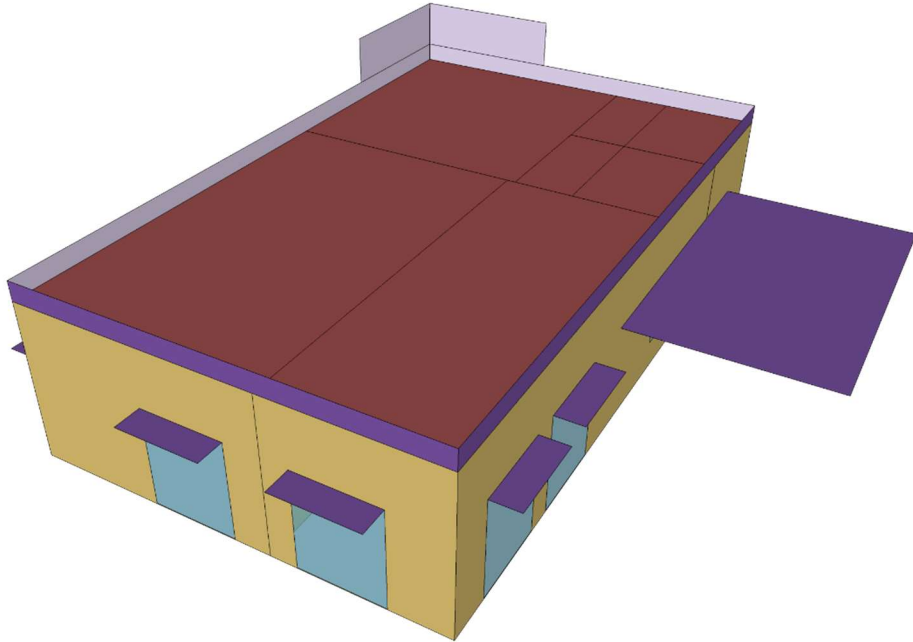


Figure 6.3: View of bank's south corner

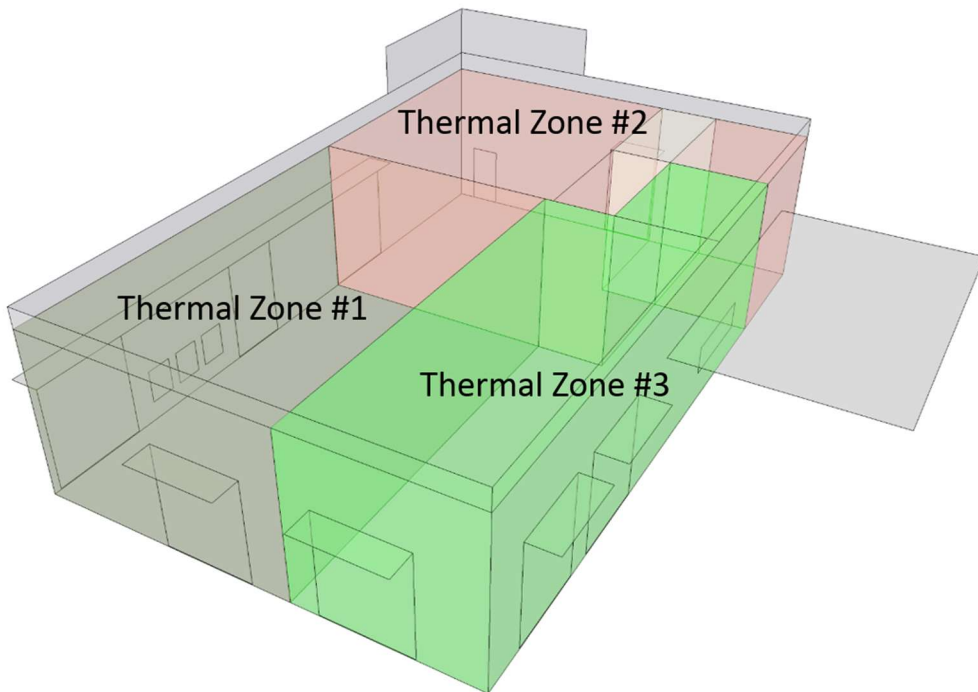


Figure 6.4: Thermal zones of retail bank

### 6.1.2. Energy Model Calibration Methodology through Thermal Response Analysis

As described above, it is very important for the envelope characteristics of a building to be accurately described in an energy model that is to be used for optimizing the envelope design of similar buildings. Current energy model calibration methods lack the ability to precisely calibrate building envelope parameters for main two reasons. First, they focus on monthly aggregate energy usage. In this case, interactions between model parameters make for the possibility of many model parameter value sets that match monthly aggregate energy usage data. It is very difficult, without detailed inspection, to know if a “calibrated” model parameter value set is a faithful representation of the actual building. Second, they focus on energy usage or temperature profiles of individual components but do not account for interactions between HVAC parameters and envelope and internal load parameters. The same co-solution problem can exist even when calibrating to granular time step energy and/or temperature data. A common example of this is when a cooling system is using excessive energy because of improper control or a system fault. In the “calibrated” model, this effect can be falsely accounted for most easily by increasing infiltration rates or equipment load rates until the artificially high loads on the modeled cooling system cause its energy usage to match actual values. This situation is common because it is much easier to adjust such envelope or equipment parameters than to explore parameter values representative of a malfunctioning cooling system.

As presented in Chapter 3, many of the effects of an HVAC system can be removed so that the thermal response of a zone can be analyzed. In Chapter 3, several items were listed whose effects on a zone’s thermal response are difficult to account for.

Furthermore, HVAC systems often cause pressure differences between the building interior and the exterior environment, impacting infiltration rates when operational. A reasonable method to account for such unmeasurable effects in an energy model is to perform a sensitivity analysis on these factors to understand them and estimated upper and lower bounds of their effect on building thermal performance. The assumption, here, is that the thermal response of the building can only be analyzed when the building is unoccupied to avoid subjecting building occupants to potentially uncomfortable conditions.

As previously discussed, it is possible to largely determine all be the factors impacting a zone's thermal response, except those in the envelope category. This is accomplished through measurement and data collection. For example, it is possible to measure the weather and internal heat gain factors impacting a zone's thermal response. The collection of hourly local weather measurements is often available. Hourly energy usage data of key electrical circuits can be measured by commercially available BASs and BMSs. Thus, the effects of weather factors and heat gains from lights and equipment can be reasonably determined and accounted for in a building energy model. With these two categories of thermal response factors accounted for, a detailed study of envelope parameters, as the only undetermined values impacting the thermal response of a zone, can be conducted. It is here that energy model optimization methods can aid in the determining of envelope parameters. The below case study describes the process of thermal response analysis, and subsequent model calibration, through a similar optimization method as presented previously for optimizing building design for thermal and lighting performance.

### 6.1.3. Method of Thermal Response Analysis of Case Study Building

To measure the thermal response of the retail bank building, the bank's VRF and DOAS systems were disabled over a period of time on weekends, so as to not disturb the normal operations of the bank. Temperatures in the three main thermal zones of the building were measured and recorded by the BMS. In addition, the BMS measured and recorded hourly electrical energy usage of all circuits, including lighting and equipment, in the bank. Over each test period, the lights were turned on in the same manner as when the building is occupied on weekdays. This was done on four occasions. Each time, the VRF and DOAS systems were turned off on a Saturday at 4:00 PM through the following Monday at 3:00 AM. Weather data was acquired from a local weather station over this time period as well. Table 6.2 outlines the Sunday each test was associated with and key weather conditions. As can be seen, three warm/hot weather days were used in this study and one cool day was used.

Table 6.2: Sundays associated with each thermal response weekend period and weather conditions associated with each test period

Test Sunday Date	Temperature (°F)			Sky Conditions
	High	Low	Average	
February 15 <sup>th</sup>	73	44	58	Clear
July 19 <sup>th</sup>	93	75	83	Partly Cloudy
August 2 <sup>nd</sup>	91	78	84	Partly Cloudy
August 16 <sup>th</sup>	91	77	84	Partly Cloudy

At the conclusion of the thermal response data collection phase, acquired data included the points outlined in Table 6.3.

Table 6.3: Hourly measurements collected during each thermal response test period

Hourly Weather Data	Hourly Zonal Data
Dry Bulb Temperature	Dry Bulb Temperature (recorded at thermostat)
Dew Point	Lighting Energy Usage
Humidity	Equipment Energy Usage
Barometric Pressure	
Wind Direction	
Wind Speed	
Precipitation Amount	
Sky Conditions	

Using these datasets, an energy model of actual conditions was created using EnergyPlus. EnergyPlus' *Weather Statistics and Conversion Tool* was used to convert measured hourly weather data to the format required by EnergyPlus. The *Weather Statistics and Conversion Tool* also generated hourly solar radiation values based on its internal model which determines these values based on sky conditions and time of day and year. Actual lighting and equipment energy usages were integrated into the model using "Schedule:File" EnergyPlus objects which allow for hourly values to be read in from a file. The building geometry and material attributes were modeled according to construction documents made available, as can be seen in Figures 6.2 and 6.3 and summarized in Table 6.1. Ground temperatures have a strong effect on single-story buildings; therefore, ground temperature below the bank were modeled in detail by EnergyPlus' *Slab Preprocessor* utility.

With the weather and internal loads determined and accounted for in the energy model, focus could be given to the calibration of envelope factors. An initial energy model simulation, with model parameters based on information from construction documents, resulted in a poor fit between modeled and measured space temperatures (Figure 6.5). Key parameter values of this model are given in Table 6.4.

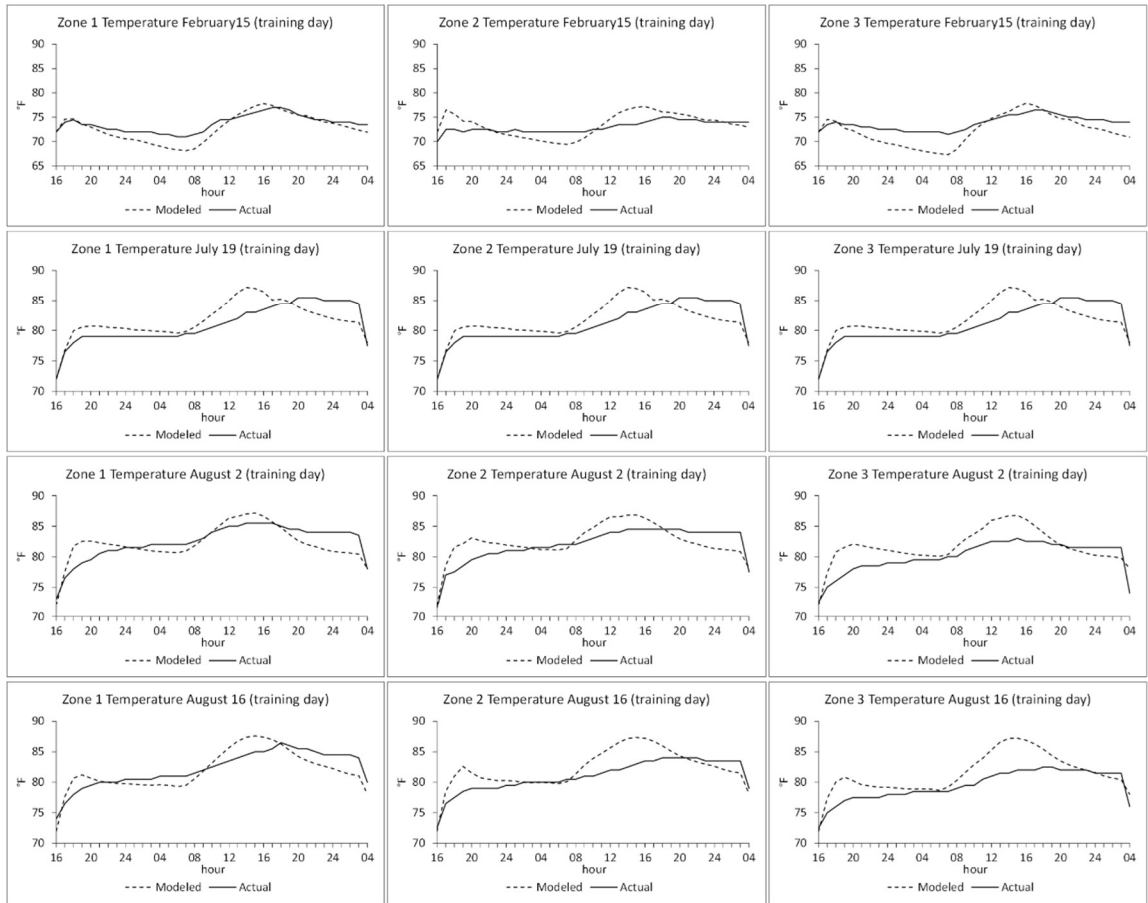


Figure 6.5: Thermal response of original uncalibrated model: Modeled and actual zone temperatures on thermal response analysis days

Table 6.4: Envelope parameters of original uncalibrated model – values based on construction documents

Envelope Parameter Factor	Minimum -Maximum
SHGC - electrochromic glass not tinted (fraction solar radiation transmitted)	0.4
SHGC - electrochromic glass tinted (fraction solar radiation transmitted)	0.09
Window U-value (W/m <sup>2</sup> °C)	2.0
Roof Insulation Conductivity (W/m °C)	0.066
Floor Conductivity (concrete slab) (W/m °C)	1.311
Floor Slab Insulation R-value (m <sup>2</sup> °C/W)	not modeled*
Floor Carpet R-value (m <sup>2</sup> °C/W)	0.1
Infiltration Rate (air changes per hour)	0.3**
Heat Gain from Lights - fraction radiant	0.7
Heat Gain from Equipment - fraction radiant	0.7
Exterior Ground Reflectance	0.4
Interior Mass – zone1, zone2, zone3 (m <sup>2</sup> of interior walls)	10.34, 12.1, 10.34

*\*not modeled because no slab insulation was shown in construction documents, however this parameters was included in calibration runs to account for a possible insulation effect not captured in the modeled floor construction*

*\*\*based on commonly used value for office buildings*

These envelope parameters were then the focus of calibration as outlined in Table 6.5. Because the uncalibrated model seemed to be more sensitive to outside temperature than the actual building, infiltration and thermal mass were included in the set of optimized parameters. Infiltration was important because if too high, zone temperatures would be heavily influenced by the temperature of the outdoor air entering the building. Internal mass was important because it can help dampen the interior's response to conducted gains and solar gains. Some fraction of heat from these sources can be absorbed by the internal mass instead of by the air mass of a zone. As can be seen, ground reflectance was considered in this calibration process. Although ground reflectance is not an inherent attribute of the building, the building's surroundings, paved surfaces and landscape features affect the effective ground reflectance experienced by the

building. Because of these considerations, and the fact that ground reflectance could not be easily measured, it was included as a parameter to be optimized.

Table 6.5: Envelope parameters calibrated

Envelope Parameter Factor	Minimum -Maximum
SHGC - electrochromic glass not tinted (fraction solar radiation transmitted)	0.3 – 0.5
SHGC - electrochromic glass tinted (fraction solar radiation transmitted)	0.01 - 0.135
Window U-value (W/m <sup>2</sup> °C)	2.0 – 6.0
Roof Insulation Conductivity (W/m °C)	0.02 – 0.1
Floor Conductivity (concrete slab) (W/m °C)	1 - 4
Floor Slab Insulation R-value (m <sup>2</sup> °C/W)	0.001 – 1.0
Floor Carpet R-value (m <sup>2</sup> °C/W)	0.001 – 1.2
Infiltration Rate (air changes per hour)	0.20 – 0.76
Heat Gain from Lights - fraction radiant	0.01 – 0.90
Heat Gain from Equipment - fraction radiant	0.01 – 0.90
Exterior Ground Reflectance	0.1 – 0.6
Interior Mass – zone1, zone2, zone3 (m <sup>2</sup> of interior walls)	0 – 1000 (each zone)*

*\*allowed to be very large to account for other sources of mass, such as underestimated mass of exterior walls, furniture, and bank vault*

To calibrate these parameters, an optimization problem was formulated. Values of these parameters were explored with the objective of minimizing the error, measured as root mean squared error (RMSE), between the measured and modeled thermal responses of each zone. A similar method as presented earlier for optimizing envelope parameters for thermal and lighting performance was used. The method employed the use of GenOpt to modify the identified parameters and search for the parameter value set that minimized RMSE as defined above. The hybrid PSOC/HJ algorithm was selected because it consistently produced solutions close to the true optimum in a reasonable number of simulations, as demonstrated above.

It was desirable to know how accurate found model solutions were at predicting zonal thermal responses for days that had not been included in the calibration of the

model. Doing this give one a sense of the ability of the model to predict thermal responses of conditions unavailable for calibration “training”. To accomplish this, a cross-validation approach was taken whereby three of the four thermal response days were used to optimize or train the model’s envelope parameters. The remaining day was used as a testing day by which the model’s prediction accuracy was tested. Training days and testing days were cycled through such that each day served as a testing day once, resulting in a four-fold cross validation set by which to evaluate this method of envelope parameter calibration.

#### 6.1.4. Results of Thermal Response Analysis and Model Calibration

Table 6.6 and Figures 6.7, 6.8, 6.9, and 6.10 show the modeled and measured thermal responses of the bank on each test day and for each thermal zone. In each figure, a different training day set and testing day is shown. Several observations can be made about the prediction accuracy of the energy model. By observing the fit of the modeled zonal temperature to measured temperature in the figures, and by cross-referencing the associated RMSE values in Table 6.6, it seems that an RMSE of less than 1 yields a reasonably good fit between modeled and measured thermal responses. For each set of training day combinations, an acceptable RMSE of less than 0.9 was achieved. However, when these model solutions where used to predict the thermal response of the testing day, results were varied. In the worst case, a testing day RMSE of 1.69 was produced by the model trained on July 19<sup>th</sup>, August 2<sup>nd</sup>, and August 16<sup>th</sup>. It is worth noting that this is perhaps a result of some issue that arises when the model parameters values are trained only on warm/hot days and tested on a cool day. This issue may also stem from an anomalous relationship between the training days of February 15<sup>th</sup> and August 16<sup>th</sup>.

When either is excluded from the training set and used as the testing day, a relatively poor testing RMSE results. For example, in addition to the testing RMSE of 1.69 when February 15<sup>th</sup> is used as the testing day, a poor testing RMSE of 1.06 was produced when August 16<sup>th</sup> was used as the testing day. It is possible that the Zone 2's temperature was kept lower on February 14<sup>th</sup> leading into the February 15<sup>th</sup> training day and that this is the source of discrepancy. It is evident in the graph that Zone 2's actual temperature was conditioned to 70 °F instead of the normal 72 °F. Despite this issue, the energy model calibration method seems to predict the building's thermal response with a reasonable degree of accuracy. Thus, it is acceptable as a means to produce a calibrated instance of an energy model to serve as a base model from which optimized designs are explored.

Next, a calibrated model instance was created by training the model parameters on all 4 thermal response days. This is show in Table 6.6 as Case 5 and in Figure 6.11. This calibrated model instance resulted in a relatively good training RMSE of 0.82. Because the cross-validation results showed reasonable good prediction capabilities of the model, it was determined that this calibrated model instance was a good base model to use in the optimization of the bank prototype design.

The envelope parameters specified in construction documents (Case 6) and their calibrated versions (Cases 1-5) are compared in Figure 6.6. Several observations can be made about the calibrated models. Firstly, interior mass values of all calibrated models closely matched and were much greater than the values of the uncalibrated model, particularly in Zone 3. This seems to be correct because the thermal response of the uncalibrated model (Figure 6.5) responds much more quickly to outside temperature and solar radiation than the measured thermal response of the building. The thermal mass

absorbs heat before it can cause a change in air temperature. The amount of thermal mass predicted by the calibrated models may seem excessive, particularly in Zone 3; however, this mass accounts for the effect of all thermally engaged mass in each zone, not just that of the surface area of interior walls. Things such as furniture, the bank vault, and underestimated mass in exterior walls and floor must be accounted for. Another observation is that calibrated models Case 2 and Case 3 generally agree with Case 5 (which was trained on all test days) while Case 1 and Case 4 show some discrepancy with Case 5, and each other. This points to the possibility of some unaccounted for anomalous condition on the test days associated with Case 1 and Case 4, February 15<sup>th</sup> and August 16<sup>th</sup>. Notable discrepancies between the model based on construction documents (Case 6) and the calibrated models include a greater SHGC of tinted electrochromic glass, greater roof conductivity, some insulating effect of the floor slab not accounted for in the construction documents, and a lower than originally estimated ground reflectance. The following section presents the optimization of the calibrated model for thermal and lighting performance.

Table 6.6: RMSE results of modeled and actual space temperatures (based on degrees Fahrenheit)

	Thermal Response Day Type				Training RMSE	Testing RMSE
	Feb 15th	Jul 19th	Aug 2	Aug 16		
Case 1	<i>Testing</i>	Training	Training	Training	0.74	1.69
Case 2	Training	<i>Testing</i>	Training	Training	0.82	0.82
Case 3	Training	Training	<i>Testing</i>	Training	0.88	0.86
Case 4	Training	Training	Training	<i>Testing</i>	0.86	1.06
Case 5	Training	Training	Training	Training	0.82	-
Case 6	- original uncalibrated model -				2.18	-

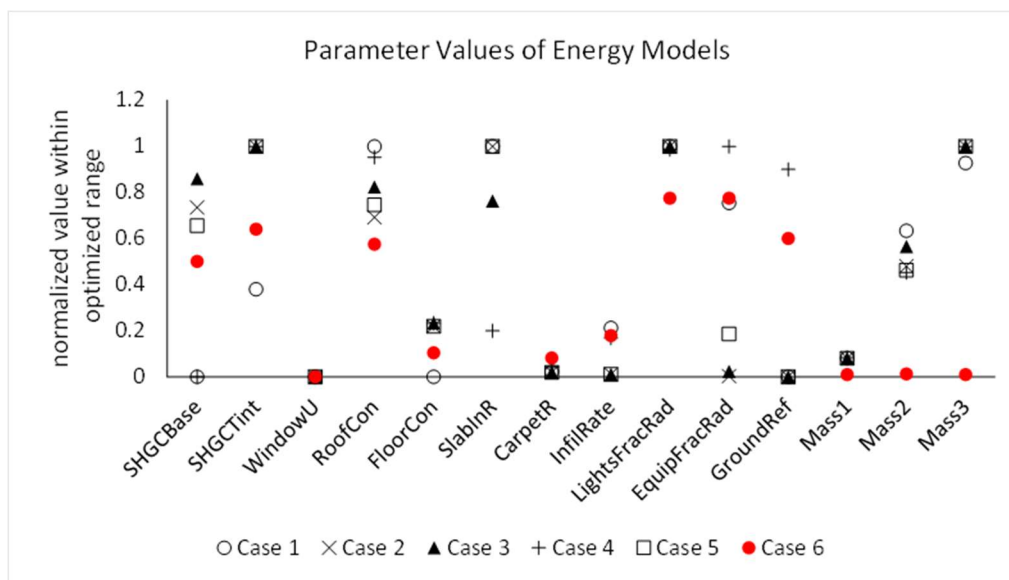


Figure 6.6: Graph of values (normalized) of calibrated parameter values for each case in Figure 6.6

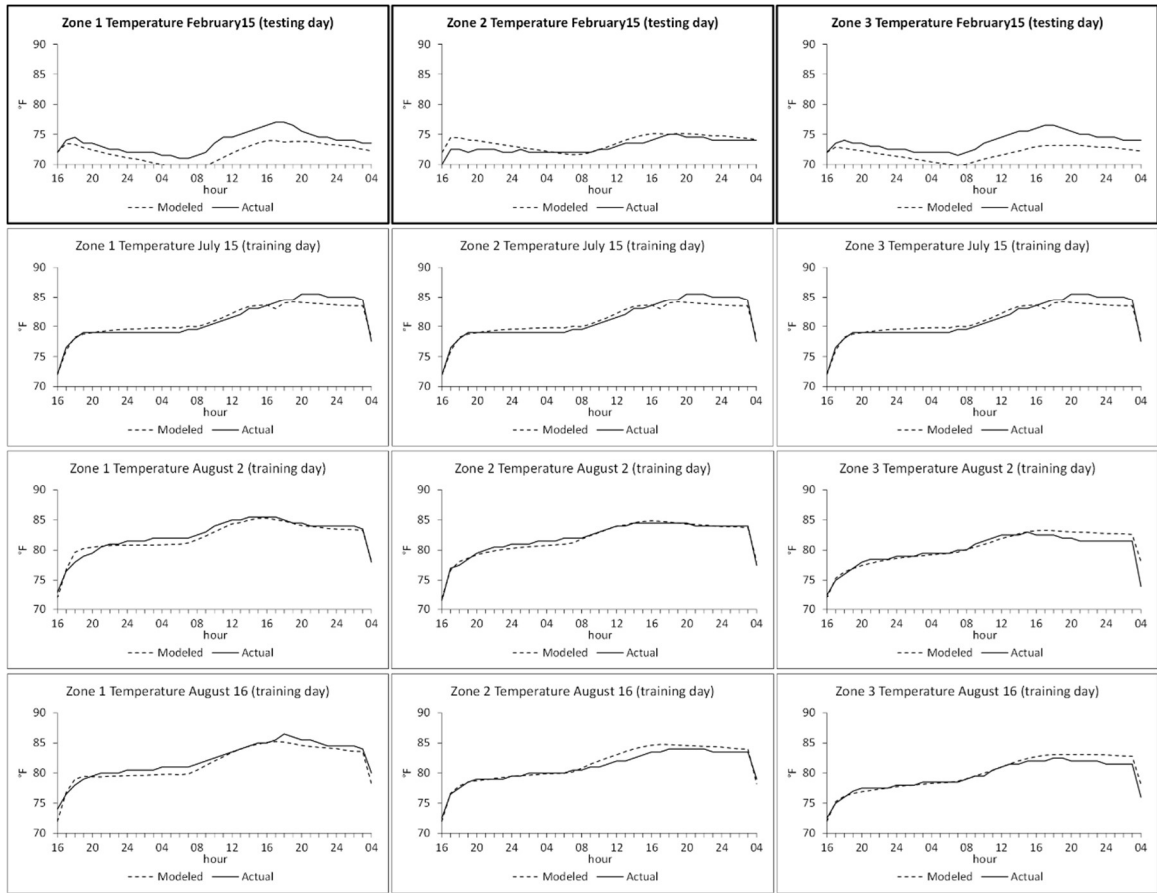


Figure 6.7: Thermal response Case 1: Modeled and actual zone temperatures on thermal response analysis days with February 15<sup>th</sup> as the testing day

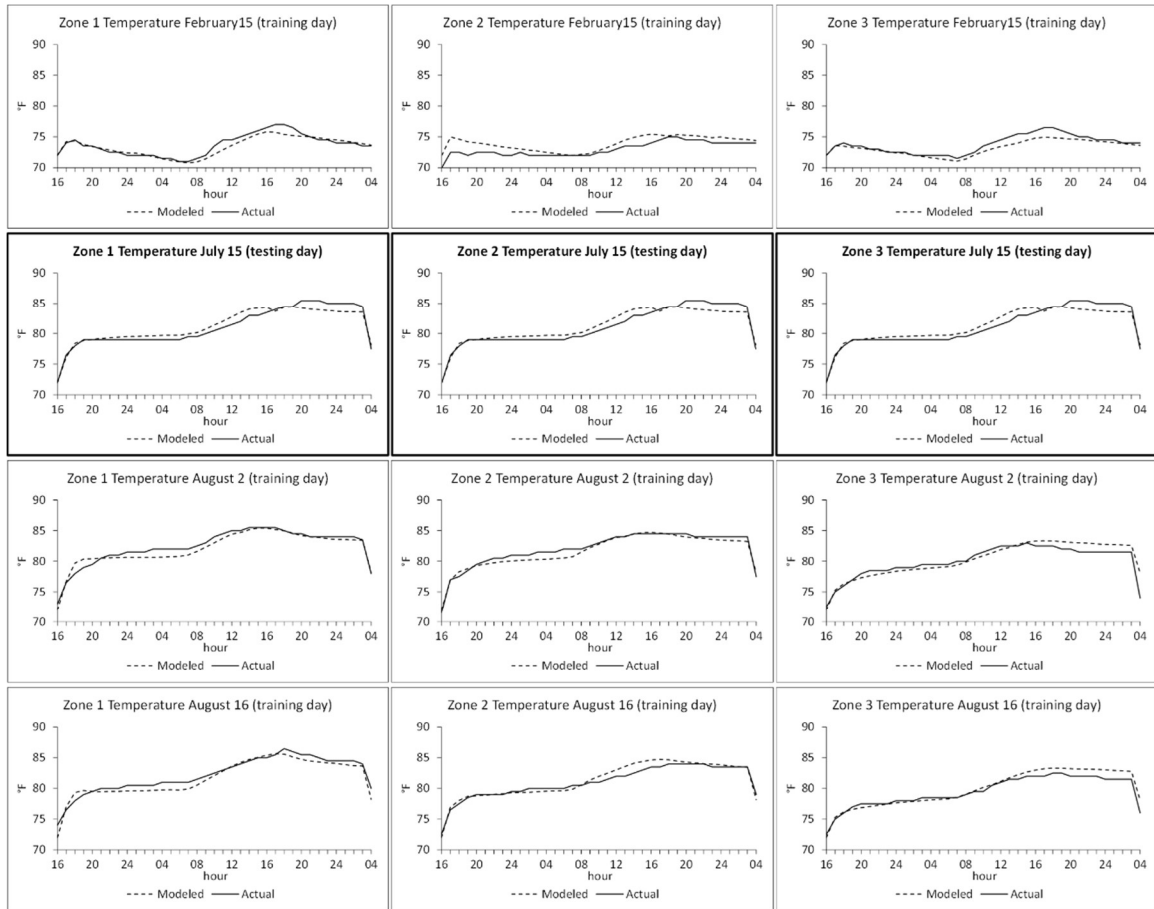


Figure 6.8: Thermal response Case 2: Modeled and actual zone temperatures on thermal response analysis days with July 19<sup>th</sup> as the testing day

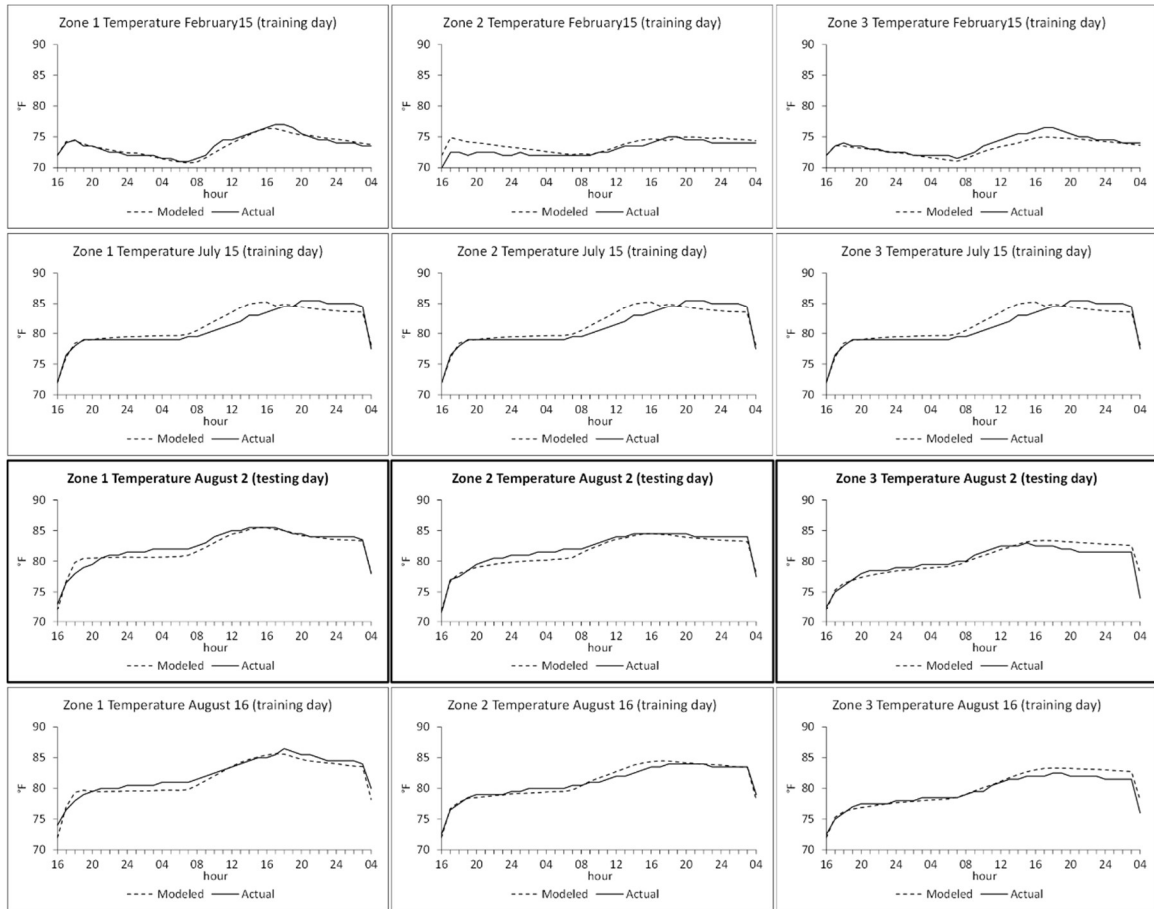


Figure 6.9: Thermal response Case 3: Modeled and actual zone temperatures on thermal response analysis days with August 2<sup>nd</sup> as the testing day

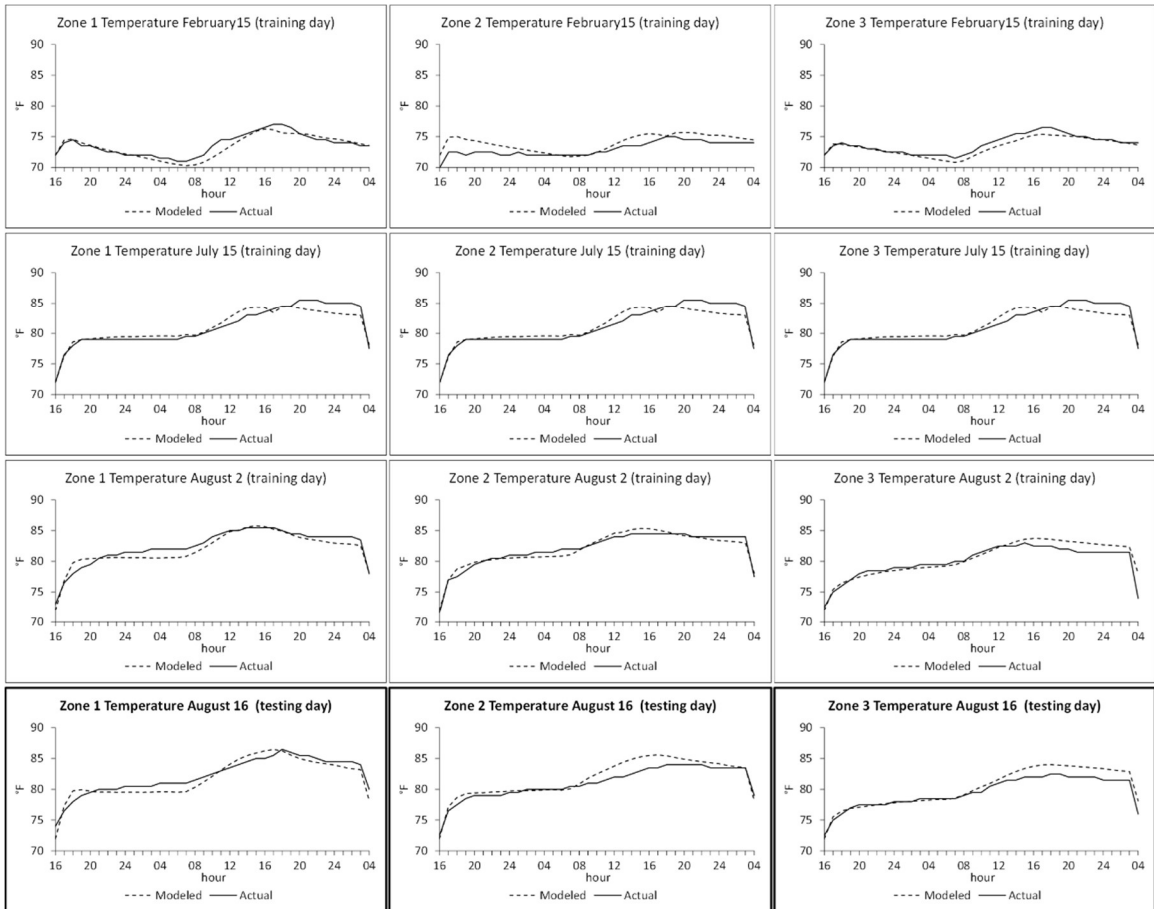


Figure 6.10: Thermal response Case 4: Modeled and actual zone temperatures on thermal response analysis days with August 16<sup>th</sup> as the testing day

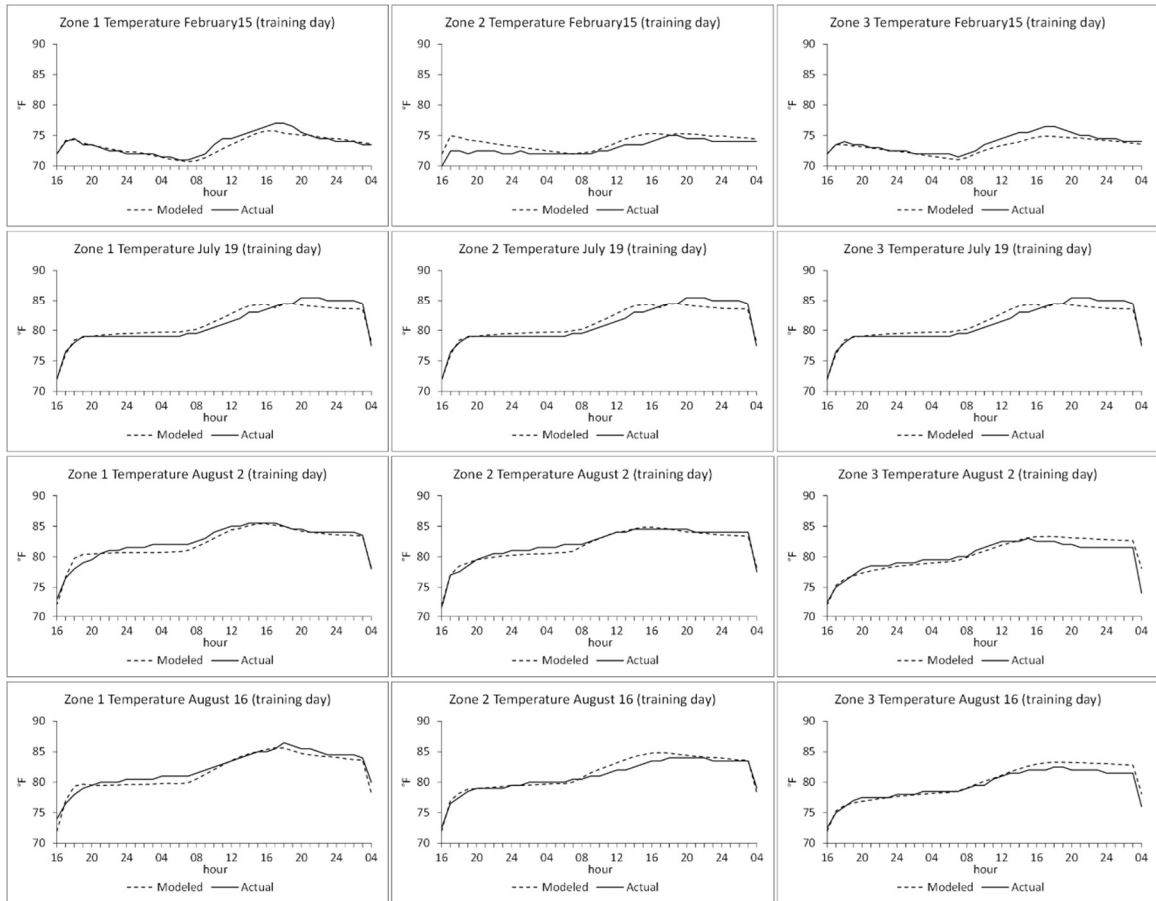


Figure 6.11: Thermal response Case 5: Modeled and actual zone temperatures on thermal response analysis days with all days used for training

## 6.2. Optimization of Retail Bank Building for Thermal and Daylighting Performance

The open office area of the retail bank is daylit by large windows of electrochromic glass. It is of interest to know the best trade-off between daylighting performance and thermal performance associated with the design of these windows, principally their size. Each window has a shading device that also impacts its solar and light transmittance. An optimization experiment was setup such that each window was allowed to maximize or minimize its vertical and horizontal size and location (i.e., the location of the window's center on its wall). Each window's shading device followed the location and width of its

window and was allowed to shorten or lengthen its extension from the building. These optimized parameters are illustrated in Figure 6.12.

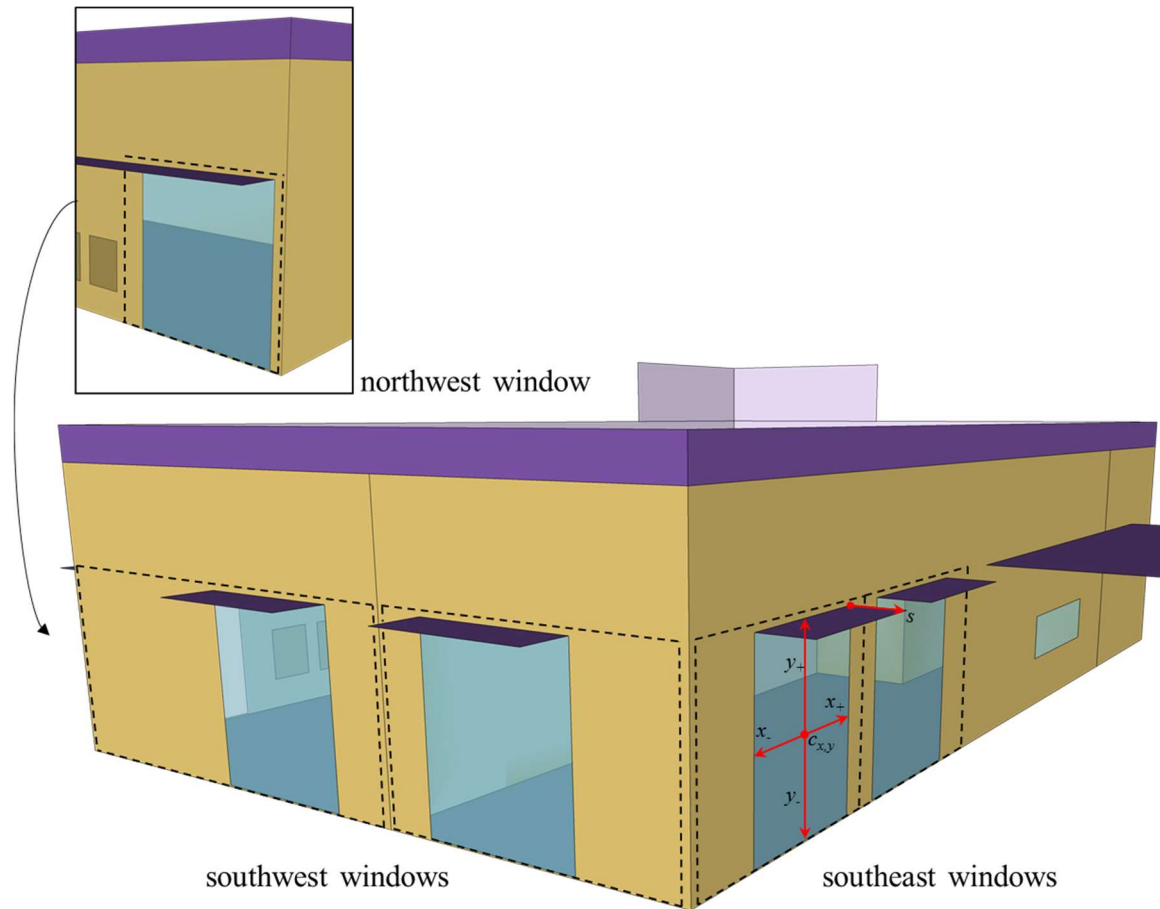


Figure 6.12: Illustration of window parameters optimized for thermal and daylighting performance. Each window was allowed to independently vary its location ( $c_{x,y}$ ) and extends from this point ( $x_+$ ,  $x_-$ ,  $y_+$ ,  $y_-$ ) within the boundaries defined by dashed lines. The length of the shading device ( $s$ ) was also allowed to vary up to 3' from the building. These parameters are illustrated on a single window but apply to all optimized windows.

The daylighting performance of the open office area was evaluated by analyzing the contribution of daylight to the illuminance of calculation points on two grids. One grid was located in the open office area of Zone 1. The other grid was located in the open office area of Zone 3. Both grids were placed at workplane height, or 0.75m above the floor (Figure 6.13).

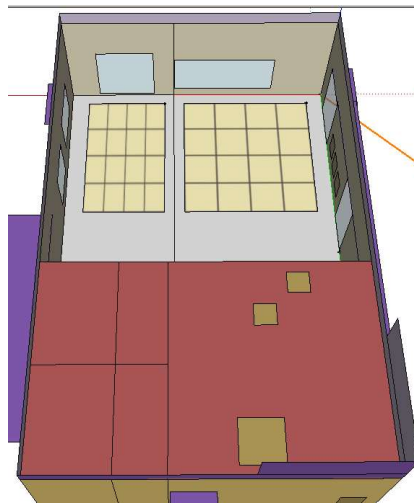


Figure 6.13: Location of grids of illuminance calculation points in zones 1 and 3.

Daylighting performance was evaluated based on Equation 5.2 and the method presented in Chapters 4 & 5. Energy performance was also evaluated based on Equation 5.2 but with a slight modification. The windows of interest for this optimization only impact the heating, cooling, and open office area lighting loads of the building. They do not impact the lighting loads in other spaces and they do not impact equipment loads. Because of this, energy performance was defined as the sum of energy used by the VRF cooling system and open office area lights on an annual basis measured in units of kWh.

Heating energy was not considered because in the Miami climate zone heating is a rare condition and results in negligible energy on an annual basis.

As in Chapter 5, the Epsilon constraint method was used to approximate the Pareto front related to lighting and thermal performance. Thermal performance was chosen as the objective to be constrained. Different values for the constraint were explored until a well define Pareto front was established.

Figure 6.14 shows the Pareto front of design solutions found by the PSOC/HJ algorithm. Three designs (*a*, *b*, and *c*) are identified on the Pareto front and are illustrated in Figures 6.15, 6.16, and 6.17. Design *a* represents a design at the extreme left of the Pareto front which fully optimized for thermal performance without regard for daylighting performance. Design *c* represents a design at the extreme right of the Pareto front which fully optimized for lighting performance without regard for thermal performance. Design *b* represents a point near the middle of the Pareto front and is a design that balanced thermal and lighting performance. It can be seen that a very small difference in energy performance is present across the bounds of the Pareto front, less than 250 kWh/year and daylighting performance ranges from 48 to 56 *P*. This suggests that smaller windows tend to save energy by reducing window area and the associated heat transmission while larger windows tend to save energy by reducing lighting loads and relying on electrochromic glass to prevent excessive solar gains. In either scenario, annual energy usage is virtually the same. This leads one to focus on daylighting performance as the main determining factor in final design selection. It can be seen in Figures 6.15, 6.16, and 6.17 that smaller windows are associated with lower daylighting performance and larger windows are associate with greater daylighting performance. It

should be noted that, normally, excessive window area leads to poor daylighting performance due to over-illumination, but that does not appear to be the case for this building. The electrochromic glass seems to be reducing the majority of over-illumination from direct sunlight, allowing larger windows to deliver more daylight deeper into the space thus resulting in high daylighting performance scores. The key knowledge gained from this optimization exercise is that, because of the electrochromic glass, there is not a strong trade-off between energy and daylighting performance for this retail bank building design; larger windows produce higher daylighting performance results with little energy increase.

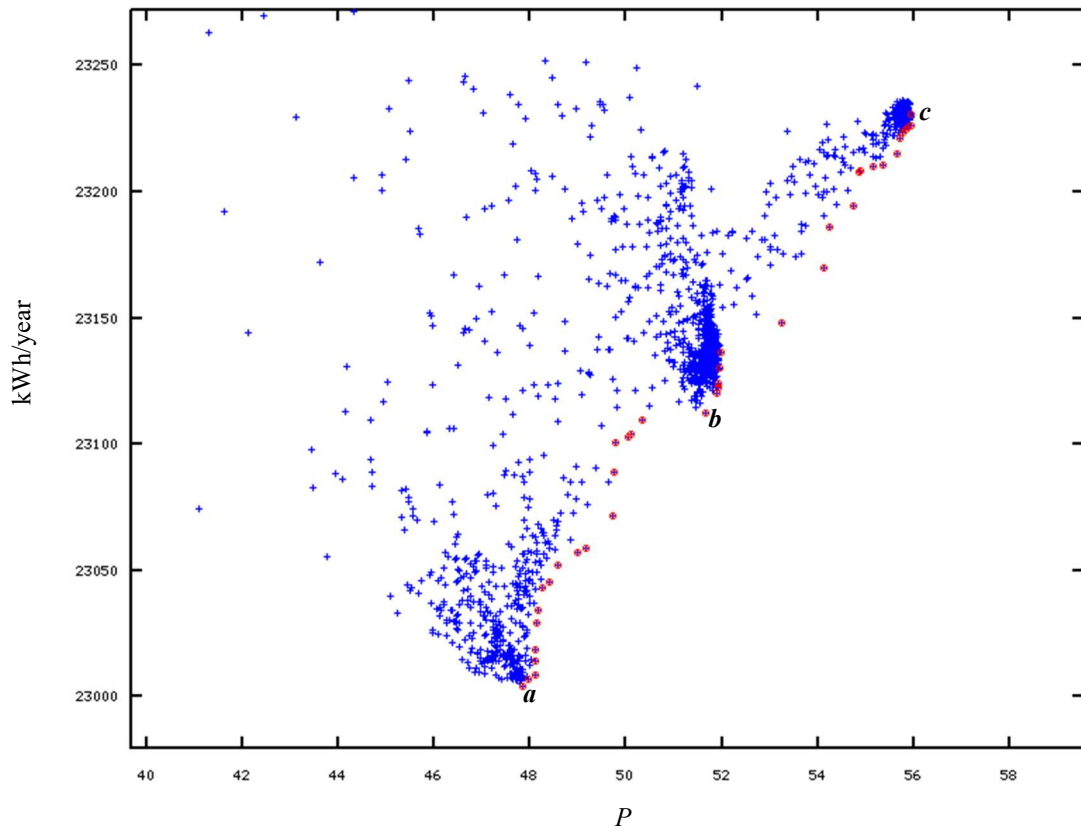
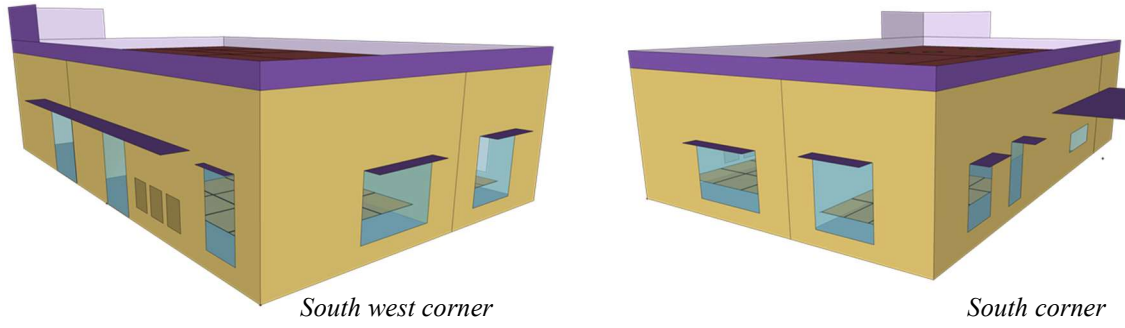
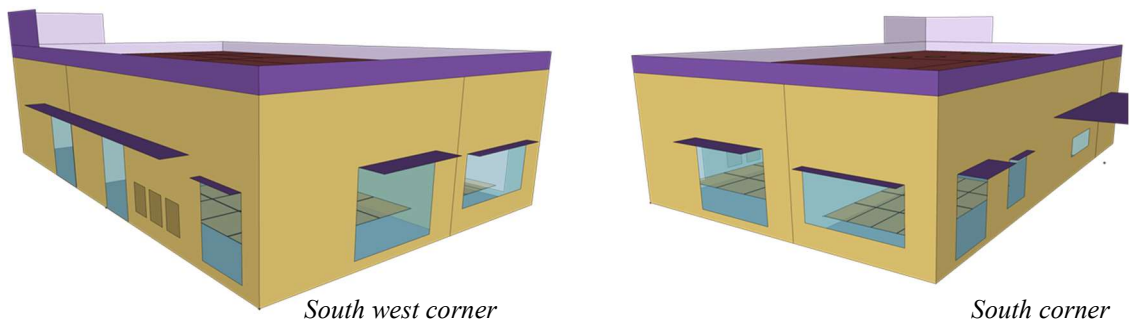
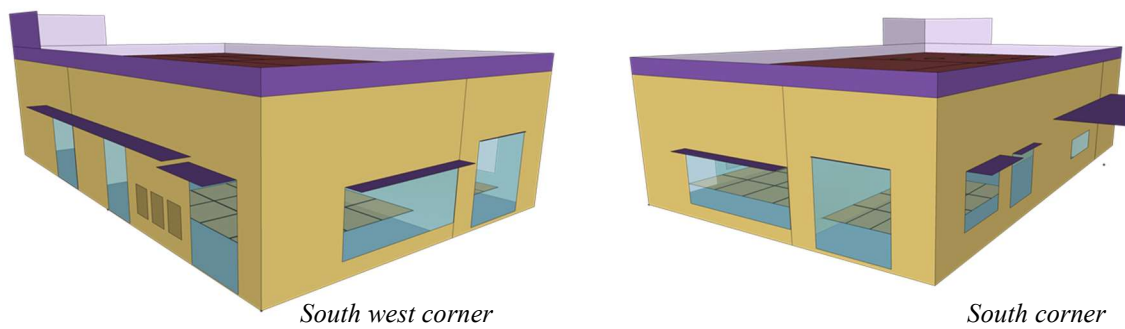


Figure 6.14: Pareto front of design solutions for the retail bank building. Pareto solutions are identified in red.

Figure 6.15: Visualization of Pareto solution *a*Figure 6.16: Visualization of Pareto solution *b*Figure 6.17: Visualization of Pareto solution *c*

## CHAPTER 7: CONCLUSION

### 7.1. Summary

This dissertation has demonstrated how the problem of designing buildings to both minimize energy demand and maximize the appropriate admission of natural light, two objectives that are generally in conflict with one another, can be solved by coupling advanced simulation programs with optimization algorithms. These two objectives are not often considered together when evaluating building energy performance. When they have been, simplifications of the problem are used in either the building geometry parameters investigated or the means of evaluating daylighting performance. This work has advanced earlier approaches to solving the building design problem by employing new techniques of searching complex geometry and state-of-the art dynamic daylighting metrics.

For the results of a building optimization to be trustworthy, there must be a certain degree of confidence in the prediction accuracy of the energy model that was used in the optimization. To this end, in Chapter 3, a framework for model calibration was demonstrated through a simulation based example. This example showed that when the true parameter set of an energy model is not known, it can be approximated by comparing the thermal response of the model to measured values. The parameter set of the energy model can then be explored with the goal of minimizing the error between its thermal response and that which was measured. In Chapter 4, an advanced method of evaluating

daylighting performance was presented and four optimization algorithms were evaluated based on how efficiently solutions were found and the consistency of found solutions, with respect to their design attributes. Algorithm/heuristic based optimization techniques were appropriate for this problem because of the complexities inherent in the formulations for evaluating daylighting and thermal performance. The four algorithms evaluated were the Simplex Algorithm of Nelder and Mead with the Extension of O'Neill (SA), Hooke Jeeves (HJ), Particle Swarm Optimization using Inertia Weight (PSOIW), and a hybrid PSO Constriction/Hooke Jeeves (PSOC/HJ) algorithm. PSOIW consistently found the best solution, while PSOC/HJ was slightly less consistent in finding the best solution, but always came close with much fewer simulations than PSOIW. In Chapter 5, the work in Chapter 4 was extended and used in the development of a method of bi-objective optimization of building energy and daylighting performance. Pareto-efficient solutions were found for the design of a classroom for various orientations. This information is valuable for design decision makers who are interested in better understanding the trade-offs between daylighting and thermal performance. In Chapter 6, the method of energy model calibration presented in Chapter 3 was applied to a case study example. The calibration method minimized the error between the model predicted thermal response and measured thermal response of the building of interest. This calibration method is unique in that it is based on hourly end uses of energy and zone temperatures, unlike other methods that are based on monthly aggregate values or hourly aggregate uses of energy. The calibrated building model was then used as the basis of a building energy and daylighting performance optimization which resulted in Pareto efficient designs available for consideration by the building designer.

Some of the main contributions of the work are listed below.

- Identification of well-performing optimization algorithms for the building envelope design problem.
- Bi-objective optimization using state-of-the-art annual thermal and lighting simulation techniques.
- Modification of annual daylighting performance metrics to aid the optimization process.
- Simultaneous optimization of solar and light transmittances of glass for thermal and lighting performance with appropriate constraints.
- Dynamic sizing and modeling of economizer cycle for thermal performance.
- Development of a model calibration method that operates on envelope parameters in isolation of HVAC system interactions.

## 7.2. Limitations and Future Work

The results presented in this dissertation demonstrate that the developed methods are useful in finding Pareto efficient building designs for energy and daylighting performance. However, when a building designer is presented with a set of Pareto efficient designs, it is not necessarily evident which one is the best choice. In addition, it may not be obvious how a particular design achieves high energy and daylighting performance. This knowledge may be of use when determining how to modify a building for cost control or how to design future buildings to achieve desired results. These limitations present several opportunities for the extension of this work. In addition, this work may be extended by the inclusion of complex fenestration systems and dynamic shading systems along with advanced methods of accounting for visual comfort.

### 7.2.1. Building Element Performance

Windows are the weakest thermal barrier in buildings and, of course, determine a building's daylighting performance. A deeper understanding of how they achieve thermal and daylighting results is desirable. To this end, a possible post-optimization analysis of Pareto-efficient design solutions is the determination of each window element's contribution to the lighting and thermal performance of the overall design. Such a method could operate on a design's discrete window elements (a single window may be divided in to discrete elements of similar area for a more granular understanding of its performance) and express their additive value to the overall performance of the design. Knowledge of the performance of window elements is important because windows are expensive (per unit area) and performance-impactful elements of the building envelope. For each window element, key questions include: is it admitting too much light, or too little light; too much solar heat, or too little; too much conducted heat, or too little; could the same lighting and thermal performance be achieved with less window area? Also important is the knowledge of which components of the building are the most significant so that they are not easily dropped from the design due to concerns such as budget constraints.

### 7.2.2. Analysis of Pareto Efficient Designs

In the building design process, the building designer ultimately has to select one design from the set of Pareto-efficient designs. This can be cumbersome due to the potentially large number of designs in this set. To aid in the selection of a single design, the set of Pareto-efficient solutions can be pruned to prototypes representative of clusters of similar designs along the Pareto front. A clustering algorithm may be used to reduce

the full set of Pareto-efficient designs to a smaller representative set. Once a reduced set is created, a multi-criteria decision making framework, such as Analytic Hierarchy Process (AHP), can be used to evaluate trade-offs between designs. Such a framework can include the decision makers' subjective valuation of energy and daylighting performance values. If desired, additional attributes of the reduced designs can also be assessed through a multi-criteria decision analysis framework. Possible additional attributes follow.

- Aesthetic appeal
- Visual comfort
  - Daylighting performance was evaluated based on the percentage of time within a desired range. This has been shown to control glare/visual comfort, but there are more advanced ways of evaluating visual comfort.
- Outdoor connection
  - In addition to energy performance and quality of lighting environment, many designers value windows for the connection they give occupants to the outdoors.
- Construction cost
  - General costs per area of building materials can be accessed. Using this information, along with the area of floor, walls, roofing, and windows, the construction cost of a design can be determined.
- Peak energy demand
  - Peak electrical power demand is of interest for environmental and economic reasons. Most building energy simulation programs calculate peak energy demand.
- Annual utility costs
  - Differences in fuel costs and time of use charges complicate the relationship between annual energy use and annual utility costs. Most building energy simulation programs allow for a rate structure to be specified for a detailed estimate of annual utility costs.

### 7.2.3. Model Calibration Improvements

A limitation of the model calibration method is the lack of direct determination of thermal effects present during normal building operations but not during thermal response test periods. Such effects include heat gain from occupants and infiltration caused by the opening of exterior doors and other fenestration elements by occupants. Heat gain from building occupants was estimated by first estimating the number of occupants in the building on an hourly basis (from observations) and the rate at which an occupant emits heat while performing office-like activities. Infiltration rates during occupied times were estimated based on cooling equipment energy use. This seemed a reasonable approach since all other thermal loads acting on the cooling system were largely determined and cooling system energy use in response to thermal loading conditions can be approximated by referencing the system's performance curves, assuming proper function of the system. A possible extension is the verification of this approach to estimate unaccounted for thermal effects and/or the development of a better approach. BAS data, such as logs from occupant sensors, door and window sensors, and HVAC performance, could possibly be useful for determining energy model parameters that account best for these effects.

Another extension of this work is to determine the number and type (e.g., average temperature, humidity, solar radiation, etc.) of test days needed to create a sufficiently calibrated energy model. In addition, the calibration method could automatically receive relevant information from the BAS to possibly perform a continuous calibration of the energy model. This would, in effect, create an operational energy model of the building that could be used for continuous commissioning and fault detection of building systems.

#### 7.2.4. Integration into Building Design Practice

A limitation of this work is the study of how the building design optimization method could fit into building design practice. Issues to consider are the time required to setup an optimization model, the time required for the simulations of the optimization sequence, and the quality of found designs. As discussed, some algorithms converge very quickly to good, but less than global optimal, solutions. Other algorithms take considerably more time to converge but find higher quality designs very close to global optimal.

Unanswered questions include the following. Do the good designs found by fast algorithms sufficiently satisfy the desires or requirements of the design team? Is the longer simulation time of the high-quality and consistent design finding algorithms a critical issue such that the results are not produced quickly enough for them to be useful? Can the optimization method be integrated into building modeling software commonly used by building design teams?

Another extension is the creation of greater visibility of optimized solutions, and/or high-performing solutions found while searching for the optimum solution, that happen to be heterogeneous with regard to design features. This issue was discussed. One point made was that dissimilar designs can have similar daylighting and thermal performance. An understanding of such designs is important to building designers because they may have different attributes in other categories, such as construction cost. A framework to make visible and explore such designs and their attributes may prove valuable to the building design team.

## REFERENCES

- [1] "Annual Energy Review 2011," U.S. Department of Energy, Energy Information Administration, 2011.
- [2] "2003 Commercial Buildings Energy Consumption Survey," U.S. Department of Energy, Energy Information Administration, 2003.
- [3] L. Doulos, A. Tsangrassoulis, and F. Topalis, "Quantifying energy savings in daylight responsive systems: The role of dimming electronic ballasts," *Energy and Buildings*, vol. 40, pp. 36-50, 2008.
- [4] R. Embrechts and C. Van Bellegem, "Increased Energy Savings by Individual Light Control," in *Right Light 4*, Copenhagen, pp. 179-182.
- [5] E. S. Lee and S. E. Selkowitz, "The New York Times Headquarters daylighting mockup: Monitored performance of the daylighting control system," *Energy and buildings*, vol. 38, pp. 914-929, 2006.
- [6] D. H. Li, T. N. Lam, and S. Wong, "Lighting and energy performance for an office using high frequency dimming controls," *Energy Conversion and Management*, vol. 47, pp. 1133-1145, 2006.
- [7] S. Onaygıl and Ö. Güler, "Determination of the energy saving by daylight responsive lighting control systems with an example from Istanbul," *Building and Environment*, vol. 38, pp. 973-977, 2003.
- [8] K. Opdal and B. Brekke, "Energy saving in Lighting by Utilisation of Daylight," in *Right Light 3*, Newcastle, 1995, pp. 67-74.
- [9] B. Roisin, M. Bodart, A. Deneyer, and P. D'herdt, "Lighting energy savings in offices using different control systems and their real consumption," *Energy and Buildings*, vol. 40, pp. 514-523, 2008.
- [10] C. E. Ochoa, M. B. Aries, and J. L. Hensen, "State of the art in lighting simulation for building science: a literature review," *Journal of Building Performance Simulation*, vol. 5, pp. 209-233, 2012.
- [11] J. Mardaljevic, "Validation of a lighting simulation program under real sky conditions," *Lighting Research and Technology*, vol. 27, pp. 181-188, 1995.
- [12] R. Compagnon, "RADIANCE: a simulation tool for daylighting systems," The Martin Centre for Architectural and Urban Studies University of Cambridge Department of Architecture, 1997.
- [13] J. Mardaljevic, "Validation of a lighting simulation program: a study using measured sky brightness distributions," *Lux Europa*, vol. 97, pp. 555-569, 1997.

- [14] C. F. Reinhart and O. Walkenhorst, "Validation of dynamic RADIANCE-based daylight simulations for a test office with external blinds," *Energy and Buildings*, vol. 33, pp. 683-697, 2001.
- [15] C. F. Reinhart and M. Andersen, "Development and validation of a Radiance model for a translucent panel," *Energy and Buildings*, vol. 38, pp. 890-904, 2006.
- [16] M. J. Witte, R. H. Henninger, J. Glazer, and D. B. Crawley, "Testing and validation of a new building energy simulation program," *Proceedings of Building Simulation 2001*, pp. 353-360, 2001.
- [17] B. Eisenhower, Z. O'Neill, V. A. Fonoberov, and I. Mezić, "Uncertainty and sensitivity decomposition of building energy models," *Journal of Building Performance Simulation*, vol. 5, pp. 171-184, 2011.
- [18] M. Wetter, "Design optimization with GenOpt," *Building Energy Simulation User News*, vol. 21, pp. 19-28, 2000.
- [19] L. G. Caldas and L. K. Norford, "A design optimization tool based on a genetic algorithm," *Automation in Construction*, vol. 11, pp. 173-184, 2002.
- [20] J. Gagne and M. Andersen, "A generative facade design method based on daylighting performance goals," *Journal of Building Performance Simulation*, vol. 5, pp. 141-154, 2012.
- [21] B. Lartigue, B. Lasternas, and V. Loftness, "Multi-objective optimization of building envelope for energy consumption and daylight," *Indoor and Built Environment*, vol. 23, pp. 70-80, 2013.
- [22] T. Rakha and K. Nassar, "Genetic algorithms for ceiling form optimization in response to daylight levels," *Renewable Energy*, vol. 36, pp. 2348-2356, 2011.
- [23] G. Zemella, D. De March, M. Borrotti, and I. Poli, "Optimised design of energy efficient building façades via Evolutionary Neural Networks," *Energy and Buildings*, vol. 43, pp. 3297-3302, 2011.
- [24] J. Hu and S. Olbina, "Simulation-Based Model for Integrated Daylighting System Design," *Journal of Computing in Civil Engineering*, vol. 28, p. A4014003, 2014.
- [25] M. Manzan and R. Padovan, "Multi-criteria energy and daylighting optimization for an office with fixed and moveable shading devices," *Advances in Building Energy Research*, pp. 1-15, 2015.
- [26] D. Coakley, P. Raftery, and M. Keane, "A review of methods to match building energy simulation models to measured data," *Renewable and Sustainable Energy Reviews*, vol. 37, pp. 123-141, 2014.

- [27] F. Karlsson, P. Rohdin, and M.-L. Persson, "Measured and predicted energy demand of a low energy building: important aspects when using Building Energy Simulation," *Building Services Engineering Research and Technology*, vol. 28, pp. 223-235, 2007.
- [28] ASHRAE, "Standard 90.1-2010, Energy standard for buildings except low-rise residential buildings," *ASHRAE/IESNA Standard*, 2010.
- [29] C. Turner and M. Frankel, "Energy performance of LEED for new construction buildings," New Buildings Institute, Vancouver, WA, 2008.
- [30] J. H. Scofield, "Do LEED-certified buildings save energy? Not really...", *Energy and Buildings*, vol. 41, pp. 1386-1390, 2009.
- [31] C. M. Stoppel and F. Leite, "Evaluating building energy model performance of LEED buildings: Identifying potential sources of error through aggregate analysis," *Energy and Buildings*, vol. 65, pp. 185-196, 2013.
- [32] T. A. Reddy, I. Maor, and C. Panjapornpon, "Calibrating Detailed Building Energy Simulation Programs with Measured Data—Part II: Application to Three Case Study Office Buildings (RP-1051)," *HVAC&R Research*, vol. 13, pp. 243-265, 2007.
- [33] T. A. Reddy, I. Maor, and C. Panjapornpon, "Calibrating Detailed Building Energy Simulation Programs with Measured Data—Part I: General Methodology (RP-1051)," *HVAC&R Research*, vol. 13, pp. 221-241, 2007.
- [34] T. Agami Reddy, "Literature review on calibration of building energy simulation programs: Uses, problems, procedures, uncertainty, and tools," *ASHRAE Transactions*, pp. 226-240, 2006.
- [35] "M&V Guidelines: Measurement and Verification for Federal Energy Projects Version 3.0," U.S. Department of Energy, 2008.
- [36] "International Performance Measurement & Verification Protocol," U.S. Department of Energy, 2002.
- [37] "ASHRAE Guideline 14-2002," ASHRAE, 2002.
- [38] P. Raftery, M. Keane, and J. O'Donnell, "Calibrating whole building energy models: An evidence-based methodology," *Energy and Buildings*, vol. 43, pp. 2356-2364, 2011.
- [39] Z. O'Neill and B. Eisenhower, "Leveraging the analysis of parametric uncertainty for building energy model calibration," *Building Simulation*, vol. 6, pp. 365-377, 2013.

- [40] P. Raftery, M. Keane, and A. Costa, "Calibrating whole building energy models: Detailed case study using hourly measured data," *Energy and Buildings*, vol. 43, pp. 3666-3679, 2011.
- [41] J. D. Bynum, D. E. Claridge, and J. M. Curtin, "Development and testing of an Automated Building Commissioning Analysis Tool (ABCAT)," *Energy and Buildings*, vol. 55, pp. 607-617, 2012.
- [42] G. P. Henze, "Model predictive control for buildings: a quantum leap?," *Journal of Building Performance Simulation*, vol. 6, pp. 157-158, 2013.
- [43] K. Xu, P. Delgoshaei, S. Wagner, and J. D. Freihaut, "Creating "As-Operated" Whole-Building Energy Models for Existing Commercial Medium Sized Office Buildings-A Case Study," in *AEI 2013*, 2013, pp. 534-543.
- [44] K. P. Lam, J. Zhao, E. B. Ydstie, J. Wirick, M. Qi, and J. Park, "AN ENERGYPLUS WHOLE BUILDING ENERGY MODEL CALIBRATION METHOD FOR OFFICE BUILDINGS USING OCCUPANT BEHAVIOR DATA MINING AND EMPIRICAL DATA " presented at the 2014 ASHRAE/IBPSA-USA Building Simulation Conference, Atlanta, 2014.
- [45] S. Wilcox and W. Marion, *Users manual for TMY3 data sets*: National Renewable Energy Laboratory Golden, CO, 2008.
- [46] G. J. Ward, F. M. Rubinstein, and R. D. Clear, "A ray tracing solution for diffuse interreflection," *ACM SIGGRAPH Computer Graphics*, vol. 22, pp. 85-92, 1988.
- [47] A. Nabil and J. Mardaljevic, "Useful daylight illuminance: a new paradigm for assessing daylight in buildings," *Lighting Research and Technology*, vol. 37, pp. 41-57, 2005.
- [48] "LM-83-12 IES Spatial Daylight Autonomy (sDA) and Annual Sunlight Exposure (ASE)," IESNA, 2012.
- [49] A. Nabil and J. Mardaljevic, "Useful daylight illuminances: A replacement for daylight factors," *Energy and Buildings*, vol. 38, pp. 905-913, 2006.
- [50] C. F. Reinhart, J. Mardaljevic, and Z. Rogers, "Dynamic daylight performance metrics for sustainable building design," *Leukos*, vol. 3, pp. 7-31, 2006.
- [51] H. Shen and A. Tzempelikos, "Daylighting and energy analysis of private offices with automated interior roller shades," *Solar Energy*, vol. 86, pp. 681-704, 2012.
- [52] H. Shen and A. Tzempelikos, "Sensitivity analysis on daylighting and energy performance of perimeter offices with automated shading," *Building and Environment*, vol. 59, pp. 303-314, 2013.

- [53] E. C. Özelkan and L. Duckstein, "Fuzzy conceptual rainfall–runoff models," *Journal of Hydrology*, vol. 253, pp. 41-68, 2001.
- [54] P. Tregenza and I. Waters, "Daylight coefficients," *Lighting Research and Technology*, vol. 15, pp. 65-71, 1983.
- [55] "3ds Max 2013," Autodesk.
- [56] "AGI32 Version 2.36," Lighting Analysisists Inc.
- [57] G. J. Ward, "The RADIANCE Lighting Simulation and Rendering System," in *Proceedings of the 21st Annual Conference on Computer Graphics and Interactive Techniques*, 1994, pp. 459-472.
- [58] M. Wetter, "Generic Optimization Program User Manual Version 3.1.0," LBNL, 2011.
- [59] R. O'Neill, "Algorithm AS 47: function minimization using a simplex procedure," *Applied Statistics*, pp. 338-345, 1971.
- [60] M. Bell and M. Pike, "Remark on algorithm 178 [E4] direct search," *Communications of the ACM*, vol. 9, pp. 684-685, 1966.
- [61] R. De Vogelaere, "Remark on algorithm 178: Direct search," *Communications of the ACM*, vol. 11, p. 498, 1968.
- [62] R. Hooke and T. A. Jeeves, "'Direct Search' Solution of Numerical and Statistical Problems," *Journal of the ACM (JACM)*, vol. 8, pp. 212-229, 1961.
- [63] L. B. Smith, "Remark on algorithm 178 [E4]: direct search," *Communications of the ACM*, vol. 12, p. 638, 1969.
- [64] R. C. Eberhart and Y. Shi, "Particle swarm optimization: developments, applications and resources," in *2001 Congress on Evolutionary Computation*, 2001, pp. 81-86.
- [65] R. Poli, J. Kennedy, and T. Blackwell, "Particle swarm optimization," *Swarm Intelligence*, vol. 1, pp. 33-57, 2007.
- [66] Y. Shi and R. Eberhart, "A modified particle swarm optimizer," in *The 1998 IEEE International Conference on Evolutionary Computation 1998*, pp. 69-73.
- [67] "Input Output Reference: The Encyclopedic Reference to EnergyPlus Input and Output," U.S. Department of Energy, 2013.
- [68] M. Deru, K. Field, D. Studer, K. Benne, B. Griffith, P. Torcellini, *et al.*, "US Department of Energy Commercial Reference Building Models of the National Building Stock," 2011.

- [69] "EnergyPlus Engineering Reference," U.S. Department of Energy, 2010.
- [70] K. Field, M. Deru, and D. Studer, "Using DOE commercial reference buildings for simulation studies," in *Proceedings of the 4th National Conference of IBPSA-USA*, 2010, pp. 85-93.
- [71] D. B. Crawley, L. K. Lawrie, F. C. Winkelmann, W. F. Buhl, Y. J. Huang, C. O. Pedersen, *et al.*, "EnergyPlus: creating a new-generation building energy simulation program," *Energy and Buildings*, vol. 33, pp. 319-331, 2001.
- [72] C. Audet, G. Savard, and W. Zghal, "Multiobjective optimization through a series of single-objective formulations," *SIAM Journal on Optimization*, vol. 19, pp. 188-210, 2008.
- [73] Y. Y. Haimes, L. S. Lasdon, and D. A. Wismer, "On a bicriterion formulation of the problems of integrated system identification and system optimization," *IEEE Transactions on Systems Man and Cybernetics*, pp. 296-297, 1971.
- [74] D. C. Montgomery, *Design and Analysis of Experiments*: John Wiley & Sons, 2008.
- [75] G. J. Ward, "RCONTRIB," 2005.